Electrochemical Studies on Hydride Ion and Hydrogen Absorbing Alloys in Molten Salt Systems

Toshiyuki Nohira

1998

Electrochemical Studies on Hydride Ion and Hydrogen Absorbing Alloys in Molten Salt Systems

Toshiyuki Nohira

1998

Contents

Chapter 1

General Introduction

1.1 Electrochemical reactions involving hydride ion and their applications

Hydride ion (H^-) is produced by dissolution of a saline hydride like LiH in molten alkali halides such as LiCl-KCl [1]. It is a unique anion existing only in molten salts. It has a strong reducing power and is stable in reducing atmosphere. Existence of the half-cell reaction of H_2/H^- has been reported by Sharer et al. [2]. Though the definition is not clear, the electrode potential for the H_2/H^- system has been estimated to be around 0.5 V (vs. Li^+/Li) from the work of Plambeck et al. [3]. Thus, precise equilibrium potential of the H_2/H^- system seems not to have been reported so far.

Electrochemical reactions involving H^- ion in molten salts are important from various engineering aspects [4]. For instance, a Li-H_2 thermally regenerative fuel cell can be constructed using the reaction of the H_2/H^- system [2, 5]. Since the Li-H_2 thermally regenerative fuel cell converts heat to electricity with high efficiency, it seems to be a promising method for efficient utilization of waste heat. It looks also promising for space applications due to its high energy density. Electrochemical reactions involving H^- ion and hydrogen in molten salts are also important in the field of nuclear energy; for example for tritium recovery from molten salt nuclear reactors [6] and nuclear fusion reactors [7] because the H^- ion resembles T^- ion. Furthermore, the half-cell reactions of M-H/H^- systems have the possibility to provide a convenient and precise means to investigate hydrogen behavior in metals at high temperature [8, 9]. Concerning this subject, it is referred to section 1.3.

1.2 Electrochemical behavior of hydride ion

With the background described above, the author studied the electrochemical behavior of H^- ion in a molten LiCl-KCl-LiH system due to its importance for the understanding of all the reactions involving H^- ion. Only a few studies have so far been carried out on this subject. In 1966, Plambeck et al. reported basic results including a diffusion coefficient of H^- ion of 1.67×10^{-5} cm^2 s^{-1} at 648 K [3]. Later, Takenaka and Ito studied the electrochemical behavior of H^- ion on an Fe electrode at 698 K using cyclic voltammetry, chronopotentiometry, chronoamperometry and gas analysis [4]. The study showed that the electrode reaction is similar to a one-electron reversible reaction and that the product after long-term anodic electrolysis was pure hydrogen gas. The hydride ion diffusion coefficient was estimated to be 3.0×10^{-5} cm^2 s^{-1} at 698 K. In the case of short-term measurements, the produced hydrogen was found mainly to diffuse into the Fe electrode, and this explained the near-reversible electrode behavior. This is reasonable, considering the not negligible sizes of hydrogen solubility, 1.9×10^{-5} (H/Fe, at 1 atm hydrogen), and diffusion coefficient, 4.6×10^{-4} cm^2 s^{-1}, in Fe at 673 K (values are averages of literature data [10]).

However, the electrochemical behavior of H^- ion using a non-hydrogen absorbing electrode does not seem to have been reported so far. If the hydrogen absorption into the electrode is negligible, the electrode reaction would become simpler than for the Fe electrode case. Therefore, a Mo electrode was chosen for investigation of the H^- ion behavior in a LiCl-KCl eutectic melt, see chapter 2. Since the solubility and diffusion coefficient of hydrogen in Mo at 673 K have been reported to be as small as 5.7×10^{-7} (H/Mo, at 1 atm hydrogen) [11] and 9.9×10^{-7} cm^2 s^{-1} [12], hydrogen absorption into the electrode might be regarded as negligible. The purpose of the study presented in chapter 2 was to examine both the anodic oxidation of H^- ion and the cathodic reduction of hydrogen. It was attempted to determine the diffusion coefficient of H^- ion and to describe the reaction mechanism for H_2 evolution. Also, the cathodic reduction of H_2 gas was directly investigated by a gas electrode.

1.3 High temperature hydrogen absorbing alloy

The author also attempted to investigate hydrogen behavior in metals at high temperature. Hydrogen behavior in metals at high temperature are worth investigating from various reasons. For hydrogen energy systems, which have attracted much attention because of their cleanness and permanence, higher operating temperatures have the advantages of higher reactivity. Furthermore, if the total generated heat is efficiently utilized in the system, higher overall energy efficiency can be expected. These high temperature operations require the development of new hydrogen absorbing alloys which work at the required temperatures. At the same time, understanding of hydrogen behavior in structural materials at high temperature is necessary to prevent hydrogen embrittlement. For a D-T neutron generator, the development of new metal-tritide targets is important because the desorption of tritium caused by generated heat prevents high neutron output and long term operation for conventional Ti-T targets [13]. This can be overcome by developing a hydrogen absorbing alloy with a very low hydrogen desorption pressure at high temperatures. Metal alloys having high hydrogen permeability at high temperatures are promising both as cathode materials for a Li-H_2 thermally regenerative fuel cell [2, 5] and as a hydrogen diffusion membrane for hydrogen purification [14].

Despite these potential uses, few studies on high temperature hydrogen absorbing alloys exist. Therefore, high temperature hydrogen absorbing alloys were investigated by electrochemical methods using a molten LiCl-KCl-LiH system. Electrochemical methods have several advantages; high sensitivity, simple apparatus, safe handling of hydrogen gas, possibility to change hydrogen pressure instantaneously by controlling electrode potential, etc.

As a first step of such a study, Pd and Pd-Li alloys were selected to be investigated for the following reasons. Firstly, Pd is well known as a hydrogen absorbing metal, and has been studied intensively at room temperature [15]. Also, Pd-Li alloys seemed to have high hydrogen absorbing ability at high temperatures according to Nacken *et al.* who reported that

PdLi absorbs hydrogen to form $PdLiH_x$ (x=0.73-0.82) at 873 K [16]. There is also an interesting report on hydrogen absorbing behavior of Pd-Li alloy at moderate temperatures (298-348 K). Sakamoto *et al.* reported that Pd_7Li dissolves considerable amounts of hydrogen to form a more stable hydride phase than Pd despite the lattice contraction which occurs on alloying Pd with Li [17].

However, in order to study hydrogen absorbing behavior of Pd and Pd-Li alloys in a LiCl-KCl-LiH system, it is important to determine previously the formation potentials of various Pd-Li alloys. In chapter 3, formation potentials of several Pd-Li phases were determined by potential measurements and X-ray diffraction analysis. The results were used in the hydrogen absorbing study both for preparing the Pd-Li alloys and for interpreting the observed potential-charge curves, see chapter 5. The obtained data, presented in chapter 3, are also of importance for studies of the electrochemical formation of Pd-based alloys, e.g., Pd-Y or Pd-La in molten LiCl-KCl systems [18].

The electrochemical study of the Pd-Li system was continued, as described in chapter 4. In this chapter, thermodynamic properties of various Pd-Li alloy phases were determined using potential data obtained at various temperatures (673, 698, 723, 748 and 773 K). To date, there are only two reports that deal with the thermodynamic properties of Pd-Li alloys. One reports the partial molar excess free energy of Li in an α-Pd phase between 1073 and 1373 K [19]. The other report presents a phase diagram and thermodynamic parameters for several known solid Pd-Li compounds using computer calculation [20]. Thus, no measurement data on neither solid Pd-Li compounds nor a liquid Pd-Li alloy seem to appear in the literature.

Based on the results presented in chapters 3 and 4, chapter 5 deals with the electrochemical hydrogen absorbing/desorbing behavior of Pd and Pd-Li alloys in a molten LiCl-KCl-LiH system. Potential-charge curve measurements were used for estimating the amount of hydrogen in the electrode. The hydrogen absorbing ability of Pd-Li alloys is discussed in terms of the Li concentration in the Pd-Li alloys. The rate of electrochemical hydrogen desorption from a PdLi electrode is also discussed.

1.4 SiH_4 production

The author studied the possibility of developing a novel method for SiH_4 production by utilizing anodic oxidation of H^- ion on a Si electrode, as described in chapter 6. SiH_4 gas is an important material in the field of Si semiconductors, because purification of Si is conducted by decomposition of SiH_4 [21]. Especially, low cost SiH_4 production is crucial for mass production of inexpensive Si solar cells. The two conventional methods of SiH_4 production are reviewed in the following.

The method using catalytic disproportionation of chlorosilane

This method was developed into practical use by Union Carbide Corporation. It is the largest scale method of SiH_4 production in the world at present [22].

The method is using the following disproportionation reactions:

$$3\ SiCl_4 + Si + 2\ H_2 \rightleftharpoons 4\ SiHCl_3 \quad (1)$$

$$2\ SiHCl_3 \rightleftharpoons SiCl_4 + SiH_2Cl_2 \quad (2)$$

$$3\ SiH_2Cl_2 \rightleftharpoons 2SiHCl_3 + SiH_4 \quad (3)$$

The net reaction is thus expressed as

$$Si + 2\ H_2 \rightarrow SiH_4 \quad (4)$$

Since this method is conducted by a chemical plant, it is suitable for mass production. However, it requires a lot of energy and a large space, because it proceeds by a multistage reaction of gas materials at high temperatures. Furthermore, since there is a large amount of chlorosilane to be taken care of, a special disposal facility is necessary to handle the large amount of chlorides.

The conventional molten salt method

The conventional SiH_4 production method using molten salt electrolysis was first proposed by Sundermeyer in 1965 [23]. When $SiCl_4$ is introduced to molten LiCl-KCl-LiH,

SiH_4 is produced by the following reaction:

$$4\ LiH + SiCl_4 \rightleftharpoons SiH_4 + 4\ LiH \qquad (5)$$

LiH is produced by hydrogenation of Li, and $SiCl_4$ is generated by chlorination of Si. Thus, if Li and Cl_2 are prepared by electrolysis of molten LiCl-KCl, a completely closed recycling system might be constructed. This method has advantages both due to high reaction rate and high SiH_4 purity.

Industrialization of the method was attempted by Yatsurugi [24], however, the practical use has not yet been attained because of the complexity of the apparatus.

In order to develop a novel and low cost production method of SiH_4, electrode behavior of Si and evolution of SiH_4 in molten LiCl-KCl-LiH systems were studied, as described in chapter 6. The results are presented both for a single crystal Si electrode and for a metal grade Si electrode. The effect of F^- ion addition to the SiH_4 evolution reaction was also examined. The reaction scheme of the SiH_4 evolution and the current efficiency are discussed.

References

[1] J. A. Plambeck, in *Encyclopedia of Electrochemistry of the Elements, volume X, Fused Salt Systems*, ed., A. J. Bard, p.16, Marcel Dekker, New York (1976).

[2] R. E. Shearer and R. C. Werner, J. Electrochem. Soc. **105,** 693 (1958).

[3] J. A. Plambeck, J. P. Elder and H. A. Laitinen, *J. Electrochem. Soc.* **113,** 931(1966).

[4] T. Takenaka and Y. Ito, *Denki Kagaku* **59,** 759(1991).

[5] P. Roy, S. A. Salamah, J. Maldonado and R. S. Narkiewicz, AIP Conf. Proc. **271,** 913 (1993).

[6] G. T. Mays, A. N. Smith and J. R. Engel, *ORNL/TM*-5759, (1977).

[7] H. Moriyama, J. Oishi and K. Kawamura, *J. Nucl. Mater.* **161,** 197(1989).

[8] B. Y. Liaw, G. Deublein and R. A. Huggins, J. Alloys and Compounds. **189,** 175 (1992).

[9] B. Y. Liaw, G. Deublein and R. A. Huggins, J. Electrochem. Soc. **142,** 2196 (1995).

[10] E. Fromm, H. Speck, H. Jehn and G. Hörz, in *Physics Data: Gases and Carbon in Metals, Part XIII: Ferrous Metals (1), Iron-Hydrogen,* p. 5 and 11, Fachinformationszentrum Energie, Physik, Mathematik Gmbh, Karlsruhe (1981).

[11] S. Yamanaka, T. Matsuura and M. Miyake, *Z. Phys. Chem.* **179,** 103(1993).

[12] V. M. Katlinskii, *Inorg. Mater.* **14,** 1299(1978).

[13] H. H. Barschall, in *Neutron Sources for Basic Physics and Applications*, S. Cierjacks, Editor, p. 57, Pergamon Press (1983).

[14] M. L. Doyle and I. R. Harris, *Platinum Metals Rev.* **32,** 130(1988).

[15] Y. Fukai, *The Metal-Hydrogen System*, Springer-Verlag (1993).

[16] B. Nacken and W. Bronger, *J. Less-Common Met.* **52,** 323(1977).

[17] Y. Sakamoto, T. Hisamoto, M. Ura and R. Nakamura, *J. Alloys Comp.* **200,** 141(1993).

[18] E. O. Ahlgren, T. Nohira and Y. Ito, *J. Electrochem. Soc.*, to be submitted.

[19] H. Brodowsky and H. Schumacher, *Report at CALPHAD XI,* Argonne, IL(1980),

Summary in L. Kaufman, *CALPHAD* **6**, 178(1982).

[20] R. A. Howald, *CALPHAD* **14,** 1(1990).

[21] W. Simmler, in *Ullmann's Encyclopedia of Industrial Chemistry*, Vol. A24, p.1, VCH Publishers (1993).

[22] R. Hayashi, in *Surface Science Technology Series Vol. 3, Science of Silicon,* ed. UCS study group on semiconductor basic technology, Realize Corporation (1996), in Japanese.

[23] W. Sundermeyer and L. M. Litz, *Chem. Ing.Tech.*, **37,** 14(1965).

[24] Y. Yatsurugi, *Molten Salt*, **31,** 77(1988), in Japanese.

Chapter 2

Hydride Ion Behavior in a Molten LiCl-KCl-LiH System*

2.1 Introduction

In molten alkali halides such as LiCl-KCl, hydride (H^-) ion is produced by dissolution of a saline hydride like LiH [1]. Electrochemical reactions involving H^- ion in molten salts are finding several useful and promising applications [2]. For instance, the half-cell reactions of M-H/H^- systems have the possibility to provide a convenient and precise means to investigate hydrogen behavior in metals at high temperature [3, 4]. To further develop this electrochemical method as a useful investigation means for hydrogen behavior in metals, including kinetic considerations, it seems necessary to obtain the data as to H^- ion, *e.g.*, reversibility of electron transfer process and a diffusion coefficient of H^- ion.

Also a Li-H_2 thermally regenerative fuel cell can be constructed using the reaction of the H_2/H^- system [5, 6]. Since the Li-H_2 thermally regenerative fuel cell converts heat to electricity with high efficiency, it seems to be a promising method for efficient utilization of waste heat. It looks also promising for space applications due to its high energy density. To develop the Li-H_2 thermally regenerative fuel cell, anodic oxidation of H^- ion and cathodic reduction of H_2 gas have to be clarified. Also a diffusion coefficient of H^- ion is important basis.

Electrochemical reactions involving T^- ion in molten salts are also important in the field of nuclear energy; for example for tritium recovery from molten salt nuclear reactors[7] and

---

*To be submitted to *J. Electrochem. Soc.*

nuclear fusion reactors [8]. Therefore, data as to H^- ion and D^- ion are important to predict the T^- ion behavior in molten salts.

Despite these possibly useful and important applications, only a few studies have so far been carried out on the electrochemical behavior of H^- ion in a LiCl-KCl eutectic melt. In 1966, Plambeck et al. reported basic results including a diffusion coefficient of H^- ion of 1.67 x 10^{-5} cm^2 s^{-1} at 648 K [9]. Later, Takenaka and Ito studied the electrochemical behavior of H^- ion and D^- ion on an Fe electrode at 698 K using cyclic voltammetry, chronopotentiometry, chronoamperometry and gas analysis [2, 10]. The study showed that the electrode reaction is similar to a one-electron reversible reaction and that the product after long-term anodic electrolysis was pure hydrogen gas. The H^- ion diffusion coefficient was estimated to be 3.0 x 10^{-5} cm^2 s^{-1} at 698 K. In the case of short-term measurements, the produced hydrogen was found mainly to diffuse into the Fe electrode, which explained the near-reversible electrode behavior. This is reasonable, considering the not negligible sizes of hydrogen solubility, 1.9 x 10^{-5} (H/Fe, at 1 atm hydrogen), and diffusion coefficient, 4.6 x 10^{-4} cm^2 s^{-1}, in Fe at 673 K (values are averages of literature data [11]).

However, the electrochemical behavior of H^- ion using a non-hydrogen absorbing electrode does not seem to have been reported so far. If the hydrogen absorption into the electrode is negligible, the electrode reaction would become simpler than the case for Fe electrode case. Therefore, in the work stated in this chapter, a Mo electrode has been chosen for investigation of the electrochemical behavior of H^- ion in a LiCl-KCl eutectic melt. Since the solubility and diffusion coefficient of hydrogen in Mo at 673 K have been reported to be as small as 5.7 x 10^{-7} (H/Mo, at 1 atm hydrogen) [12] and 9.9 x 10^{-7} cm^2 s^{-1} [13], hydrogen absorption into the electrode might be regarded as negligible. The purposes of the study presented in this chapter were to determine the diffusion coefficient of H^- ion by several different techniques and to describe the reaction mechanism for H_2 gas evolution. Also, an investigation on the electrochemical reduction of H_2 was carried out using a gas electrode. The difference between gas electrodes using Mo and Ni wires is discussed.

2.2 Experimental

The experimental setup is shown in Fig. 2.1. The cell was operated in a furnace attached to the base of an argon glove box with gas circulating purifier (MBN-R-07; Japan Pionics Co., Ltd.), resulting in a water contamination level less than 1 ppm. The LiCl-KCl eutectic (LiCl:KCl = 58.5:41.5 mol%, m.p. 625 K; reagent grade, Wako Pure Chemical Co., Ltd.) was contained in a high purity alumina crucible (99.5 % Al_2O_3; Nippon Kagaku Togyo Co., Ltd., SSA-S). It was kept under vacuum for more than 72 hours at elevated temperatures (473-573 K) to remove water. The eutectic mixture was then melted in a dry argon atmosphere at 673 K. Pre-electrolysis using a Pt wire cathode and a glassy carbon anode was carried out with a terminal voltage of 2.5 V in order to remove residual water. When the cathodic current density became less than 0.5 mA cm^{-2} the pre-electrolysis was terminated. LiH (Wako Pure Chemical Co., Ltd., 95 %) was directly added to the melt as a H^- ion source. Chromel-Alumel thermocouples were used for both temperature measurement and control. The temperature was maintained within ± 1 K by a temperature control unit (DSM-2; Shimaden Co., Ltd.).

The working electrode was a square-shaped sheet of Mo (5 mm x 3 mm x 0.2 mm, Nilaco Corp., 99.95 %). Also, Mo or Ni wire (ϕ1 mm) bundled type electrode covered with a high purity alumina tube was used as a gas electrode. Pure argon (99.998 %) or pure hydrogen (99.9999%) was supplied from the top of the gas electrode. The counter electrode was a glassy carbon rod (70 mm x ϕ5 mm, Tokai Carbon Co., Ltd.) or an Al-Li alloy prepared by electrolytic deposition of Li on an Al rod (70 mm x ϕ4 mm, Nilaco Corp., 99.99 %). The reference electrode was an Al-Li alloy in the coexisting (α+β) phase state prepared electrochemically from an Al wire (10 mm x ϕ1 mm, Nilaco Corp., 99.99 %). The equilibrium potential of this electrode is determined by the following reversible reaction [14, 15, 16]:

$$Al(\alpha) + Li^+ + e^- \rightleftharpoons AlLi(\beta) \qquad (1)$$

The potential of this reference electrode was calibrated with reference to that of Li^+/Li

electrode, which was prepared by electrodepositing lithium metal on a nickel wire [17]. This electrode can be regarded as the Li^+/Li electrode since Ni has a small solubility of Li with no intermetallic phase formation [18]. All potentials in the present thesis are given in reference to this Li^+/Li electrode potential.

A potentio/galvanostat (HZ-3000; Hokuto Denko Corp.) connected to a personal computer (FMVS31673; Fujitsu) was used for the cyclic voltammetry, chronopotentiometry and double potential step chronoamperometry measurements.

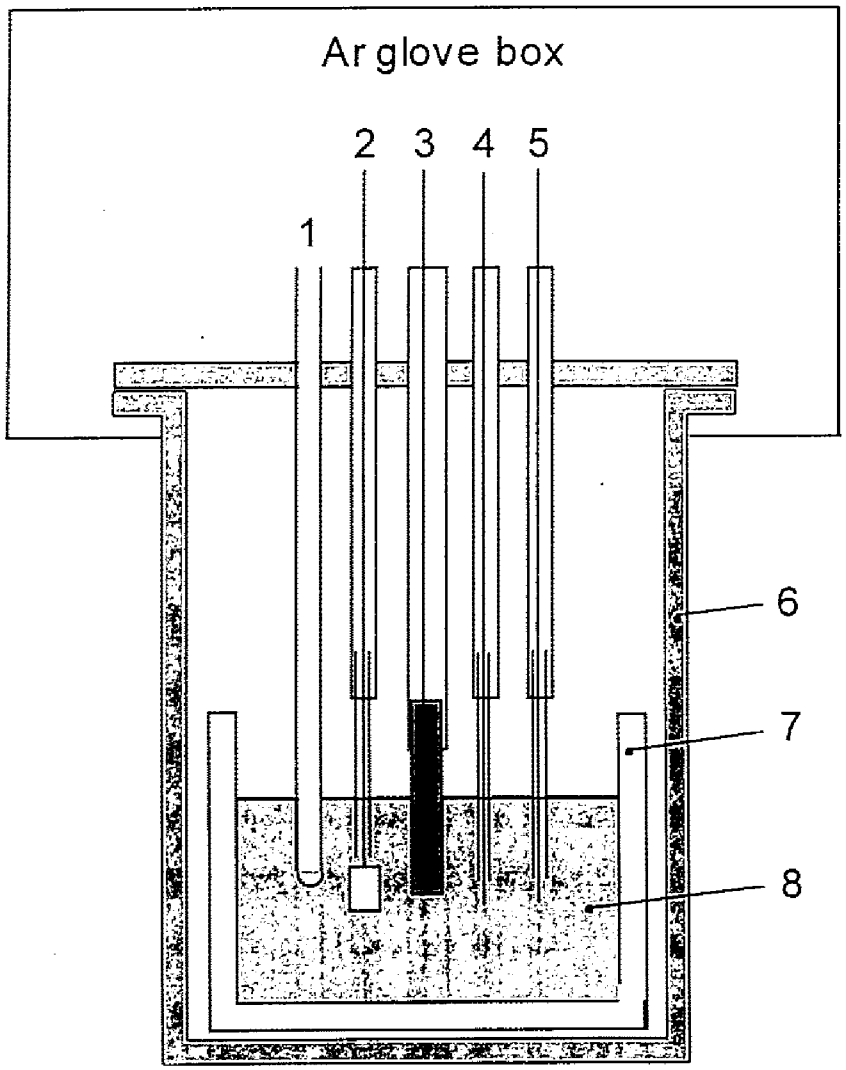

Fig. 2.1. Schematic representation of the experimental apparatus. (1) thermocouple, (2) working electrode, (3) counter electrode, (4) Al-Li reference electrode, (5) Li^+/Li electrode (Ni wire), (6) stainless holder, (7) alumina crucible and (8) LiCl-KCl eutectic melt.

2.3 Results and discussion

The electrochemical behavior of H^- ion in a LiCl-KCl melt was investigated at 673 K using a Mo electrode. All values reported below were determined at this temperature. In the following sections, the discussion was divided according to the employed electrochemical method, voltammetry, chronopotentiometry and double potential step chronoamperometry.

2.3.1 Cyclic voltammetry

Figure 2.2 shows typical voltammograms obtained at various scan rates in a melt with 0.4 mol% LiH added. Ohmic drops were compensated after the measurements, considering the measured solution resistance, 0.3 Ω. The anodic currents are believed to correspond to the oxidation of H^- ion:

$$H^- \rightarrow H_{ad} + e^- \qquad (2)$$

where H_{ad} is a hydrogen atom adsorbed at the electrode. At all scan rates, the anodic peak potentials, E_{ap}, seem to be independent of scan rates having a constant value, E_{ap} = 0.8 V. For the voltammograms obtained at high scan rates (2.0 and 5.0 V s^{-1}), the ratio of cathodic peak current to anodic peak current, i_{cp}/i_{ap}, is nearly unity considering the actual i_{ap} baseline [19]. These are typical behaviors for a reversible system, in which both reactants and products are soluble [20]. On the other hand, for the voltammograms obtained at lower scan rates, i_{cp}/i_{ap} decreases from unity with decreasing scan rate. The decrease indicates that species of anodically oxidized H^- ion are disappearing from the vicinity of the electrode. It is believed to proceed as H_2 bubble formation since, in an earlier study, the electrolysis product was found to be pure H_2 gas using gas analysis [2]. This shows that H^- ion is first oxidized to H_{ad} then is dissolved to the melt and that H_2 bubble formation finally occurs. It is believed that the dissolution of H_{ad} to the electrolyte proceeds by a reversible process, because the observed reversible behavior cannot be explained assuming an irreversible process at this step. The

reaction is, thus, regarded as a reversible electrochemical reaction followed by a reversible chemical reaction in the first and an irreversible chemical reaction in the second ($E_rC_rC_i$ mechanism). Since a reversible following chemical reaction scarcely affects the result of electrochemical measurements, the $E_rC_rC_i$ mechanism can be regarded as similar to an E_rC_i mechanism.

It is worth noting that a cyclic voltammogram of reversible electrochemical reaction followed by a chemical reaction (E_rC case) may show essentially reversible behavior in certain conditions. This is especially true in the case of small values of λ. λ is a dimensionless kinetic parameter and defined as

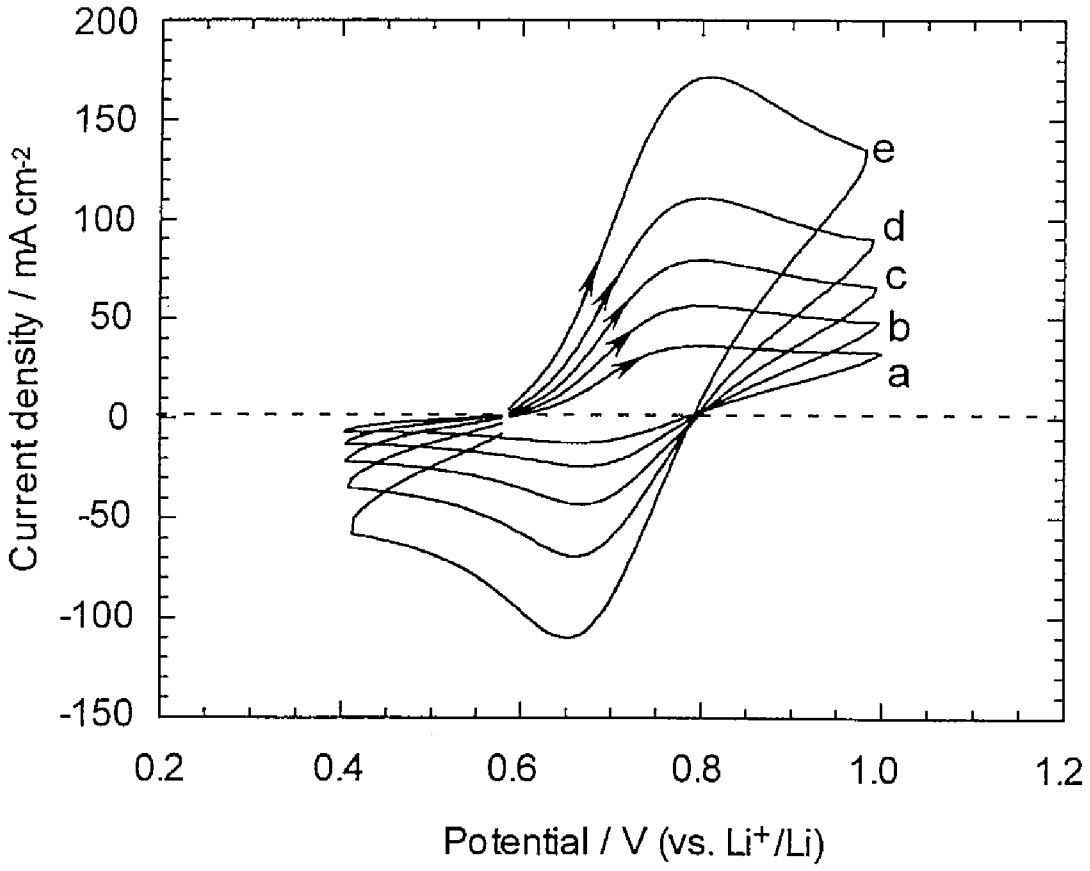

Fig. 2.2. Cyclic voltammograms for a Mo electrode in a molten LiCl-KCl-LiH (0.4 mol% LiH added) system at 673 K. Scan rates: (a) 0.2, (b) 0.5, (c) 1.0, (d) 2.0 and (e) 5.0 V s^{-1}.

$$\lambda = \frac{kRT}{nFv} \tag{3}$$

where k is the rate constant of a following chemical reaction and v is the scan rate [20]. It has been shown that cyclic voltammograms with λ =0.1 and 0.01 are almost identical to reversible behavior except that the height of the reverse wave is slightly small for λ =0.1. This is in agreement with the observed cyclic voltammograms shown in Fig. 2.2. In the case of small λ, it is possible to obtain information concerning the electrochemical reactions treating the system as reversible. Therefore, the observed reversible behavior will be firstly discussed. Then, consideration on the E_rC_i mechanism described above will be discussed in the section of double potential step chronoamperometry since the method provides a more convenient interpretation than cyclic voltammetry.

Here, discussion will be conducted on the voltammogram obtained at 5.0 V s^{-1} which seems to show high reversibility. In the case of reversible system, the following relation holds [18, 21]:

$$\left|E_{ap} - E_{ap/2}\right| = 2.2\frac{RT}{nF} \tag{4}$$

where $E_{ap/2}$ is the anodic half-peak potential, R and T are the gas constant and temperature, respectively, n is the number of electrons and F is Faraday constant. Using equation 4, n is calculated to be 1.1, consistent with reaction 2.

The $E_{ap/2}$ value can also be used to estimate the polarographic half-wave potential, $E_{1/2}$, which for the anodic reaction is given by [19]

$$E_{1/2} = E_{ap/2} + 1.09\frac{RT}{nF} \tag{5}$$

Using equation 5 and the values from Fig. 2.2, the $E_{1/2}$ value was found to be 0.75 V. The $E_{1/2}$ value is in turn related to the formal potential, $E^{0'}$ [20]:

$$E_{1/2} = E^{0'} - \frac{RT}{nF}\ln\frac{D_O^{1/2}}{D_R^{1/2}} \tag{6}$$

where D_O is the diffusion coefficient of the species of anodically oxidized H^- ion and D_R is the H^- ion diffusion coefficient.

To confirm the reversibility of the voltammogram, the convolution technique was applied. The convoluted current, $I(t)$, is calculated by

$$I(t) = \frac{1}{\pi^{1/2}} \int_0^t \frac{j(u)}{(t-u)^{1/2}} du \qquad (7)$$

where $j(t)$ is the observed current at time t [19]. Since the $I(t)$ is extremely sensitive to slight deviation from the ideally reversible shape of the cyclic voltammograms, the convolution technique can be used as a very sensitive test of the reversibility [22]. Figure 2.3 shows a convoluted cyclic voltammogram in which the backward scan curve slightly deviates from the forward scan curve. For a completely reversible reaction, the curves for forward and backward scans superimpose. However, only a slight shift means still high reaction reversibility since quasi-reversible reaction curves do not coincide at all [23].

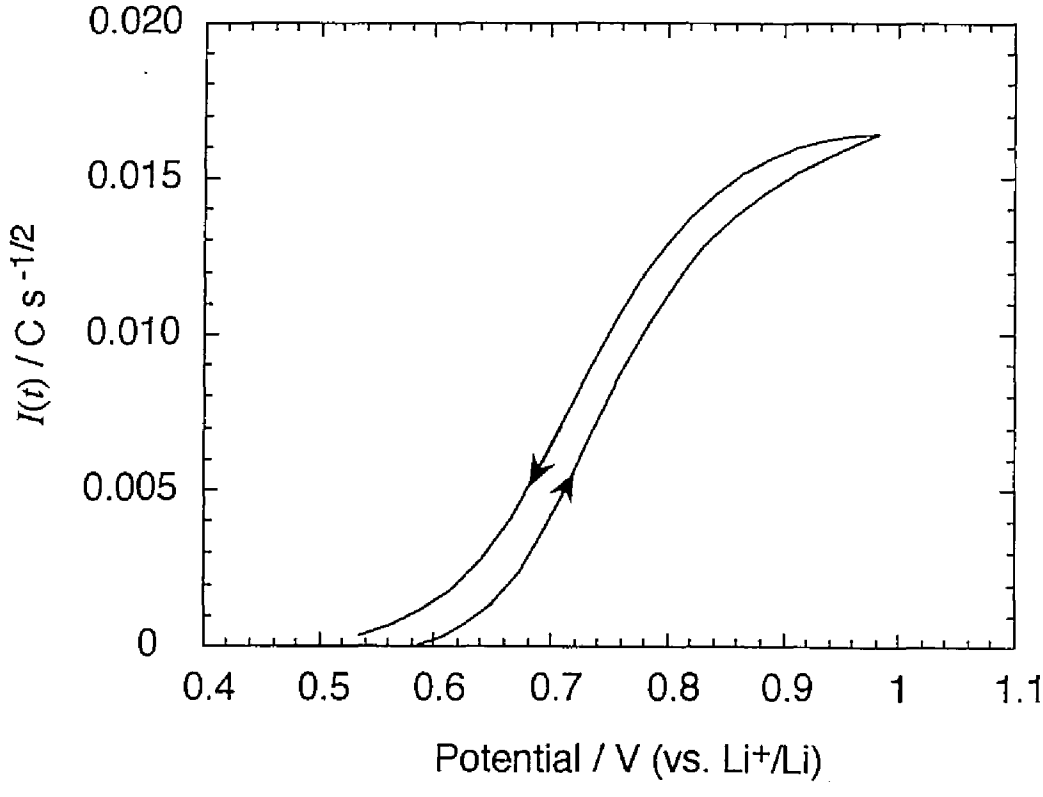

Fig. 2.3. Convoluted cyclic voltammogram for a Mo electrode in a molten LiCl-KCl-LiH (0.4 mol% LiH added) system at 673 K. Scan rate: 5.0 V s^{-1}.

In the case of a reversible wave, the following relation holds [24]:

$$E = E_{1/2} - \frac{RT}{nF} \ln \frac{I_l - I}{I} \qquad (8)$$

where I_l is the limiting value of the convoluted current. Thus, the logarithmic analysis shown in Fig. 2.4 provides direct and precise values of $E_{1/2}$ and RT/nF. The obtained $E_{1/2}$ value is 0.755 V, which is in accord with the $E_{1/2}$ value estimated earlier using equation 5. From the slope of RT/nF the n value is calculated to be 1.05, which also agrees with the n value obtained using equation 4. Moreover, D_R is obtained by the relation [19]:

$$I_l = nFAD_R^{1/2}C_R^* \qquad (9)$$

where A is the electrode area and C_R^* is the bulk concentration of H^- ion. When C_R^* is estiamted to be 0.32 mol% from the reason stated later in the discussion on Fig. 2.6, D_R is estimated as 2.0×10^{-5} cm^2 s^{-1}.

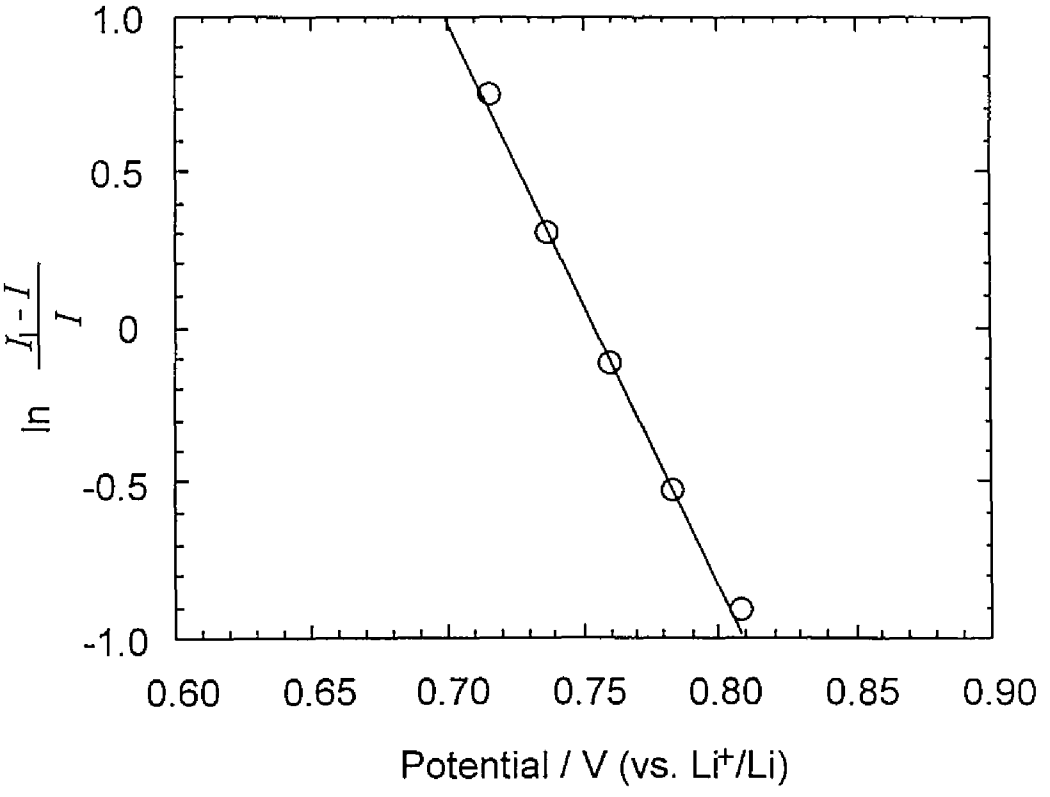

Fig. 2.4. Logarithmic analysis of the convoluted voltammogram for a Mo electrode in a molten LiCl-KCl-LiH (0.4 mol% LiH added) system at 673 K. Scan rate: 5.0 V s^{-1}.

For a reversible wave, the anodic peak current density, i_{ap}, is given by [20]

$$i_{ap} = 0.4463nFC_R^*\left(\frac{nF}{RT}\right)^{1/2} v^{1/2} D_R^{1/2} \qquad (10)$$

Furthermore, equation 10 holds for the E_rC case even in the region where E_{ap} and i_{cp} differ considerably from reversible values [20]. This may be explained by diffusion of H^- ion governing the current. To confirm the validity of equation 10 for the present electrochemical system, cyclic voltammetry was conducted at various scan rates and amounts of added LiH. Figure 2.5 shows the variations of i_{ap} with $v^{1/2}$ for various nominal LiH concentrations. Linear least square fits are shown as solid lines, and i_{ap} seems to be linearly dependent on $v^{1/2}$ for all concentrations, consistent with equation 10.

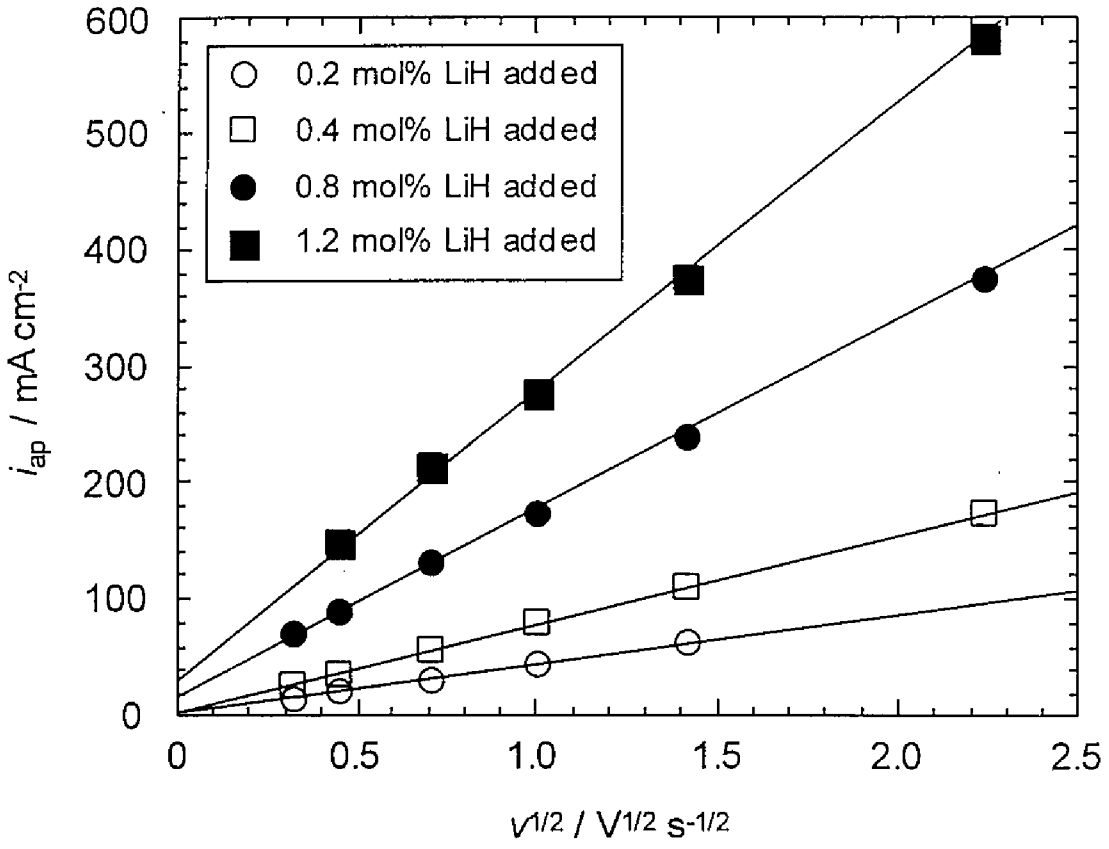

Fig. 2.5. Variation of anodic peak current density with square root of potential scan rate for different concentrations of added LiH.

Figure 2.6 shows that i_{ap} also seems to vary linearly with the amount of added LiH as expected from equation 10. However, the extrapolation to zero current in Fig. 2.6 seems to converge at around 0.08 mol% for all scan rates. This might be explained by 0.08 mol% LiH being consumed by contaminations in the melt such as water and heavy metal ion. Although the reason for the loss of H^- ion is not completely clear, it seems to be reasonable to regard 0.08 mol% as the zero point of the H^- ion bulk concentration. Values of C_R^* can be estimated by subtracting 0.08 mol% from the amount of added LiH. Since the validity of equation 10 was confirmed, the H^- ion diffusion coefficient was estimated as 2.2×10^{-5} cm^2 s^{-1}.

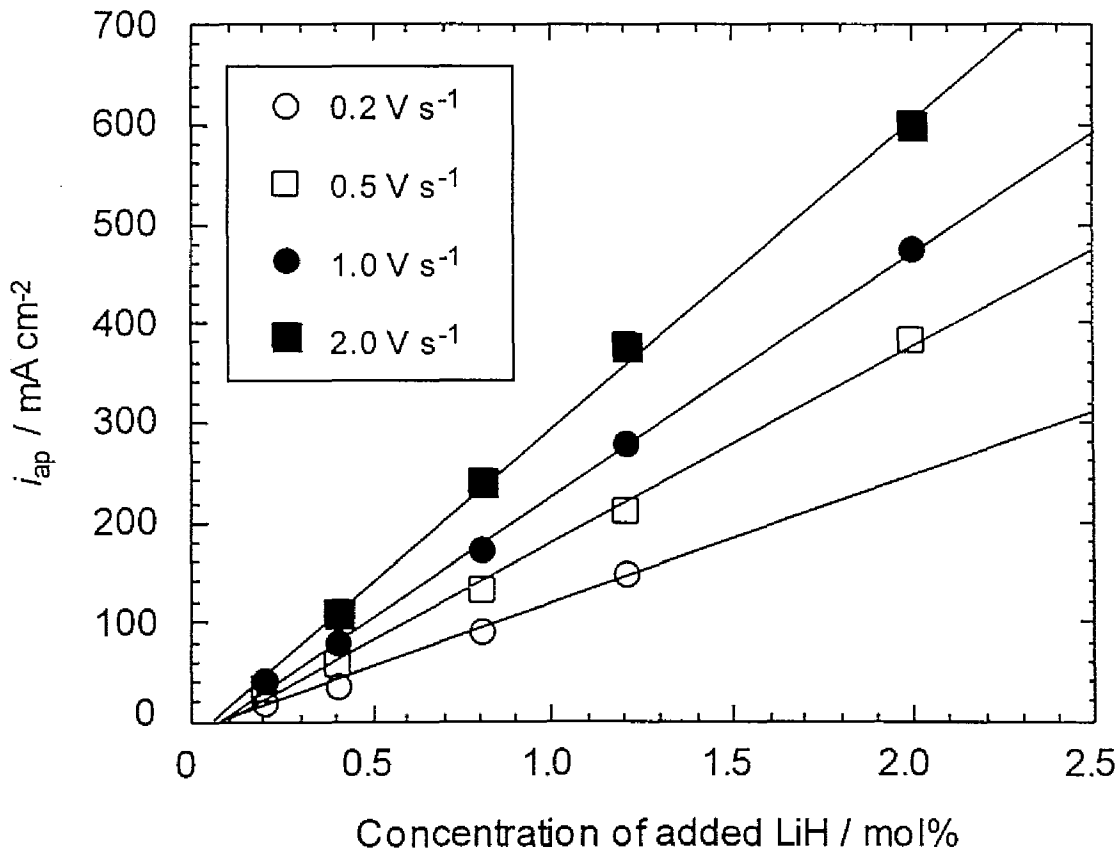

Fig. 2.6. Variation of anodic peak current density with concentration of added LiH for different potential scan rates.

2.3.2 Chronopotentiometry

Chronopotentiometry was conducted to further investigate the anodic reaction of H^- ion. Figure 2.7 shows a typical chronopotentiogram at an applied anodic current density of 250 mA cm^{-2}. Considering the results of cyclic voltammetry, the observed potential plateau is thought to be due to the oxidation of H^- ion. The duration of the potential plateau, the transition time, τ, is the most important parameter in analyzing chronopotentiometric data.

For a reversible system, the following relation is valid [25]:

$$E = E_{\tau/4} - \frac{RT}{nF} \ln \frac{\tau^{1/2} - t^{1/2}}{t^{1/2}} \qquad (11)$$

where $E_{\tau/4}$ is called the quarter-wave potential. The degree of reversibility can, therefore, be

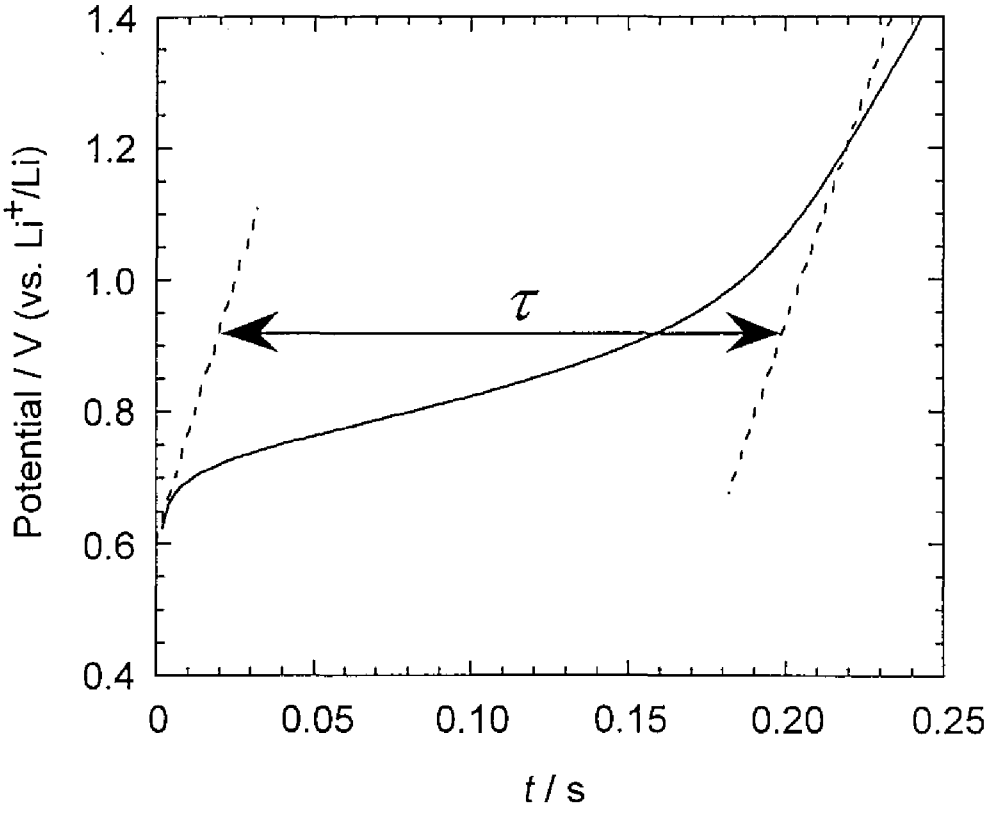

Fig. 2.7. Typical chronopotentiogram for the oxidation of H^- ion in a molten LiCl-KCl-LiH (LiH added 0.4 mol%) system at 673 K. Applied current density: 75 mA cm^{-2}.

checked by plotting the potential against $\ln((\tau^{1/2}-t^{1/2})/t^{1/2})$, as shown in Fig. 2.8. The plot shows a good linear relationship indicating high reversibility. The slope of the plot gives a n value of 0.99, almost equal to the value obtained above using voltammetry. Furthermore, $E_{\tau/4}$ is directly obtained as 0.754 V from the intercept with the potential axis. $E_{\tau/4}$ is related to $E^{0'}$ as [25]

$$E_{\tau/4} = E^{0'} - \frac{RT}{nF}\ln\frac{D_O}{D_R} \qquad (12)$$

Comparing equations 6 and 12, $E_{\tau/4}$ is expected to be close to the voltammetry $E_{1/2}$ value and the obtained $E_{\tau/4}$ is indeed nearly equal to $E_{1/2}$ estimated from the convoluted voltammogram in Fig. 2.4.

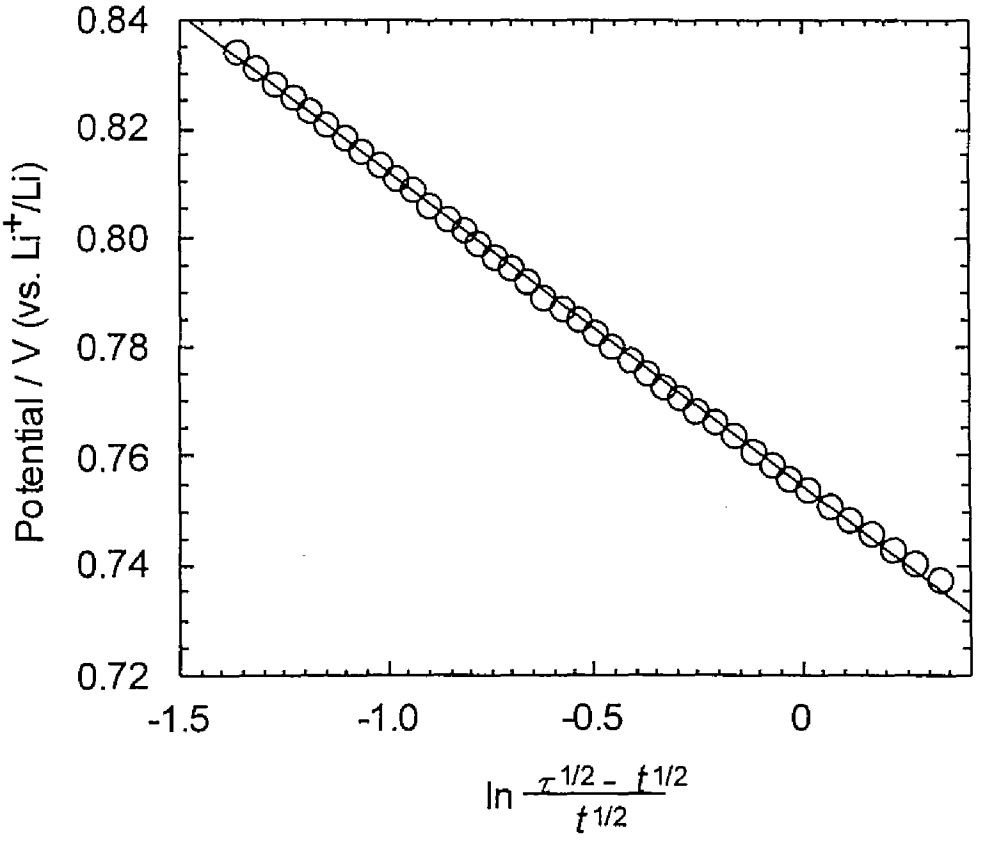

Fig. 2.8. Plot of potential against $\ln(\tau^{1/2}-t^{1/2})/t^{1/2}$ for the chronopotentiogram in a molten LiCl-KCl-LiH (LiH added 0.4 mol%) system at 673 K. Applied current density: 75 mA cm^{-2}.

For a reversible system the Sand equation holds [26]:

$$\frac{i\tau^{1/2}}{C_R^*} = \frac{nFD_R^{1/2}\pi^{1/2}}{2} \qquad (13)$$

where i is the applied current density. To confirm this relation and to estimate the value of D_R, measurements were conducted with varying applied current density and at different concentrations of LiH. Figure 2.9 shows the variation of $\tau^{-1/2}$ with i for different concentrations of added LiH. In the figure there are also shown linear least square fits as solid lines. The linearity seems to be good, thereby verifying the validity of equation 13 for this system.

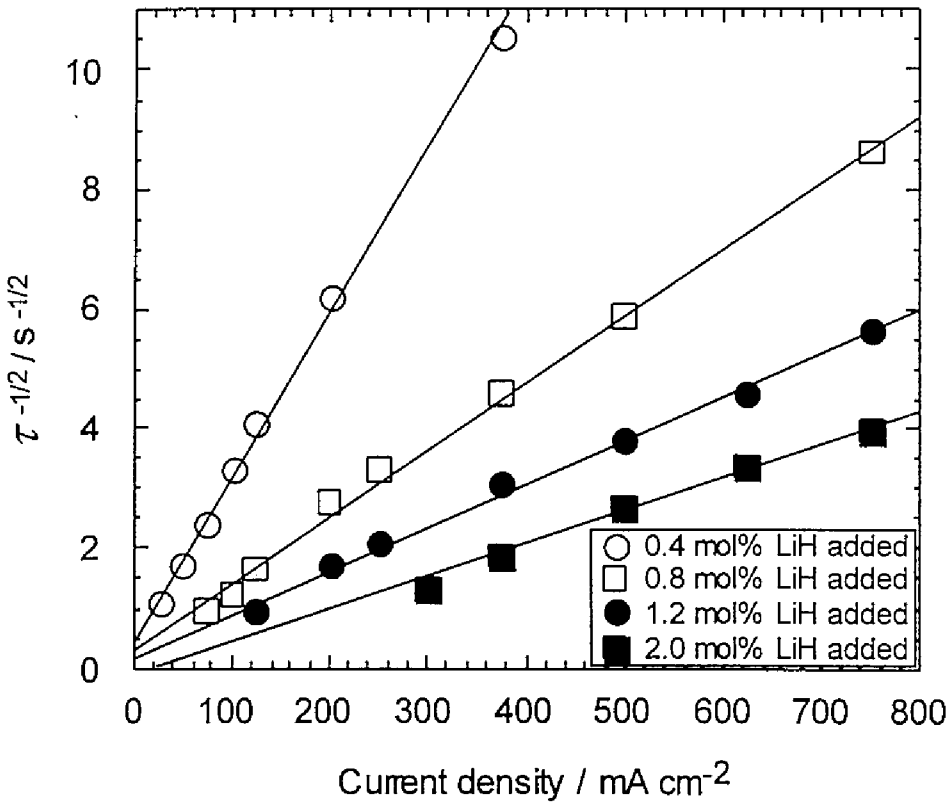

Fig. 2.9. Variation of inverse square root of transient time with applied current density for different concentrations of added LiH.

Figure 2.10 shows the relations between $\tau^{1/2}$ and the amount of added LiH for different applied current densities. Linear relations are again noticed, and the extrapolations to zero current converge again at around 0.08 mol% for all currents, in agreement with the results of the cyclic voltammetry measurements shown in Fig. 2.6. Following a similar path as described in the voltammetry section above, C_R^* was estimated by subtracting 0.08 mol% from the nominal LiH concentrations. Using these data and equation 13, the H^- ion diffusion coefficient was estimated to be 1.7 (± 0.3) x 10^{-5} cm^2 s^{-1}.

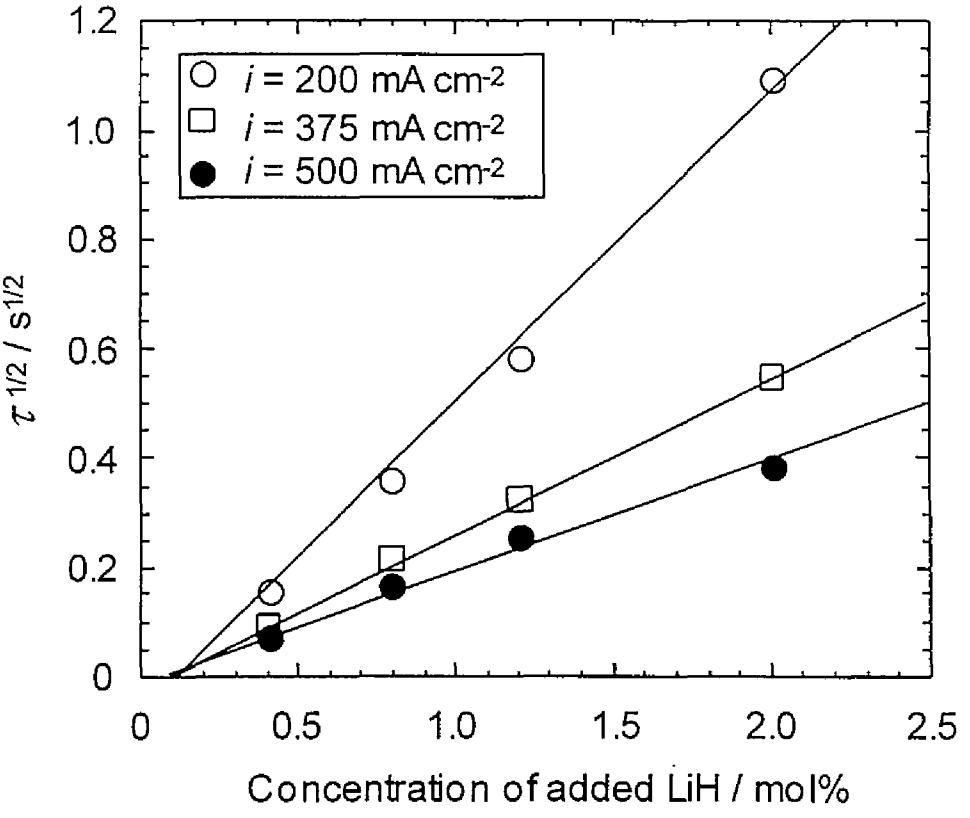

Fig. 2.10. Variation of square root of transient time with concentration of added LiH for different applied current densities.

2.3.3 Double potential step chronoamperometry

Judging from the change of the i_{cp}/i_{ap} ratio with cyclic voltammetry scan rate, the electrode reaction was considered to be an E_rC_i reaction. There are two possible types of reaction schemes following the electron transfer in reaction 2. If a certain amount of molecular hydrogen is soluble, the following scheme is valid:

$$H_{ad} + H_{ad} \rightarrow H_{2,sol} \qquad \text{(Reversible)} \qquad (14)$$

$$H_{2,sol} \rightarrow H_{2,bubble} \qquad \text{(Irreversible)} \qquad (15)$$

where $H_{2,sol}$ is the dissolved hydrogen molecule, and $H_{2,bubble}$ is the hydrogen molecule in a bubble form. Since the irreversible process governs the total behavior and the irreversible process is a bubble formation, hereafter this scheme is referred to as the *irreversible bubble formation scheme*. On the other hand, if hydrogen is soluble in the melt as hydrogen atoms or neutral species consisting of one hydrogen atom, the following scheme is suggested:

$$H_{ad} \rightarrow H_{sol} \qquad \text{(Reversible)} \qquad (16)$$

$$H_{sol} + H_{sol} \rightarrow H_{2,sol} \qquad \text{(Irreversible)} \qquad (17)$$

$$H_{2,sol} \rightarrow H_{2,bubble} \qquad \text{(Reversible or irreversible)} \qquad (18)$$

where H_{sol} is the dissolved hydrogen atom in the melt. In this scheme, a dimerization process is considered as the irreversible process, thus, it is referred to as the *irreversible dimerization scheme*.

Although cyclic voltammetry can be used for studying the E_rC_i reaction, double potential step chronoamperometry is more advantageous [27]. In particular, it is relatively easy to distinguish between first- and second-order chemical reactions. Furthermore, by analyzing the forward step response it is possible to estimate the H^- ion diffusion coefficient.

Figure 2.11 shows a typical current response in double potential step chrono-amperometry measurements. During the forward step, potential was adjusted to E_f, where theconcentration of H^- ion at the electrode surface can be regarded as zero. As a consequence of this setting, the current response during the forward step should be identical to a reversible

case, where the value of the current is determined solely by the diffusion of substance R. In such a case, the current response is given by the Cottrell equation [28]:

$$i = \frac{nFD_R^{1/2}C_R^*}{\pi^{1/2}t^{1/2}} \tag{19}$$

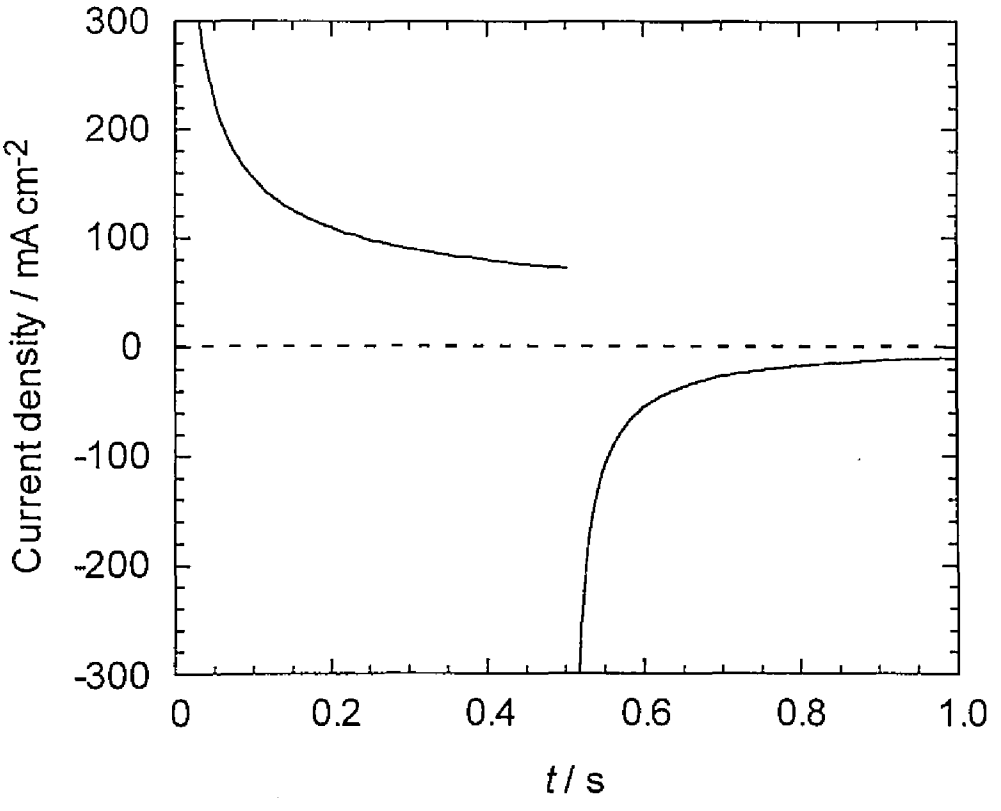

Fig. 2.11. Current response in double potential step chronoamperometry in a molten LiCl-KCl-LiH (LiH added 0.8 mol%) system at 673 K. E_f =1.2 V (vs. Li^+/Li) for 0.5 s and E_r =0.52 V for 0.5 s.

Figure 2.12 shows the plot of i vs. $t^{-1/2}$ during forward step. The near linearity is obtained except the slight deviation in the initial period of the measurement. Although the reason for the slight deviation is not clear, the obtained linearity supports the validity of equation 19. From the slope of the plot, the diffusion coefficient of H^- ion was estimated to be 1.9×10^{-5} $cm^2\ s^{-1}$.

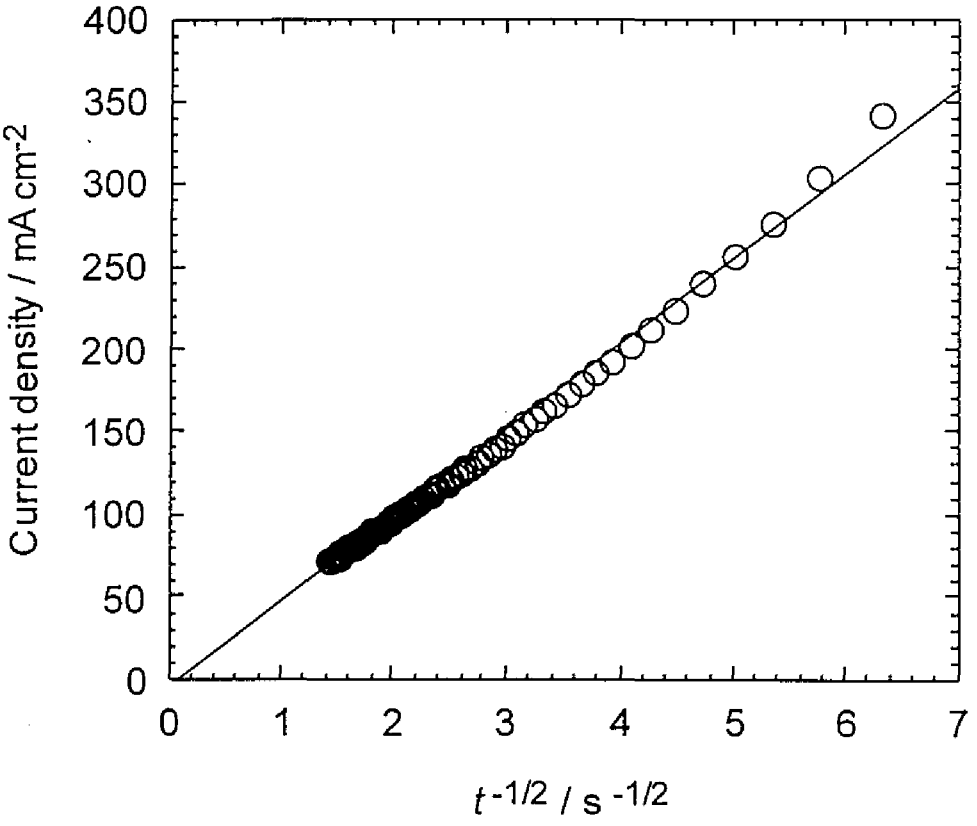

Fig. 2.12. Plot of current density against $t^{-1/2}$ for the chronoamperogram during the forward step in a molten LiCl-KCl-LiH (LiH added 0.8 mol%) system at 673 K. E_f =1.2 V (vs. Li^+/Li).

Irreversible bubble formation scheme

On the other hand, during the reverse step, the potential was changed to E_r where the reverse reaction occurs. The analysis of the cathodic current response was carried out by plotting $-i_r/i_f$ vs. $(t-\tau)/\tau$, where i_f and i_r are current densities during forward and reversal steps, respectively, and τ is forward step duration. This is shown in Fig. 2.13 for different values of τ. For comparison, a theoretical curve for a reversible case with no chemical reaction is also shown in Fig. 2.13, which shows the obvious discrepancy from the experimental data. In order to evaluate the validity of the *irreversible bubble foramtion scheme* (reaction 15), which seems to have a first-order rate constant, theoretical curves for first-order chemical reactions are plotted. Figure 2.13 shows the plots for several values of $k_1\tau$, where k_1 is the first-order rate constant.

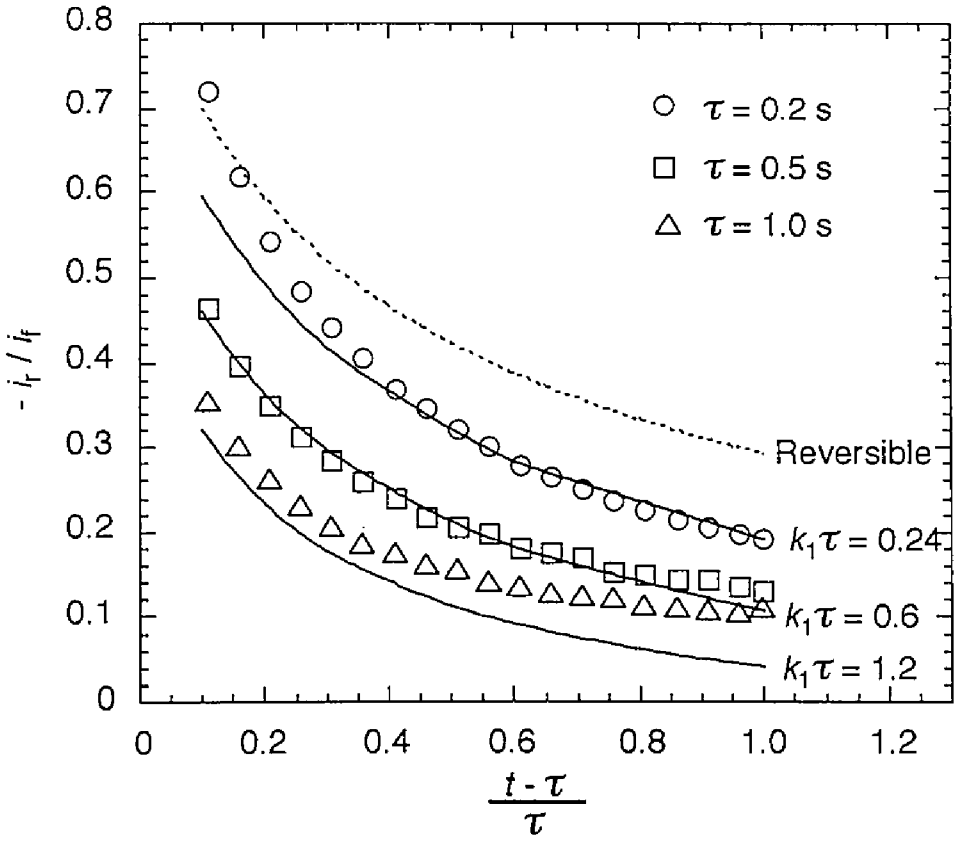

Fig. 2.13. Comparison of experimental data with the theoretical curves for first-order chemical reaction. Experiment: τ are 0.2, 0.5 and 1.0 s. Theory: $k_1\tau$ are 0.24, 0.6 and 1.2.

The $k_1\tau$, is the most important parameter to analyze the first-order chemical reaction in double potential step chronoamperometry. The theoretical curves are from the work by Schwartz and Shain [29]. Among the theoretical curves, the curve for $k_1\tau = 0.24$ was first chosen because it fits relatively well with the experimental data for $\tau = 0.2$ s. Experimental data for $\tau = 0.5$ s are then in good agreement with the theoretically expected curves for $k_1\tau = 0.6$. This indicates that the scheme is correctly describing the experimental data, giving $k_1 = 1.2\ s^{-1}$. However, experimental data for $\tau = 1.0$ s does not coincide with the theoretical curve for $k_1\tau = 1.2$ which is deduced from $k_1 = 1.2\ s^{-1}$. The deviation is particularly large at the end of measurement. Since the absolute value of i_r was as small as 6 mA cm^{-2} at the end of measurement for the $\tau = 1.0$ s case, a small residual current would affect the i_r/i_f ratio. Considering that hydrogen seems to be soluble in the melt, the deviation from the theoretical curve might then be explained by a cathodic current caused by the reduction of hydrogen already present in the melt.

Irreversible dimerization scheme

The *irreversible dimerization scheme* (reaction 17), which thought to have a second-order rate constant, was also examined by plotting the theoretical curves for second-order chemical reactions, as shown in Fig. 2.14. The theoretical curves were constructed from the work by Olmstead and Nicholson [27], and are shown for y_s=0.8 and 2.0, where y_s is the dimensionless forward step duration defined by

$$y_s = k_2 C_R^* \tau \qquad (20)$$

where k_2 is the second-order rate constant. Among the theoretical curves, the curve for y_s=0.8 was first chosen because it fits relatively well with the experimental data for $\tau = 0.2$ s. If the scheme is valid, the experimental data for $\tau = 0.5$ s is expected to agree with the theoretical curve for y_s=2.0. However, the experimental data for $\tau = 0.5$ s does not coincide with the theoretical curve for y_s=2.0. Thus, it is believed that the *irreversible dimerization scheme* is not correctly describing the present situation.

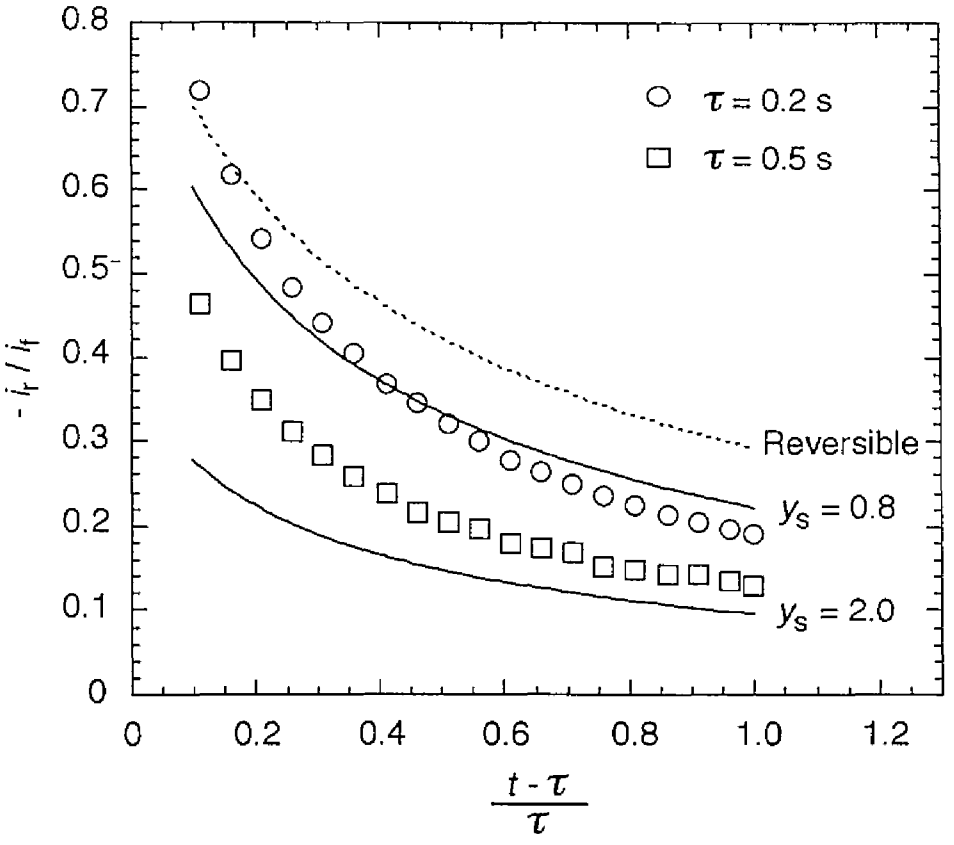

Fig. 2.14. Comparison of experimental data with the theoretical curves for second-order chemical reaction. Experiment: τ are 0.2 and 0.5 s. Theory: y_s are 0.8 and 2.0, where $y_s = k_2 C_R^* \tau$.

Comparing the results for the two proposed chemical reaction schemes, the *irreversible bubble formation scheme* seems to fit the obtained results. The rate constant is, then, estimated to be 1.2 s^{-1}. Since the present work seems to be the first attempt to describe the chemical reaction which follows the electrochemical oxidation of H^- ion, it might be used as a basis for the further investigation of this or similar systems. For a more detailed study of the chemical reaction step it is necessary to determine the amount of hydrogen dissolved in the melt, and then to calculate the theoretical values.

2.3.4 Electrochemical reduction of H_2 gas to H^- ion

Electrochemical reduction of H_2 gas was investigated using a gas electrode. The reaction is thought to form H^- ion in a LiCl-KCl eutectic melt. Figure 2.15 describes the principle of the electrochemical reduction of H_2 gas. The reaction is considered to proceed at so-called the three phase zone among a metal electrode, H_2 gas and electrolyte.

Polarization curves were measured for gas electrodes using Mo or Ni wires in a molten LiCl-KCl-LiH(2.0 mol%) system, as shown in Fig. 2.16. For comparison, polarization curves were measured under flowing only Ar gas. Even in the absence of H_2 gas, small currents were observed for both electrodes. The result suggests that a small amount of neutral H species existed in the melt before H_2 gas introduction. Under flowing only H_2 gas, rest potentials were observed at 0.48 V for both Mo and Ni electrodes. The potential is thought to be the equilibrium potential of H_2/H^- couple at 1 atm H_2 and 2.0 mol% LiH.

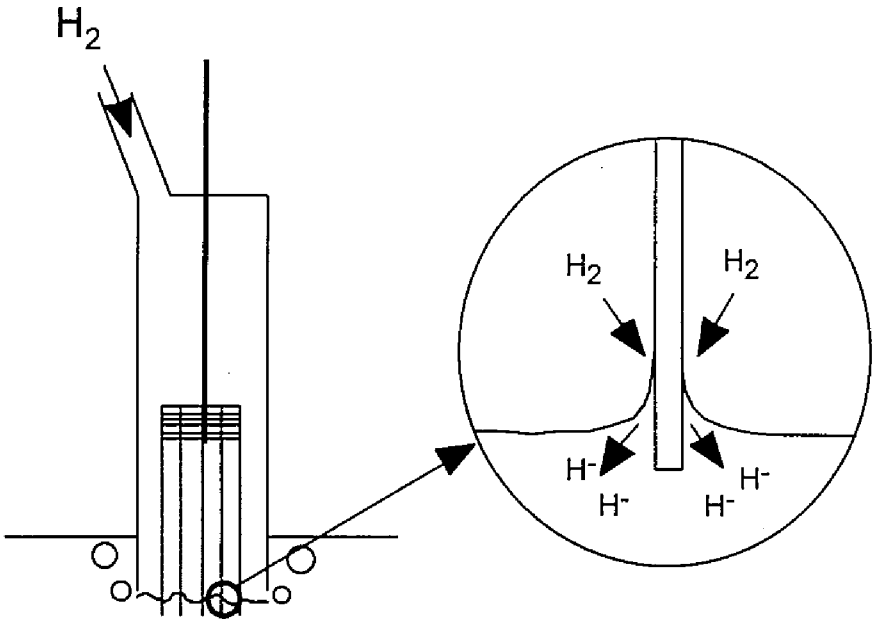

Fig. 2.15. Conceptual explanation for the principle of the electrochemical reduction of H_2 gas using a gas electrode.

Assuming the Nernst relation, the following equation might be obtained for the potential of H_2/H^- couple:

$$E = 0.25 + \frac{RT}{F}\ln\frac{P_{H_2}^{1/2}}{X_{H^-}} \qquad (21)$$

where P_{H_2} is the pressure of H_2 (atm), and X_{H^-} is the anion mole fraction of H^- ion. However, the validity of the relation has not been confirmed yet, and this is interesting future subject.

When the potential values during potentiostatic electrolysis were shifted in negative direction, the cathodic currents increased rapidly till 0.3 V and reached almost constant for both Mo and Ni. These currents are considered to correspond to the electrochemical reduction of H_2 gas. Thus, electrochemical reduction of H_2 gas in a LiCl-KCl eutectic melt is though to be possible by using a gas electrode. The cathodic current densities at 0.3 V are 4 mA cm^{-1} for Ni and 3 mA cm^{-1} for Mo. The results obtained here show that Ni electrode is superior to Mo electrode in cathodic reduction rate of H_2 gas.

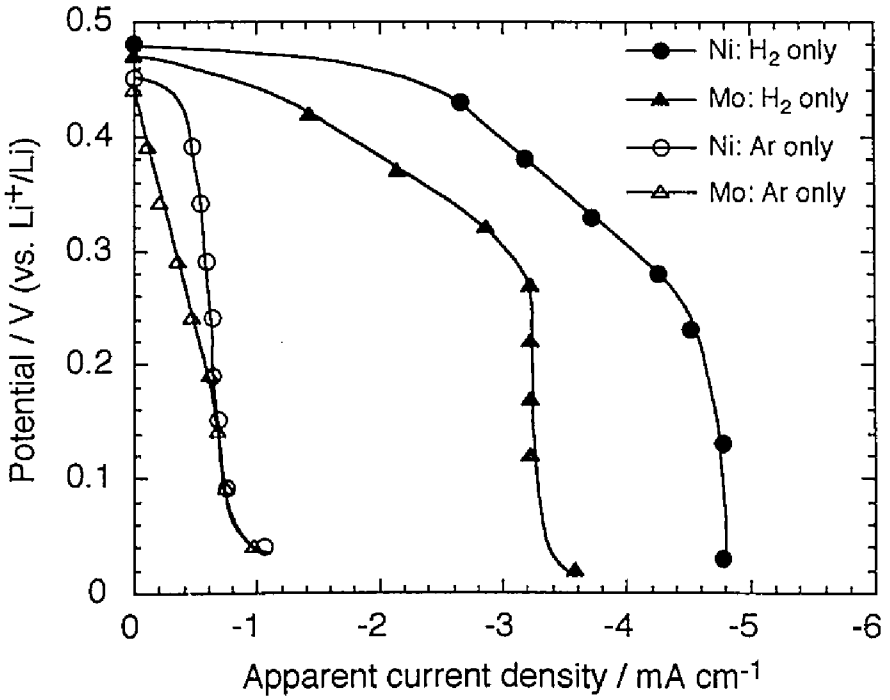

Fig. 2.16. Cathodic polarization curves for gas electrodes using Mo or Ni wires in a molten LiCl-KCl-LiH(2.0 mol%) system at 673 K. Gas flow rate: 10 ml min^{-1}.

2.4 Conclusions

The electrochemical behavior of H^- ion on a Mo electrode in a LiCl-KCl eutectic melt to which LiH was added in concentrations between 0.2 and 2.0 mol% was studied at 673 K by cyclic voltammetry, chronopotentiometry and double potential step chronoamperometry. Using a Mo electrode the hydrogen absorption into the electrode could be neglected, which made possible the investigation of the reverse cathodic reaction without any influence of absorbed hydrogen. Also, electrochemical reduction of H_2 gas was investigated using gas electrodes. The conclusions can be summarized as follows:

(1) Cyclic voltammetry showed that the electrode reaction of H^- ion proceeds by a reversible electrochemical reaction followed by a chemical reaction.

(2) The observed voltammograms showing good reversibility were analyzed by the conventional methods including a convolution technique, which gave $E_{1/2}$ = 0.755 V (vs. Li^+/Li) and $n \sim 1$ for the anodic oxidation of H^- ion.

(3) Chronopotentiometry was also applied to investigate the anodic reaction, and indicated also a reversible behavior with $E_{\tau/4}$ = 0.75 V and $n \sim 1$.

(4) Double potential step chronoamperometry was conducted to study the chemical reaction steps, and the results point to the following reaction scheme

$$H^- \rightarrow H_{ad} + e^- \qquad \text{(Reversible)}$$

$$H_{ad} + H_{ad} \rightarrow H_{2,sol} \qquad \text{(Reversible)}$$

$$H_{2,sol} \rightarrow H_{2,bubble} \qquad \text{(Irreversible)}$$

(5) Diffusion coefficients were estimated by different methods, as summarized in Table 2.1. There seem to be reasonable consistency with values in the range of 1.4-2.2 x 10^{-5} cm^2 s^{-1}. The data obtained in the present study are also compared with literature data, as shown in Table 2.1, and there seem to be good agreement.

(6) Cathodic polarization curves for gas electrodes showed that electrochemical reduction of H_2 gas was possible in a molten LiCl-KCl-LiH(2.0 mol%) system. It was also shown that Ni

was superior to Mo for cathodic reduction of H_2 gas.

Table 2.1. Diffusion coefficients of H^- ion in a LiCl-KCl eutectic melt.

Method	$10^5 D$ $cm^2\ s^{-1}$	Temperature K	Ref.
Convolution method [$I_l = nFAD_R^{1/2}C_R^*$]	2.0	673	This work
Voltammetry [$i_{ap} = f(v^{1/2})$]	2.2	673	This work
Chronopotentiometry [Sand equation]	1.7	673	This work
Chronoamperometry [Cottrel equation]	1.9	673	This work
Chronopotentiometry [Sand equation]	1.67	648	9
Voltammetry [$i_{ap} = f(v^{1/2})$]	3.0	698	2

Nomenclature

A	electrode area (cm^2)
C_R^*	bulk concentration of H^- ion (mol cm^{-3})
D_O	diffusion coefficient of the anodically oxidized species of H^- ion ($cm^2\ s^{-1}$)
D_R	diffusion coefficient of H^- ion ($cm^2\ s^{-1}$)
E	potential (V vs. Li^+/Li)
$E^{0'}$	formal potential (V vs. Li^+/Li)
$E_{1/2}$	polarographic half-wave potential in voltammetry (V vs. Li^+/Li)
E_f	forward step potential in double potential step chronoamperometry (V vs. Li^+/Li)
$E_{ap/2}$	anodic half-peak potential in voltammetry (V vs. Li^+/Li)
E_{ap}	anodic peak potential in voltammetry (V vs. Li^+/Li)
E_r	reverse step potential in double potential step chronoamperometry (V vs. Li^+/Li)

$E_{\tau/4}$	quarter-wave potential in chronopotentiometry (V vs. Li^+/Li)
F	Faraday constant (96487 C mol^{-1})
I	convoluted current in voltammetry (C $s^{1/2}$)
I_l	limiting value of convoluted current in voltammetry (C $s^{1/2}$)
i	current density (A cm^{-2})
i_{ap}	anodic peak current density in voltammetry (A cm^{-2})
i_{cp}	cathodic peak current density in voltammetry (A cm^{-2})
i_f	current density during forward step in double potential step chronoamperometry (A cm^{-2})
i_r	current density during reversal step in double potential step chronoamperometry (A cm^{-2})
j	current (A)
k_1	rate constant for first-order chemical reaction (s^{-1})
k_2	rate constant for second-order chemical reaction (mol^{-1} cm^3 s^{-1})
n	number of electrons
P_{H_2}	pressure of H_2 (atm)
R	gas constant (8.314 J K^{-1} mol^{-1})
t	time (s)
T	temperature (K)
v	scan rate in voltammetry (V s^{-1})
y_s	dimensionless forward step duration in double potential step chronoamperometry for E_rC_i reaction with second-order chemical reaction
X_{H^-}	anion mole fraction of H^- ion
λ	dimensionless kinetic parameter for E_rC_i reaction
τ	(a) transition time in chronopotentiometry (s) (b) forward step duration in double potential step chronoamperometry (s)

References

[1] J. A. Plambeck, in *Encyclopedia of Electrochemistry of the Elements, volume X, Fused Salt Systems*, ed., A. J. Bard, p.16, Marcel Dekker, New York (1976).

[2] T. Takenaka and Y. Ito, *Denki Kagaku* **59,** 759(1991).

[3] B. Y. Liaw, G. Deublein and R. A. Huggins, J. Alloys and Compounds. **189,** 175 (1992).

[4] B. Y. Liaw, G. Deublein and R. A. Huggins, J. Electrochem. Soc. **142,** 2196 (1995).

[5] R. E. Shearer and R. C. Werner, J. Electrochem. Soc. **105,** 693 (1958).

[6] P. Roy, S. A. Salamah, J. Maldonado and R. S. Narkiewicz, AIP Conf. Proc. **271,** 913 (1993).

[7] G. T. Mays, A. N. Smith and J. R. Engel, *ORNL/TM*-5759, (1977).

[8] H. Moriyama, J. Oishi and K. Kawamura, *J. Nucl. Mater.* **161,** 197(1989).

[9] J. A. Plambeck, J. P. Elder and H. A. Laitinen, *J. Electrochem. Soc.* **113,** 931(1966).

[10] T. Takenaka and Y. Ito, *Denki Kagaku* **59,** 796(1991).

[11] E. Fromm, H. Speck, H. Jehn and G. Hörz, in *Physics Data: Gases and Carbon in Metals, Part XIII: Ferrous Metals (1), Iron-Hydrogen,* p. 5 and 11, Fachinformations-zentrum Energie, Physik, Mathematik Gmbh, Karlsruhe (1981).

[12] S. Yamanaka, T. Matsuura and M. Miyake, *Z. Phys. Chem.* **179,** 103(1993).

[13] V. M. Katlinskii, *Inorg. Mater.* **14,** 1299(1978).

[14] K. Amezawa, M. Osugi, Y. Tomii and Y. Ito, *Denki Kagaku* **61,** 736(1993).

[15] R. A. Sharma and R. N. Seefurth, *J. Electrochem. Soc.* **123,** 1763(1976).

[16] C. J. Wen, B. A. Boukamp, R. A. Huggins and W. Weppner, *J. Electrochem. Soc.* **126,** 2258(1979).

[17] T. Takenaka, Y. Ito and J. Ohisi, *Denki Kagaku* **53,** 476(1985).

[18] Y. Takeuchi, K. Mochizuki, M. Watanabe and I. Obinata, *J. Jpn. Inst. Met.* **29,** 801(1966) in Japanese; TR: *Metallwiss. Tech.* **20,** 2(1966) in German.

[19] A. J. Bard and L. R. Faulkner, *Electrochemical Methods: Fundamentals and Applications,* chap. 6, John Wiley & Sons, New York (1980).

[20] R. S. Nicholson and I. Shain, *Anal. Chem.* **36,** 706(1964).

[21] T. Shimada, M. Iizuka and Y. Ito, *Denki Kagaku* **60,** 200(1992).

[22] P. E. Whitson, H. W. Vanden Born and D. H. Evans, *Anal. Chem.* **45,** 1298(1973).

[23] J. M. Savéant and D. Tessier, *J. Electroanal. Chem.* **65,** 57(1975).

[24] J. C. Imbeaux and J. M. Savéant, *J. Electroanal. Chem.* **44,** 169(1973).

[25] Z. Karaoglanoff, *Z. Elektrochem.*, **12,** 5(1906).

[26] A. J. Bard and L. R. Faulkner, *Electrochemical Methods: Fundamentals and Applications,* chap. 7, John Wiley & Sons, New York (1980).

[27] M. L. Olmstead and R. S. Nicholson, *Anal. Chem.*, **41,** 851(1969).

[28] F. G. Cottrell, *Z. Physik. Chem.*, **42,** 385(1902).

[29] W. M. Schwarz and I. Shain, *J. Phys. Chem.*, **69,** 30(1965).

Chapter 3

Electrochemical Formation of Pd-Li Alloys in a LiCl-KCl Eutectic Melt*

3.1 Introduction

Electrochemical formation of Pd-Li alloys in a LiCl-KCl eutectic melt was investigated. Because the data are important basis for studying Pd-H and Pd-Li-H systems in molten LiCl-KCl. Figure 3.1 shows the Pd-Li phase diagram [1]. There are five solid alloy phases (Pd_7Li, Pd_2Li, PdLi, Pd_2Li_3 and $PdLi_2$) and a liquid phase. It is especially important to determine the formation potentials of various Pd-Li alloys.

On the other hand, Pd-Li alloys are interesting materials for their electrocatalytic properties, magnetic properties, etc. [1]. These properties are considered to depend significantly on the compositions of these alloys. However, by metallurgical methods for producing these alloys, it is rather difficult to control their compositions. This disadvantage will be overcome by applying electrochemical formation methods. For example, when a palladium electrode is cathodically polarized in a LiCl-KCl eutectic melt, the electrochemical formation of Pd-Li alloys occurs, whose composition are determined by the applied potentials. To control the compositions of these alloys, it is necessary to determine the relationship between applied potentials and phases of Pd-Li alloys formed.

Furthermore, palladium-rare earth alloys are also promising materials for their superconductivity, magnetic properties and hydrogen diffusion properties [2]. In particular, the last property of these alloys is excellent, so that they are expected to find uses as new

---

* Published in *J. Appl. Electrochem.* **25,** 48(1995).

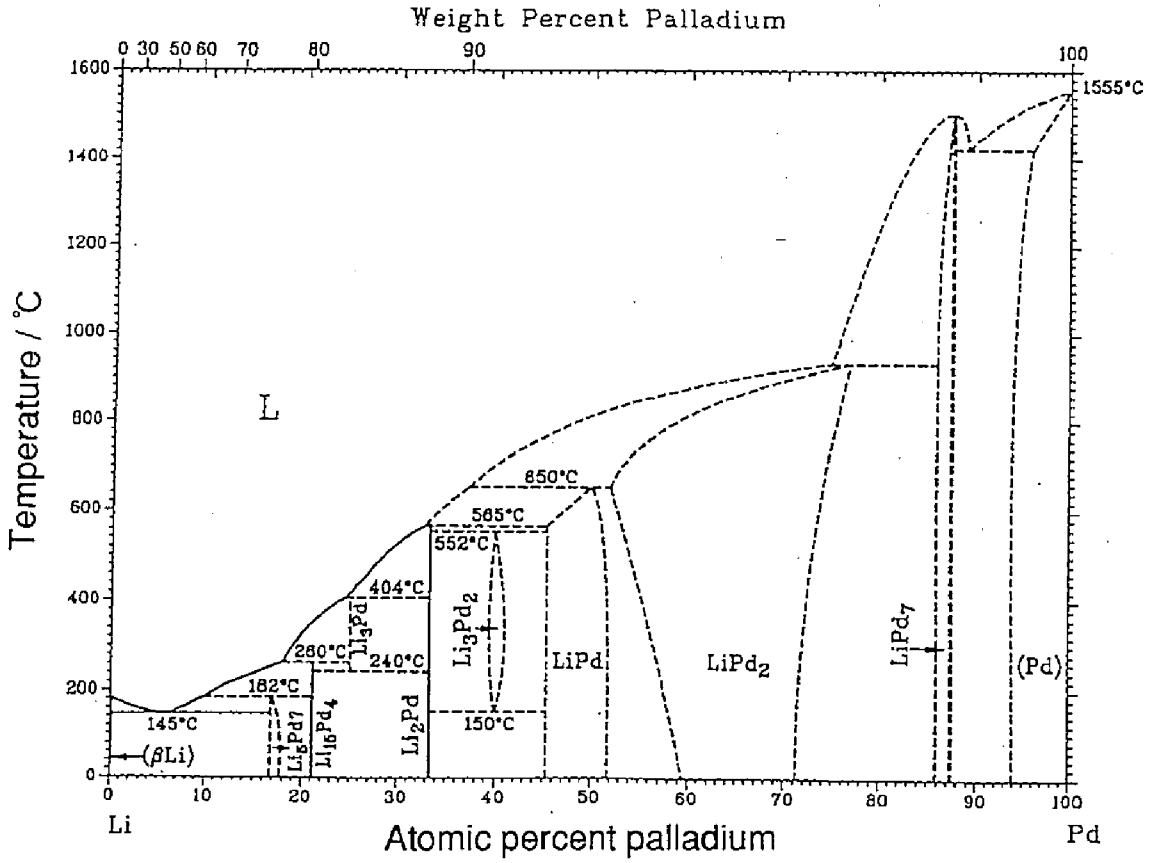

Fig. 3.1. Phase diagram of the Pd-Li system [1].

hydrogen diffusion membranes [3]. For example, a Pd-8%Y alloy has been shown to have improved permeability over the Pd-25%Ag alloy which is currently in use as a conventional hydrogen diffusion membrane [4]. One of the most useful techniques for the formation of palladium-rare earth alloys, electrochemical process using alkali halide solvents such as a molten LiCl-KCl system, will be possible when the method of electrochemical formation of Ni-Y intermetallic compounds in the molten LiCl-KCl system recently proposed by Xie et al. [5] is applied. The advantages of such an electrochemical process are low working temperature and high purity of produced alloys. However, electrochemical formation of lithium alloy is supposed to occur at a considerably more positive potential compared with

that of pure alkali metal deposition. Therefore, the electrochemical window of the solvent electrolyte may become narrow. When a palladium electrode is used in the molten LiCl-KCl system, the electrochemical formation of Pd-Li alloy is supposed to occur as mentioned above. Thus, to control the electrochemical formation of palladium-rare earth alloys, it is also important to determine previously the formation potentials of various Pd-Li alloys.

However, to date there have been no reports concerning the electrochemical formation of a Pd-Li alloy in a molten salt system.

From this background, the aim of the study presented in this chapter was to investigate the electrochemical formation reaction of Pd-Li alloys in a LiCl-KCl eutectic melt and to determine the formation potentials of various Pd-Li alloy phases.

3.2 Experimental

A schematic representation of the experimental apparatus used is shown in Fig. 3.2. The experiments were conducted in a LiCl-KCl eutectic melt at 723 K. All chemicals were reagent grade (Wako Pure Chemical Co.,Ltd.). Materials were contained in a high purity alumina crucible (99.5% Al_2O_3; Nippon Kagaku Togyo Co., Ltd., SSA-S), and were dried under vacuum for more than 72 h at 473 K to remove water. The eutectic mixture was then melted under a dry argon atmosphere at 723 K. To remove residual water contamination further, pre-electrolysis was carried out with the terminal voltage of 2.5 V, using a platinum wire cathode and a glassy carbon rod anode. When the cathodic current density became less than 0.5 mA cm^{-2}, pre-electrolysis was terminated. A Chromel-Alumel thermocouple was used for temperature measurement.

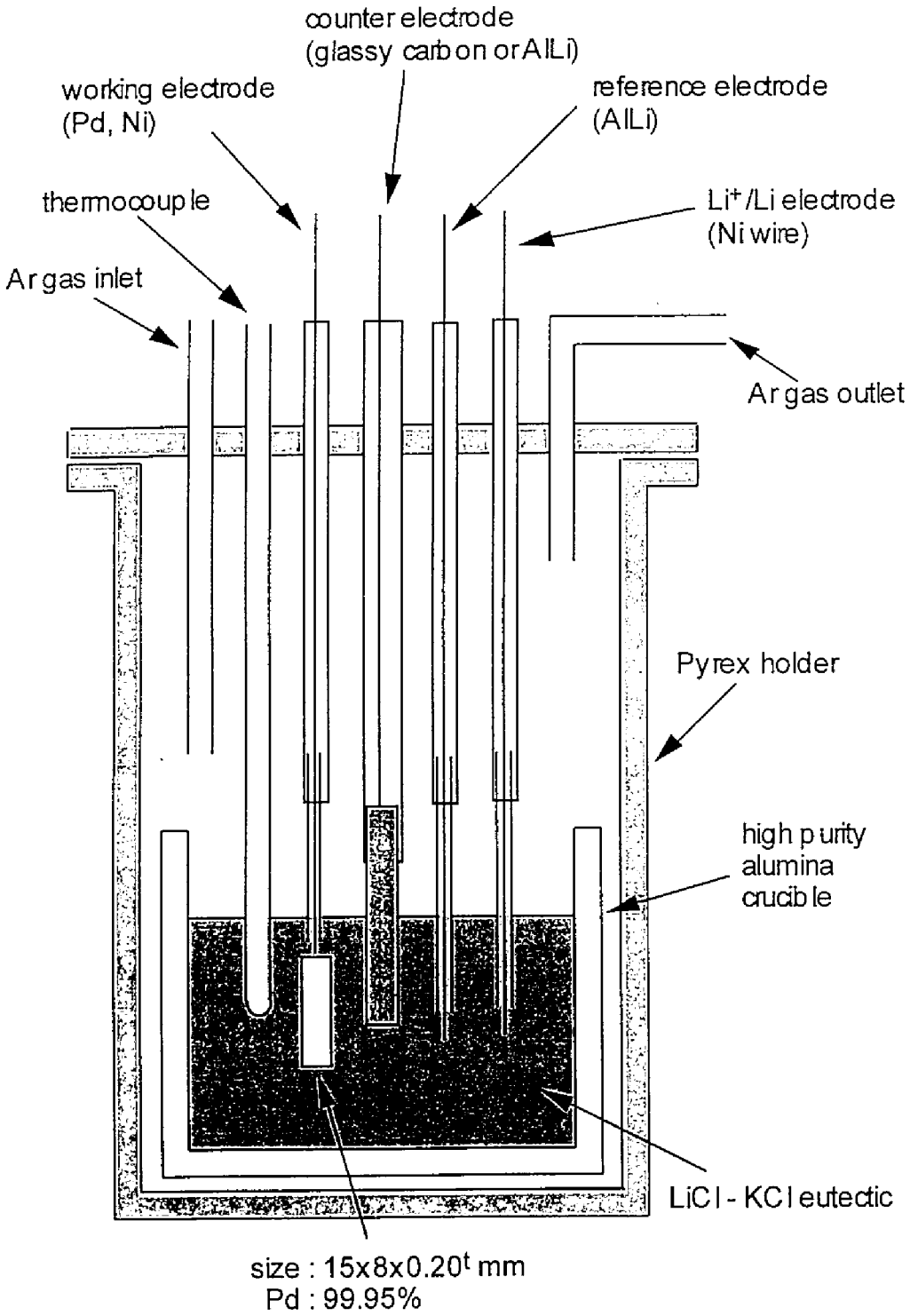

Fig. 3.2. Schematic drawing of the experimental apparatus.

Figure 3.3 shows a schematic drawing of electrodes. The working electrodes were rectangular-shaped sheets of palladium (15 mm x 8 mm x 0.05 mm, The Nilaco Corporation, 99.95%) or nickel (15 mm x 8 mm x 0.2 mm, The Nilaco Corporation, 99.95%). Pd wire (5 mm x ϕ1 mm, The Nilaco Corporation, 99.95%) was also used as the working electrode. The reference electrode was the Al-Li alloy in the coexisting (α+β) phase state, see chapter 2. The potential of this reference electrode was calibrated with reference to that of Li^+/Li electrode by the same method described in chapter 2. The counter electrodes were the Al-Li alloy in the coexisting (α+β) phase state for cyclic voltammetry and glassy carbon for galvanostatic and potentiostatic electrolysis. The Al-Li alloy used as reference and counter electrodes were prepared electrochemically from an aluminum rod (70 mm x ϕ5 mm, The Nilaco Corporation, 99.99%) in another cell.

Cyclic voltammetry and open-circuit potentiometry were applied to investigate the electrochemical behavior of palladium electrode.

Pd-Li alloy samples were prepared by potentiostatic electrolysis at 0.95 V, 0.70 V, 0.56 V, 0.30 V and 0.08 V (samples 1-5, respectively), with charging times between 11.5 hours and 23 hours. After electrolysis, the samples which were formed in the positive potential region (samples 1-3) were taken out from the bath and washed with acetone. Their XRD patterns were then measured by a diffractometer. CuKα (1.5418 Å) line was used as an X-ray source. Because samples which were formed in the negative potential region (samples 4 and 5) reacted easily with air, they were sealed with argon gas immediately after being removed from the bath. They were then ground into powder and sealed in capillaries in argon glove box, and their XRD powder data were measured by the Debye-Scherrer method. All XRD data were compared with those calculated based on the reported structure and lattice constants of each Pd-Li intermetallic compound [1].

(1) Working electrode

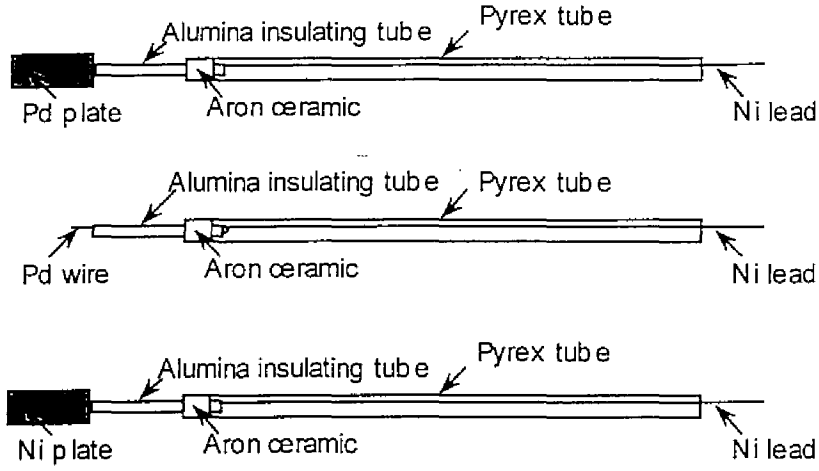

(2) Counter electrode

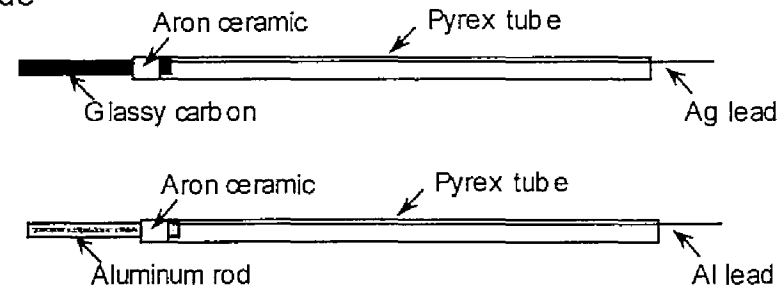

(3) Li^+/Li electrode

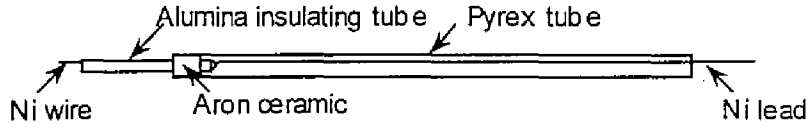

(4) Reference electrode (AlLi)

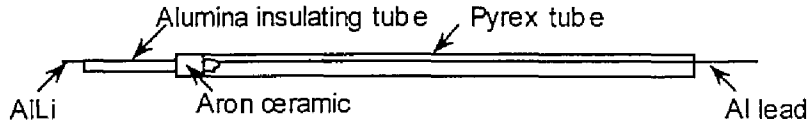

Fig. 3.3. Schematic drawing of electrodes.

3.3 Results and discussion

3.3.1 Cyclic voltammetry

Figure 3.4 shows a typical cyclic voltammogram of the palladium electrode at 723 K (reversal potential = 0.15 V; scanning rate = 1 mV s^{-1}). On the cathodic sweep, current began to flow at about 0.97 V, and there were five cathodic peaks (shoulders) where the current increased sharply at 0.97 V, 0.87 V, 0.62 V, 0.49 V and 0.19 V (peaks 1-5).

To investigate the peaks observed in the negative potential region, the reversal potential was changed to 0 V and the scan rate was lowered to 0.1 mV s^{-1}. The results are shown in Fig. 3.5. In this voltammogram, a sixth cathodic peak (peak 6) was observed, at which the current increased sharply at 0.06 V.

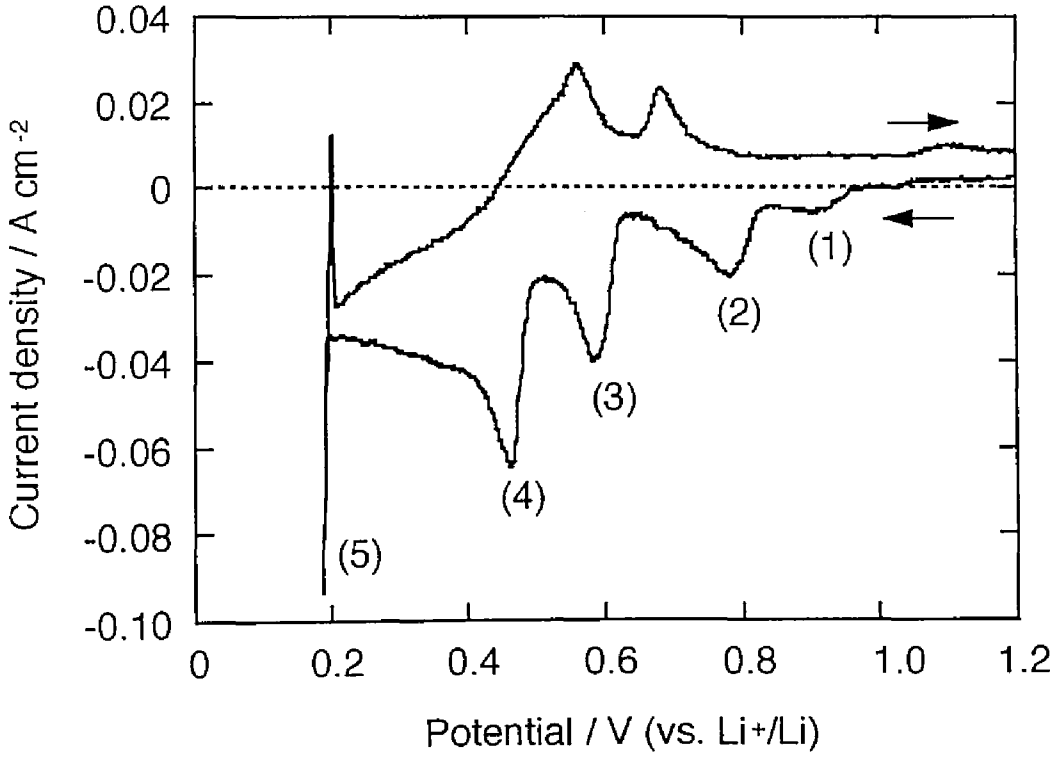

Fig. 3.4. Cyclic voltammogram of Pd electrode in a LiCl-KCl eutectic melt at 723 K. Reversal potential: 0.15 V, Scan rate: 1 mV s^{-1}.

For comparison, the cyclic voltammogram of the nickel electrode at 723 K is also shown as a dotted curve in Fig. 3.5. Because no alloys or intermetallic compounds can be formed between nickel and lithium at 723 K [6], only the peak of lithium deposition was observed.

According to the Pd-Li phase diagram [1] shown in Fig. 3.1, there were several intermetallic compounds and a liquid phase at 723 K. The above six cathodic peaks (peaks 1-6) in Figs. 3.4 and 3.5 were considered to be associated with the formation reaction of each Pd-Li alloy.

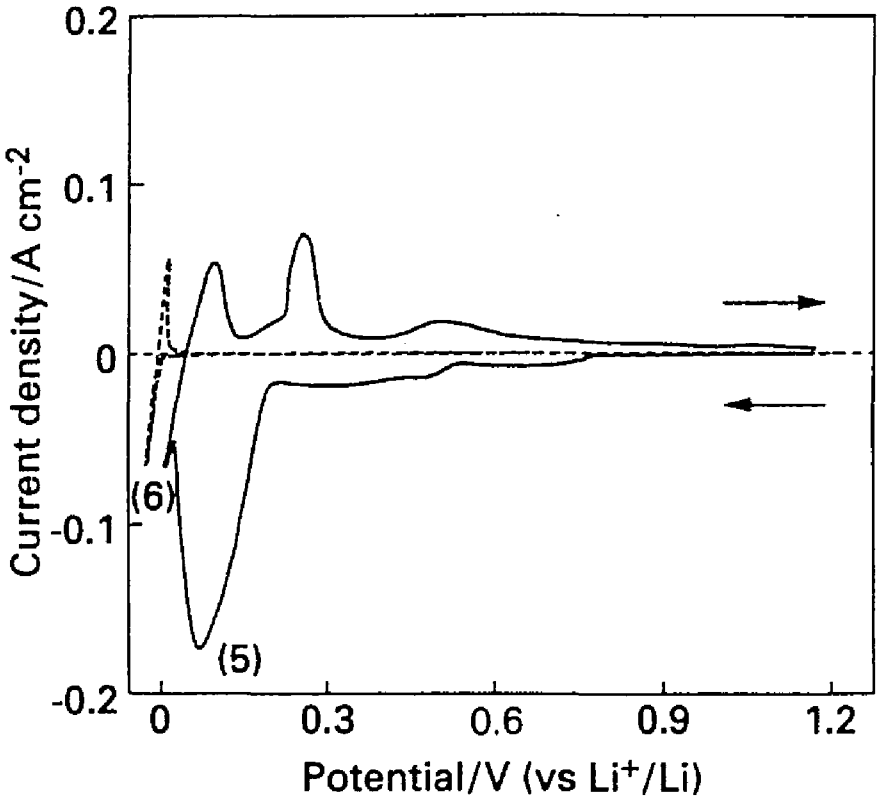

Fig. 3.5. Cyclic voltammograms of Pd (solid curve) and Ni (dotted curve) electrodes in a LiCl-KCl eutectic melt at 723 K. Reversal potential: 0 V, Scan rate: 0.1 mV s^{-1}.

3.3.2 Chronopotentiometry

Chronopotentiometry was also carried out to investigate the Pd-Li alloy formation. Figure 3.7 shows the chronopotentiogram obtained by galvanostatic cathodic electrolysis at 5 mA cm^{-2}. A small potential stagnation is observed at around 0.62 V, which is considered to correspond to peak 3 in the voltammogram. There are potential plateaus (plateaus 4-6) at around 0.49, 0.19 and 0.06 V, respectively. These potential values almost coincide with the raising potentials for peaks 4-6 in the voltammograms, respectively. However, potential plateaus have not been observed in the potential region where peaks 1-2 appeared in the voltammograms. This means the slow formation rate for the Pd-Li alloy in dilute lithium region.

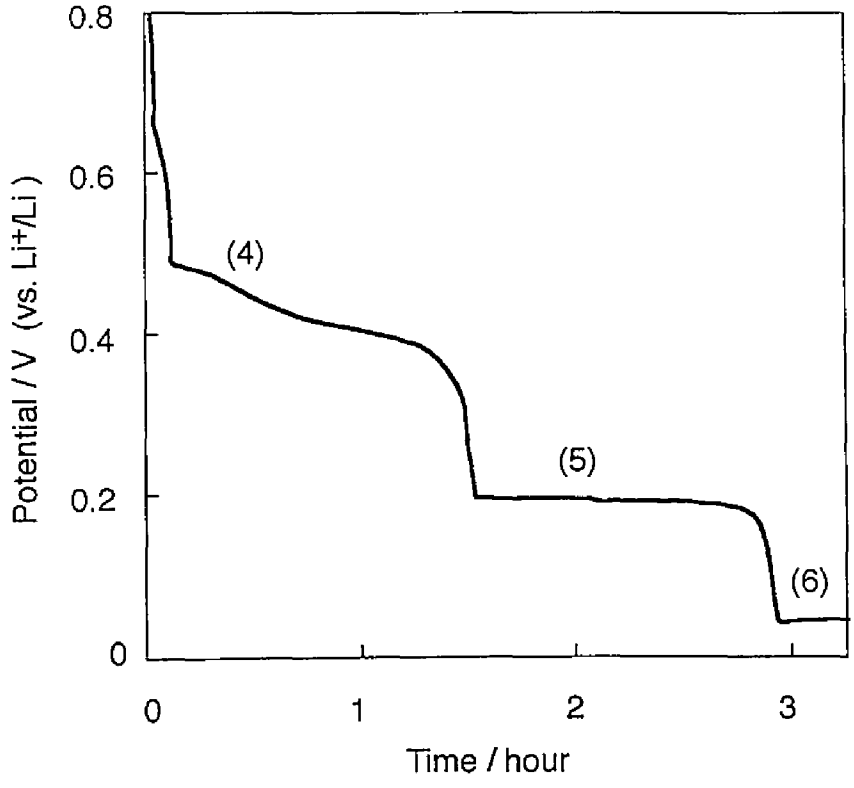

Fig. 3.6. Potential transient curve of Pd electrode in a LiCl-KCl eutectic melt at 723 K. Current density: 5 mA cm^{-2}.

3.3.3 Open-circuit potentiometry

Open-circuit potentiometry was carried out to investigate the electrochemical behavior of the palladium electrode at 723 K. After galvanostatic electrolysis for 30 s at an electrolysis current density of 1 A cm^{-2}, the current was interrupted, and the open-circuit potential transient curve of the palladium electrode was measured. Figure 3.7 shows the results. There were five potential plateaus (plateaus 1-5) at about 0.20 V, 0.53 V, 0.64 V, 0.91 V and 1.05 V, respectively. These five plateaus corresponded to the five cathodic peaks (peaks 1-5) shown in Fig. 3.4, respectively, each of which were considered to correspond to each coexisting phase state of the solid Pd-Li alloy.

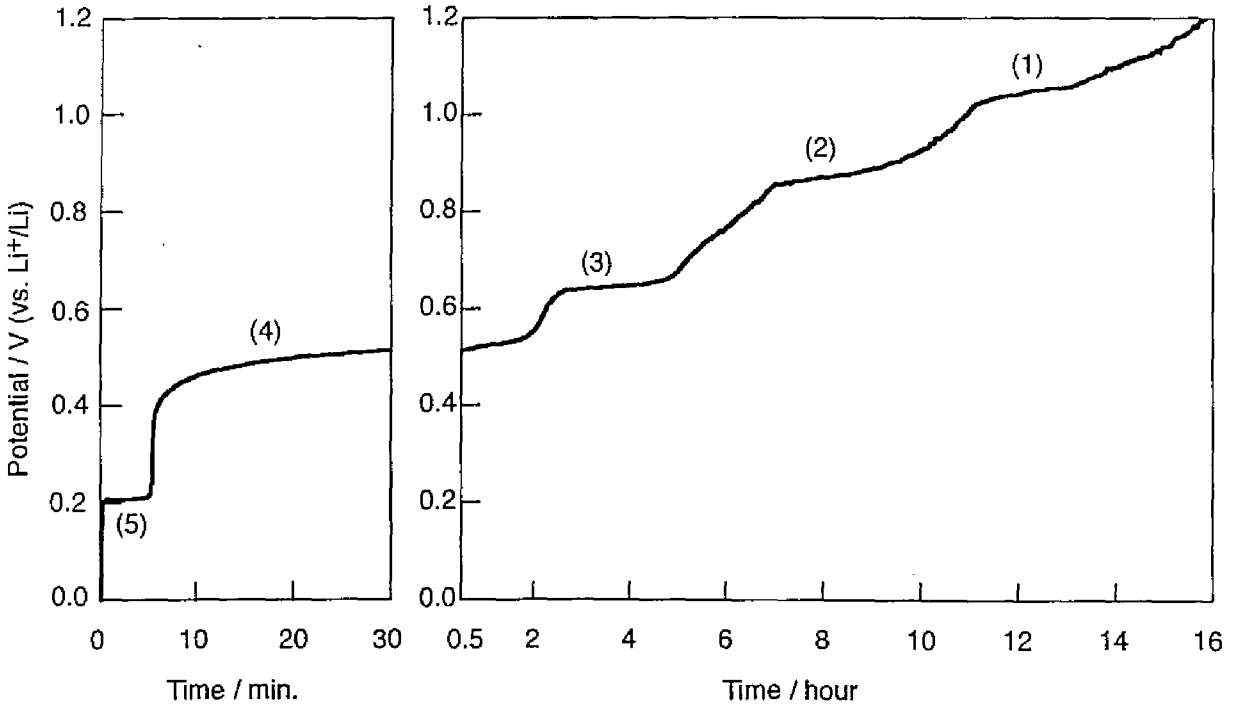

Fig. 3.7. Open-circuit potential transient curve of Pd electrode in a LiCl-KCl eutectic melt at 723 K, after galvanostatic electrolysis for 30 s at a current density of 1 A cm^{-2}.

3.3.4 Characterization of electrochemically formed Pd-Li alloys, and reaction formulas

Based on the results obtained by cyclic voltammetry and open-circuit potentiometry, potentiostatic electrolysis was conducted to form Pd-Li alloy samples with electrolysis potentials of 0.95 V, 0.70 V, 0.56 V, 0.30 V and 0.08 V, respectively (samples 1-5).

From the XRD pattern shown in Fig. 3.8, sample 1 (electrolyzed at 0.95 V) was identified as Pd_7Li. The XRD pattern of substrate Pd metal is also shown in Fig. 3.8. This result indicates that potential plateau 1 (1.05 V) shown in Fig. 3.7 corresponds to the following reaction:

$$7\,Pd + Li^+ + e^- \rightleftharpoons Pd_7Li \qquad (1)$$

A cross-section SEM image of sample 1 is shown in Fig. 3.9, in which it can be seen that surface alloy layer with 1 μm thickness was formed on the substrate Pd metal.

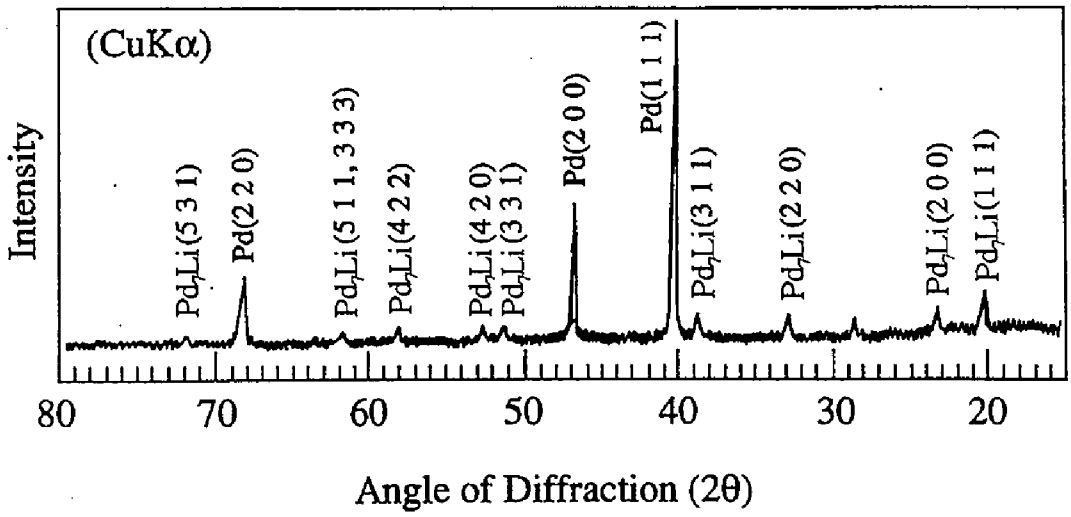

Fig. 3.8. XRD pattern of sample 1 prepared at 0.95 V for 21 h at 723 K. Pd_7Li: cubic unit cell with a=7.660 Å.

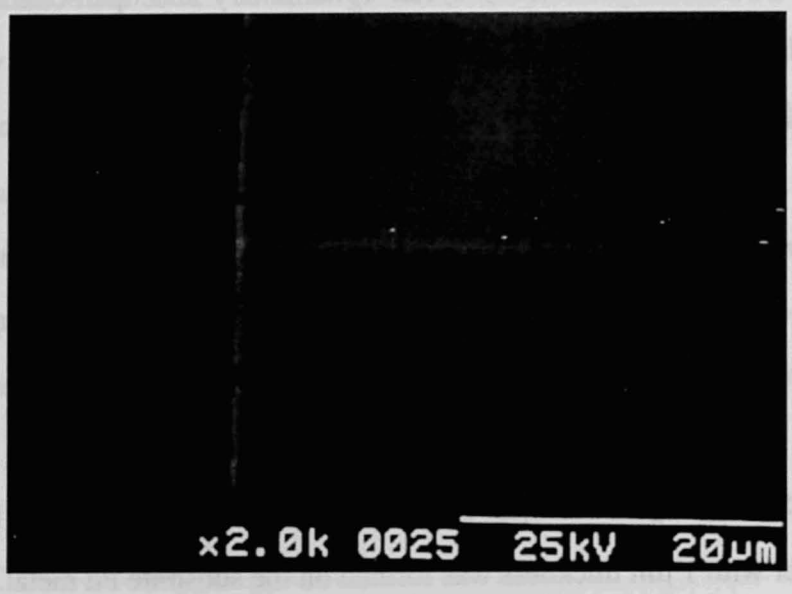

Fig. 3.9. Cross-section SEM image of sample 1 prepared at 0.95 V for 21 h at 723 K.

The XRD pattern shown in Fig. 3.10 identifies sample 2 (electrolyzed at 0.70 V) also as Pd_7Li and substrate Pd metal. This result suggests that potential plateau 2 (0.91 V) corresponds to the formation of a new metastable phase which has not been reported previously. A cross-section SEM image of sample 2 is shown in Fig. 3.11. The thickness of surface alloy layer is about 2-3 μm, showing faster growth than sample 1.

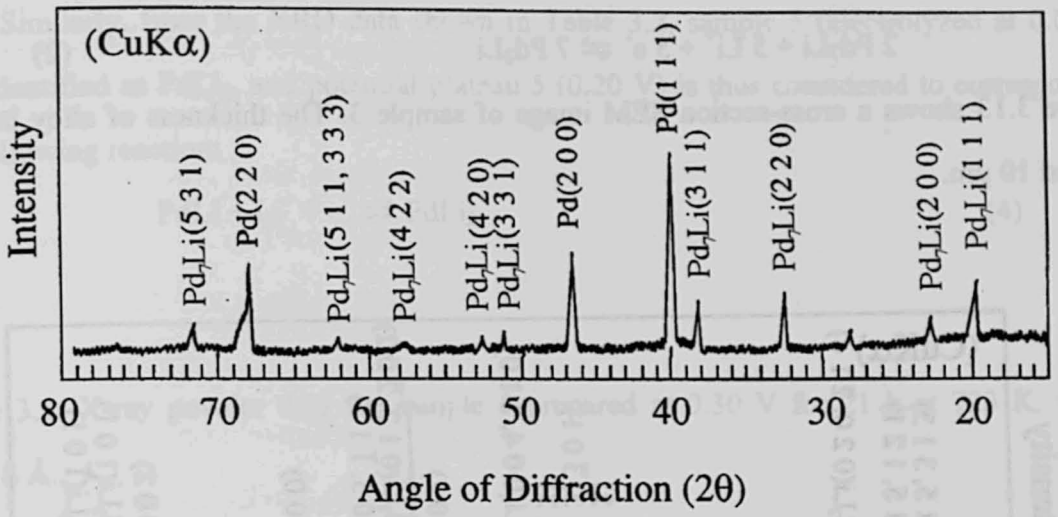

Fig. 3.10. XRD pattern of sample 2 prepared at 0.70 V for 23 h at 723 K. Pd_7Li: cubic unit cell with a=7.660 Å.

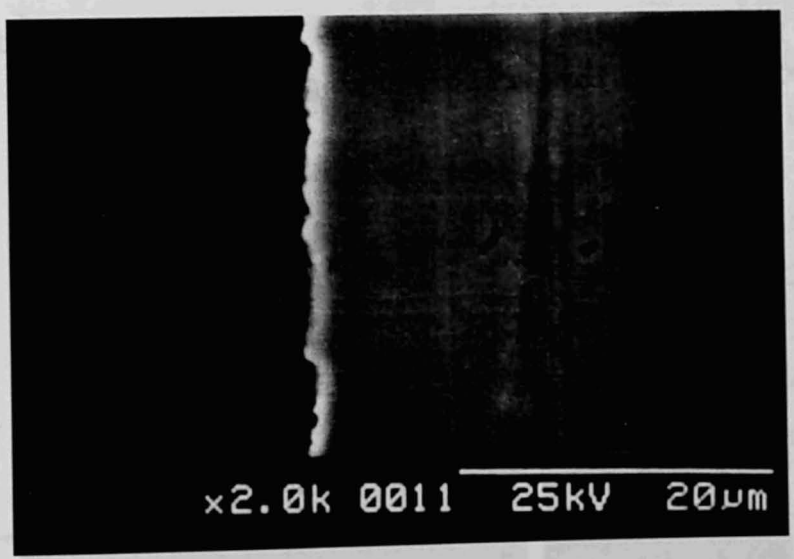

Fig. 3.11. Cross-section SEM image of sample 2 prepared at 0.70 V for 23 h at 723 K.

From the XRD pattern shown in Fig. 3.12, sample 3 (electrolyzed at 0.56 V) was identified as Pd_2Li. Potential plateau 3 (0.64 V) is then considered to represent the following reaction:

$$2\ Pd_7Li + 5\ Li^+ + 5\ e^- \rightleftharpoons 7\ Pd_2Li \qquad (2)$$

Figure 3.13 shows a cross-section SEM image of sample 3. The thickness of alloy layer is around 10 μm.

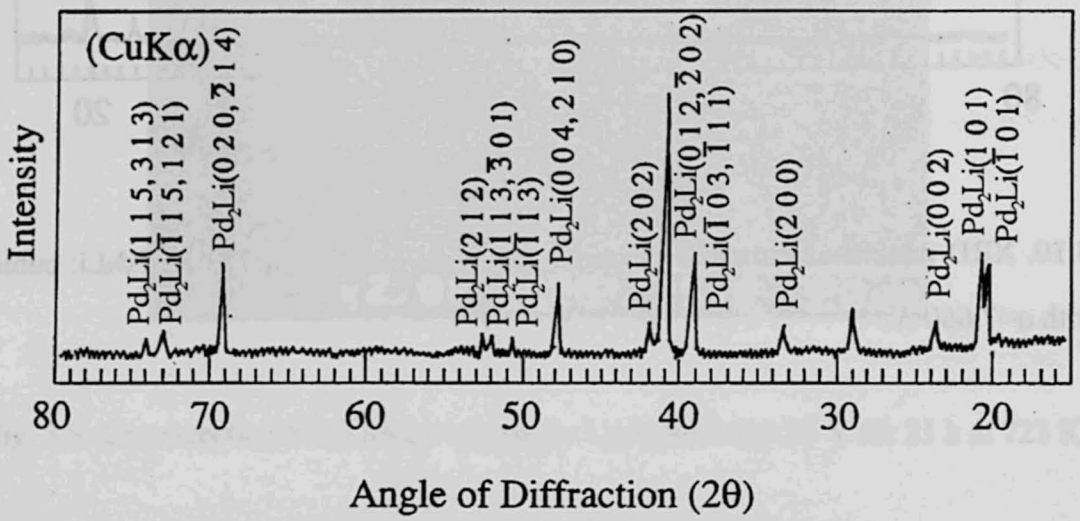

Fig. 3.12. XRD pattern of sample 3 prepared at 0.56 V for 12 h at 723 K. Pd_2Li: monoclinic unit cell with a=5.371 Å, b=2.725 Å, c=7.658 Å and β=91.09°.

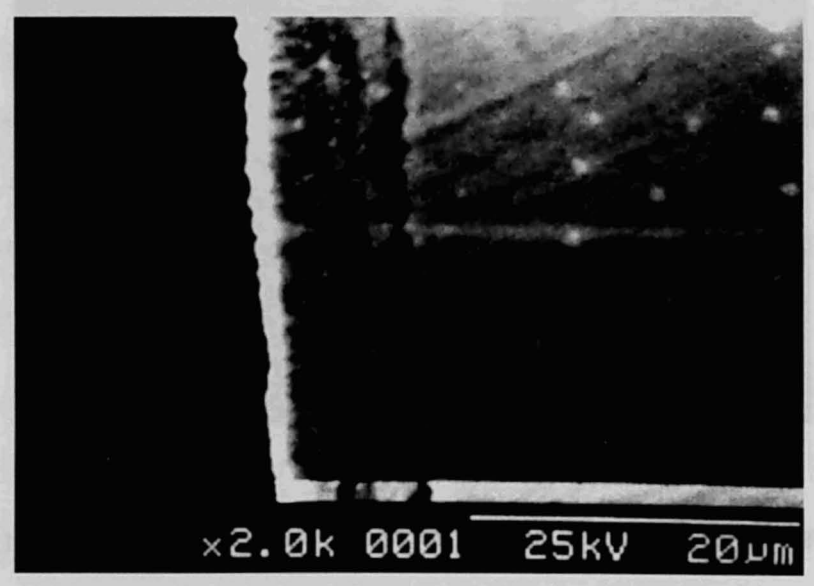

Fig. 3.13. Cross-section SEM image of sample 3 prepared at 0.56 V for 12 h at 723 K.

The XRD data for sample 4 (electrolyzed at 0.30 V) are shown in Table 3.1. Sample 4 was identified as PdLi, and the reaction at potential plateau 4 (0.53 V) can be expressed as

$$Pd_2Li + Li^+ + e^- \rightleftharpoons 2\,PdLi \qquad (3)$$

Similarly, from the XRD data shown in Table 3.2, sample 5 (electrolyzed at 0.08 V) was identified as $PdLi_2$, and potential plateau 5 (0.20 V) is thus considered to correspond to the following reaction:

$$PdLi + Li^+ + e^- \rightleftharpoons PdLi_2 \qquad (4)$$

Table 3.1. X-ray powder data for sample 4 prepared at 0.30 V for 21 h at 723 K. CuKα 1.5418 Å.

Intensity (S, M, W)	*d* / Å	*h k l* for PdLi*
S	4.064	0 0 1
M	2.388	1 0 0
VS	2.062	1 0 1
S	1.557	1 0 2
M	1.374	1 1 0
M	1.311	1 1 1
M	1.192	2 0 0, 1 0 3
M	1.149	2 0 1
W	1.035	2 0 2
W	0.976	1 1 3
W	0.947	1 0 4
W	0.905	2 1 0
W	0.885	2 1 1

* Hexagonal unit cell with a=2.763 Å, c=4.167 Å.

Table 3.2. X-ray powder data for sample 5 prepared at 0.08 V for 11.5 h at 723 K. CuKα 1.5418 Å.

Intensity (S, M, W)	d / Å	$h\,k\,l$ for $PdLi_2$*
W	3.555	1 0 0
W	2.593	0 0 1
W	2.158	1 0 1
M	2.083	1 1 0
M	1.806	2 0 0
M	1.658	1 1 1
M	1.507	2 0 1
W	1.374	2 1 0
M	1.359	0 0 2
S	1.273	1 0 2
M	1.227	2 1 1
W	1.215	3 0 0
M	1.143	1 1 2
M	1.112	3 0 1
M	1.089	2 0 2
M	1.053	2 2 0
M	1.012	3 1 0
W	0.983	2 2 1
M	0.970	2 1 2
S	0.950	3 1 1

* Hexagonal unit cell with a=4.214 Å, c=2.728 Å.

In samples 4 and 5, the palladium sheet was completely alloyed, and it was noted that the volume of sample 5 became several times as large as that of the initial palladium sheet. It is also interesting to note that the current density of peak 5 in Fig. 3.5 is much larger than that of the other peaks, which indicates that the diffusion of lithium in $PdLi_2$ is faster than that in the other phases.

Besides the five solid intermetallic compounds, there is a liquid phase in the Pd-Li phase diagram (Fig. 3.1). Thus, both peak 6 (0.06 V) in Fig. 3.5 and plateau 6 (0.06 V) in Fig. 3.6 are considered to correspond to the following reaction:

$$PdLi_2 + x\ Li^+ + x\ e^- \rightleftharpoons \text{liq. phase} \qquad (5)$$

The Pd-Li phase diagram shown in Fig. 3.1 also suggests the possibility of Pd_2Li_3 formation, which, however, was not identified in any samples under our experimental conditions. This supports the results of Van Vucht and Buschow [7] who reported that Pd_2Li_3 does not exist.

To summarize the above experimental results and discussion, the plateau potentials and the corresponding reactions are listed in Table 3.3.

Table 3.3. Formation reactions and corresponding formation potentials of each type Pd-Li alloy in a LiCl-KCl eutectic melt at 723 K.

Reaction	Equilibrium potential / V (vs. Li^+/Li)
$7\ Pd + Li^+ + e^- \rightleftharpoons Pd_7Li$	1.05
$2\ Pd_7Li + 5\ Li^+ + 5\ e^- \rightleftharpoons 7\ Pd_2Li$	0.64
$Pd_2Li + Li^+ + e^- \rightleftharpoons 2\ PdLi$	0.53
$PdLi + Li^+ + e^- \rightleftharpoons PdLi_2$	0.20
$PdLi_2 + x\ Li^+ + x\ e^- \rightleftharpoons$ liq. phase	0.06

3.4 Conclusions

To provide fundamental information concerning the electrochemical formation of Pd-Li alloys and palladium-rare earth alloys in molten LiCl-KCl systems, electrodeposition of lithium on palladium was investigated by electroanalytical techniques. The conclusions in this chapter can be summarized as follows.

(1) Electrochemical formation of various phases of Pd-Li alloy was achieved with cathodic polarization of the palladium electrode at various potentials in a LiCl-KCl eutectic melt at 723 K.

(2) The formation reactions and the corresponding formation potentials of each phase of Pd-Li alloy were determined as follows:

$7\ Pd + Li^+ + e^- \rightleftharpoons Pd_7Li$	1.05 V (vs. Li^+/Li)
$2\ Pd_7Li + 5\ Li^+ + 5\ e^- \rightleftharpoons 7\ Pd_2Li$	0.64 V (vs. Li^+/Li)
$Pd_2Li + Li^+ + e^- \rightleftharpoons 2\ PdLi$	0.53 V (vs. Li^+/Li)
$PdLi + Li^+ + e^- \rightleftharpoons PdLi_2$	0.20 V (vs. Li^+/Li)
$PdLi_2 + x\ Li^+ + x\ e^- \rightleftharpoons$ liq. phase	0.06 V (vs. Li^+/Li)

(3) These results also provide useful information concerning the electrochemical window of the molten LiCl-KCl system, which is very important in considering the electrochemical formation reactions of palladium-rare earth alloys.

References

[1] O. Loebich, Jr. and Ch. J. Raub, *J. Less-Common Met.* **55,** 67(1977).

[2] Ch. J. Raub, *Platinum Metals Rev.* **28,** 63(1984).

[3] M. L. Doyle and I. R. Harris, *Platinum Metals Rev.* **32,** 130(1988).

[4] D. T. Hughes and I. R. Harris, *J. Less-Common Met.* **61,** 9(1978).

[5] G. Xie, K. Ema and Y. Ito, *J. Appl. Electrochem.* **23,** 753(1993).

[6] Y. Takeuchi, K. Mochizuki, M. Watanabe and I. Obinata, *J. Jpn. Inst. Met.* **29,** 801(1966) in Japanese; TR: *Metallwiss. Tech.* **20,** 2(1966) in German.

[7] J. H. N. Van Vucht and K. H. J. Buschow, *J. Less-Common Met.* **48,** 345(1976).

Chapter 4

Thermodynamic Properties of Pd-Li Alloys*

4.1 Introduction

Based on the result in chapter 3, further study to determine the thermodynamic properties of Pd-Li alloys was carried out. To date, there are only two reports that deal with the thermodynamic properties of Pd-Li alloys. One is a proceeding which reports the partial molar excess free energy of Li in an α-Pd phase between 1073 and 1373 K [1]. The other report presents a phase diagram and thermodynamic parameters for several known solid Pd-Li compounds by using computer calculation [2]. So, no measurement data as to solid Pd-Li compounds and a liquid Pd-Li alloy appear in the literature.

The thermodynamic properties of Pd-Li alloys are thought to be important for studying the hydrogen absorbing natures of Pd-Li alloys at high temperature from thermodynamic aspects. Also, the thermodynamic properties of Pd-Li alloys seem to be useful in considering the following interesting hydrogen absorbing behaviors of Pd-Li alloys, which were studied at moderate temperature (298-348 K). Sakamoto *et. al* reported that Pd_7Li dissolves considerable amounts of hydrogen to form a more stable hydride phase than Pd despite the lattice contraction which occurs on alloying Pd with Li [3]. Yamazaki *et al.* found that the deposition of Li onto Pd and the formation of Pd-Li alloy during cathodic hydrogen charging in aqueous LiOH solution are likely to occur at a much more positive potential than the reported UPD potential [4].

The purpose of the study presented in this chapter was to determine the thermodynamic

---

* Published in *J. Electrochem. Soc.* **145,** 785(1998).

properties for various Pd-Li alloy phases by potential measurements at various temperatures (673-773 K).

4.2 Experimental

The apparatus and experimental method have already been described in chapter 3. Thus, several important items will be mentioned specially.

A Chromel-Alumel thermocouple was used for temperature measurement with an accuracy of ±1 K.

The reference electrode was an Al-Li alloy in the coexisting (α+β) phase state prepared electrochemically from an aluminum wire (10 mm x ϕ1 mm, The Nilaco Corporation, 99.99 %). The potential of this electrode is the equilibrium potential of the following reversible reaction [5, 6, 7]

$$Al(\alpha) + Li^+ + e^- \rightleftharpoons AlLi(\beta) \qquad (1)$$

The temperature dependence of this equilibrium potential with reference to Li^+/Li potential has been reported as

$$E = 0.4644 - 2.488 \times 10^{-4} T \qquad (2)$$

where E is the potential (V vs. Li^+/Li) and T is the absolute temperature (K) [6]. A similar relation was also obtained in the present experiments.

According to the Pd-Li phase diagram (Fig. 3.1), there are several single phases (Pd_7Li, Pd_2Li and PdLi) and a intermetallic compound ($PdLi_2$) and a liquid phase at 723 K*. In the study presented in chapter 3, formation potential of each phase of Pd-Li alloy was found by

---

* In this chapter, a "single phase" is defined as an alloy phase which has a significantly wide composition range, such as Pd_7Li, Pd_2Li and PdLi phases in Fig. 3.1. An "intermetallic compound" is defined as an alloy with a very narrow composition range, such as $PdLi_2$.

open-circuit potentiometry and chronopotentiometry in LiCl-KCl at 723 K, combined with XRD analysis of the electrochemically formed alloy samples. However, a statistical consideration or an investigation on temperature dependence were not carried out. Therefore, in the study presented in this chapter, open-circuit potentiometry and chronopotentiometry were carried out several times to obtain more precise potential data for each coexisting phase of Pd-Li alloy at some selected temperatures (673, 698, 723, 748 and 773 K).

4.3 Results and discussion

4.3.1 Potential measurement

Open-circuit potentiometry was used to measure the formation potentials of the Pd_7Li, Pd_2Li, PdLi and $PdLi_2$ phases, since this method showed more reliable reproducibility for these phases than other methods, e.g., chronopotentiometry and cyclic voltammetry. In the open-circuit potentiometry, Li was deposited onto a Pd electrode by galvanostatic cathodic electrolysis for 30 seconds at a current density of 1 A cm^{-2}, and then the open-circuit potential transient curve was measured. A typical curve obtained at 723 K is shown in Fig. 4.1. There are potential plateaus (plateaus 1-5) at 1.04, 0.91, 0.65, 0.53 and 0.20 V, respectively.

According to the result in chapter 3, plateaus 1, 3, 4 and 5 correspond to the coexisting (Pd+Pd_7Li), (Pd_7Li+Pd_2Li), (Pd_2Li+PdLi) and (PdLi+$PdLi_2$) phases, respectively. From five independent measurements, the potential value at 723 K has been determined for each coexisting phase as shown in Table 4.1 with standard deviation and numbers of data point (note: in this chapter, uncertainty is given with standard deviation for all cases). However, plateau 2 does not correspond to any coexisting phase. This suggests that plateau 2 corresponds to the formation of a new metastable phase which has not been reported previously. Furthermore, the Pd-Li phase diagram shown in Fig. 3.1 also suggests the

possibility of Pd_2Li_3 formation. However, neither a potential plateau nor an XRD pattern corresponding to the Pd_2Li_3 compound was observed. These results indicate that the Pd_2Li_3 phase does not exist. This supports the results of Van Vucht and Buschow who reported that they could not find the Pd_2Li_3 compound [8].

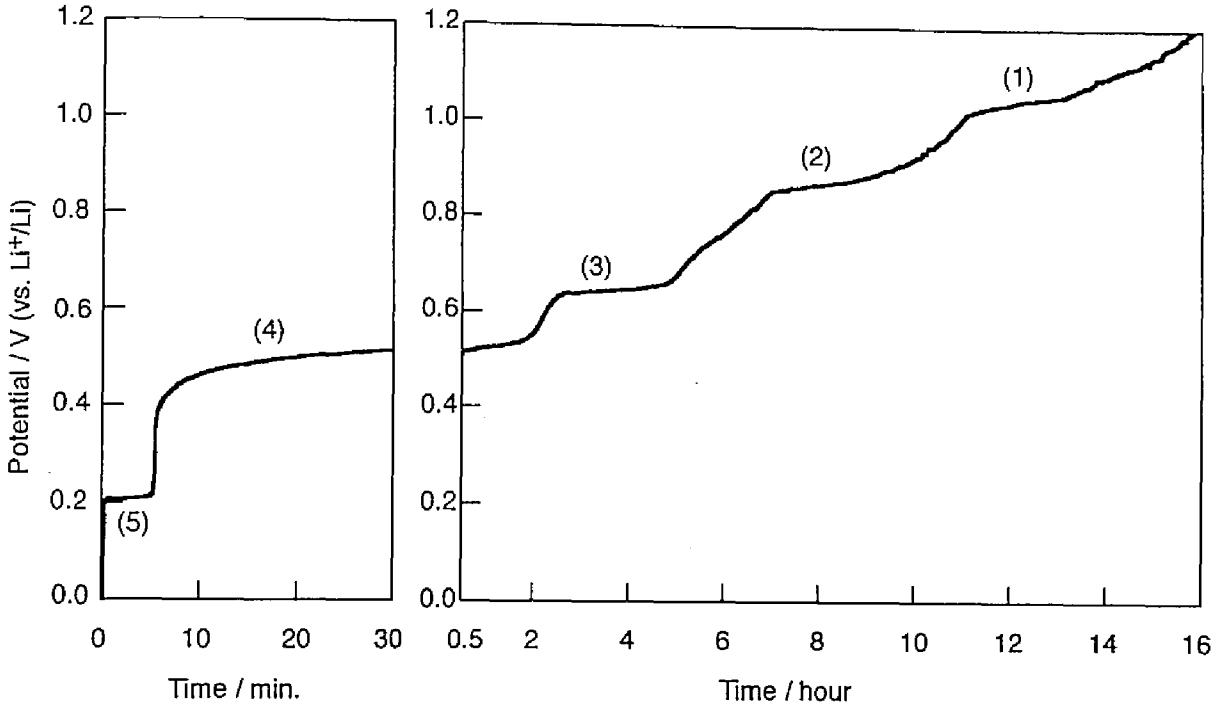

Fig. 4.1. Open-circuit potential transient curve of Pd electrode in a LiCl-KCl eutectic melt at 723 K, after galvanostatic electrolysis for 30 s at a current density of 1 A cm^{-2}.

Table 4.1. Potential values and corresponding equilibrium reactions in coexisting phase state between each phase of Pd-Li alloy in a LiCl-KCl eutectic melt at 723 K.

E V vs. Li^+/Li	Numbers of data	Reaction
1.04±0.01	5	$7\,Pd + Li^+ + e^- \rightleftharpoons Pd_7Li$
0.648±0.004	6	$2/5\,Pd_7Li + Li^+ + e^- \rightleftharpoons 7/5\,Pd_2Li$
0.531±0.002	4	$Pd_2Li + Li^+ + e^- \rightleftharpoons 2\,PdLi$
0.2029±0.0003	11	$PdLi + Li^+ + e^- \rightleftharpoons PdLi_2$
0.063±0.001	3	$PdLi_2 + x\,Li^+ + x\,e^- \rightleftharpoons$ liq. phase

Chronopotentiometry was carried out to investigate the formation potential of the liquid phase alloy. In this experiment, constant current cathodic electrolysis was conducted at a current density of 40 mA cm^{-2}. A typical potential transient curve at 723 K is shown in Fig. 4.2. Potential plateau A corresponds to plateau 5 in Fig. 4.1, at which the formation of $PdLi_2$ occurs. After further electrolysis, electrode potential shifts to negative direction because of the increase of Li activity in the Pd-Li alloy. Finally, the potential value stays almost constant at around 0.05 V, which indicates that new coexisting phase state is produced. Then the applied current was cut off to observe open-circuit potential, and stable potential plateau B was observed at 0.063 V. From the result of chapter 3, this plateau B corresponds to the coexisting ($PdLi_2$+liquid) phase. The result is also given in Table 4.1.

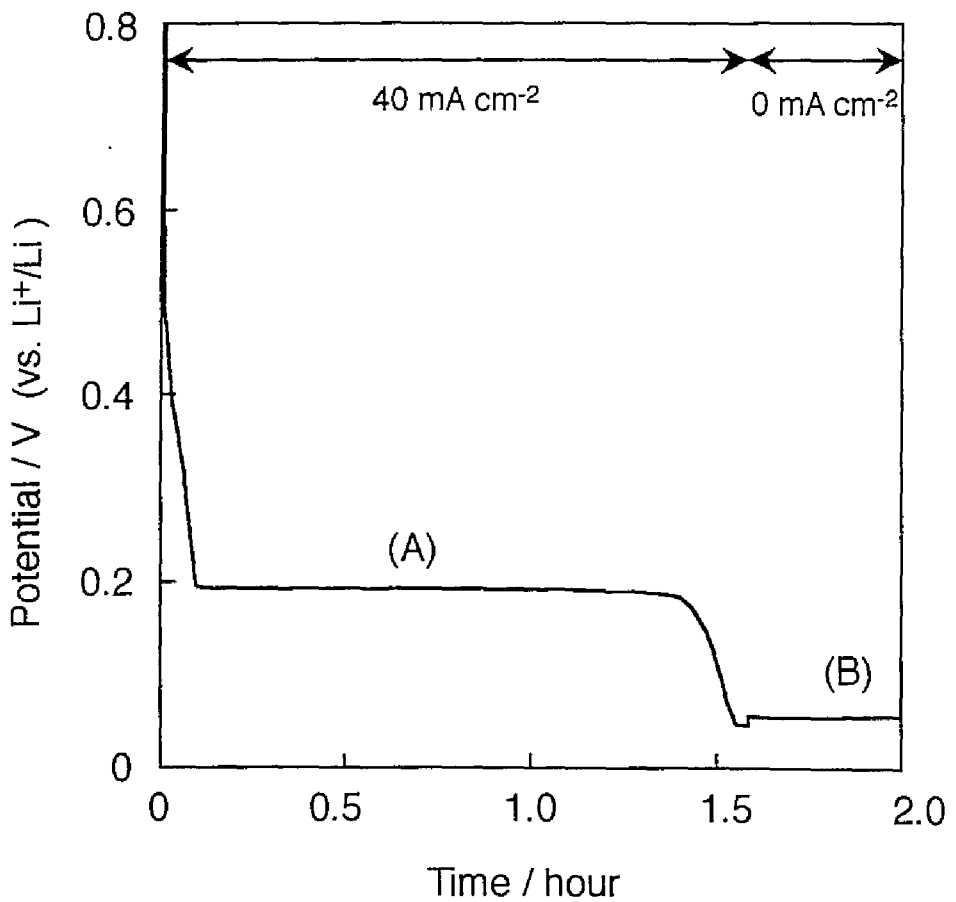

Fig. 4.2. Typical potential transient curve of Pd electrode in a LiCl-KCl eutectic melt at 723 K. Current density: 40 mA cm^{-2}.

4.3.2 Thermodynamic calculation

Further experiments by the same technique were directed to measure the formation potentials of Pd-Li alloys at other temperatures (673, 698, 748 and 773 K). The resultant potential values are summarized in Table 4.2 with numbers of data point. Using the obtained potential values, E (V vs. Li^+/Li), the relative partial molar Gibbs free energies of Li in the Pd-Li alloy, $\Delta\overline{G_{Li}}$, and the Li activities in the Pd-Li alloy, a_{Li}, were calculated from the following relations:

$$\Delta\overline{G_{Li}} = -FE \tag{3}$$

and

$$a_{Li} = \exp\left(\frac{\Delta\overline{G_{Li}}}{RT}\right) \tag{4}$$

where F is Faraday constant, R is gas constant and T is temperature (K). The calculated thermodynamic properties are also given in Table 4.2.

The Pd activities in the Pd-Li alloy with reference to pure solid Pd as the standard state, a_{Pd}, were calculated using the Gibbs-Duhem relation:

$$\ln a_{Pd} = -\int_{X_{Pd}=1}^{X_{Pd}} \frac{X_{Li}}{X_{Pd}} d\ln a_{Li} \tag{5}$$

where X is the mole fraction of the designated component. In this calculation, the following three assumptions were applied. Firstly, Raoul's law holds for a change of Pd activity in an α-Pd phase. Therefore, Pd activity is considered to be 0.94 at X_{Pd}=0.94 where the boundary of an α-Pd phase exists. Secondly, in any coexisting phase states, Li activity and Pd activity hold constant values. The final assumption is that Pd activity changes linearly with X_{Pd} in single phases, such as, Pd_7Li, Pd_2Li and PdLi. Figure 4.3 schematically explains this linear approximation, taking a single PdLi phase as an example.

Table 4.2. Thermodynamic properties of Li for Pd-Li alloys in coexisting phase states at various temperatures.

T K	E V vs. Li^+/Li	Numbers of data	$\Delta\overline{G_{Li}}$ kJ mol^{-1}	a_{Li}
In the coexisting phase state between Pd and Pd_7Li				
673	1.066± 0.006	3	-102.9± 0.5	1.0(±0.1) x 10^{-8}
698	1.054± 0.004	5	-101.7± 0.4	2.4(±0.2) x 10^{-8}
723	1.04± 0.01	5	-100.5± 1.0	5.5(±0.9) x 10^{-8}
748	1.029± 0.002	4	-99.3± 0.2	1.16(±0.03) x 10^{-7}
773	1.017± 0.004	5	-98.1± 0.4	2.4(±0.2) x 10^{-7}
In the coexisting phase state between Pd_7Li and Pd_2Li				
673	0.662± 0.004	2	-63.8± 0.3	1.11(±0.07) x 10^{-5}
698	0.658± 0.001	5	-63.5± 0.1	1.76(±0.03) x 10^{-5}
723	0.648± 0.004	6	-62.5± 0.4	3.0(±0.2) x 10^{-5}
748	0.640± 0.003	6	-61.7± 0.3	4.9(±0.3) x 10^{-5}
773	0.631± 0.003	5	-60.9± 0.3	7.7(±0.4) x 10^{-5}
In the coexisting phase state between Pd_2Li and PdLi				
673	0.542± 0.005	3	-52.3± 0.5	8.7(±0.8) x 10^{-5}
698	0.537± 0.005	4	-51.9± 0.5	1.3(±0.1) x 10^{-4}
723	0.531± 0.002	4	-51.3± 0.2	1.98(±0.06) x 10^{-4}
748	0.532± 0.002	5	-51.3± 0.2	2.62(±0.09) x 10^{-4}
773	0.522± 0.001	4	-50.4± 0.1	3.94(±0.06) x 10^{-4}
In the coexisting phase state between PdLi and $PdLi_2$				
673	0.2034± 0.0005	5	-19.63± 0.05	3.00(±0.03) x 10^{-2}
698	0.2030± 0.0003	6	-19.59± 0.03	3.42(±0.02) x 10^{-2}
723	0.2029± 0.0003	11	-19.58± 0.03	3.85(±0.02) x 10^{-2}
748	0.2032± 0.0004	7	-19.61± 0.04	4.27(±0.03) x 10^{-2}
773	0.2035± 0.0004	6	-19.64± 0.04	4.71(±0.03) x 10^{-2}
In the coexisting phase state between $PdLi_2$ and liquid Pd-Li alloy				
673	4.9(±0.1) x 10^{-2}	4	-4.7 ± 0.1	0.431± 0.009
698	5.5(±0.1) x 10^{-2}	4	-5.3 ± 0.1	0.403± 0.008
723	6.3(±0.1) x 10^{-2}	3	-6.1 ± 0.1	0.364± 0.008
748	7.2(±0.2) x 10^{-2}	4	-7.0 ± 0.2	0.33± 0.01
773	8.4(±0.3) x 10^{-2}	5	-8.1 ± 0.3	0.28± 0.01

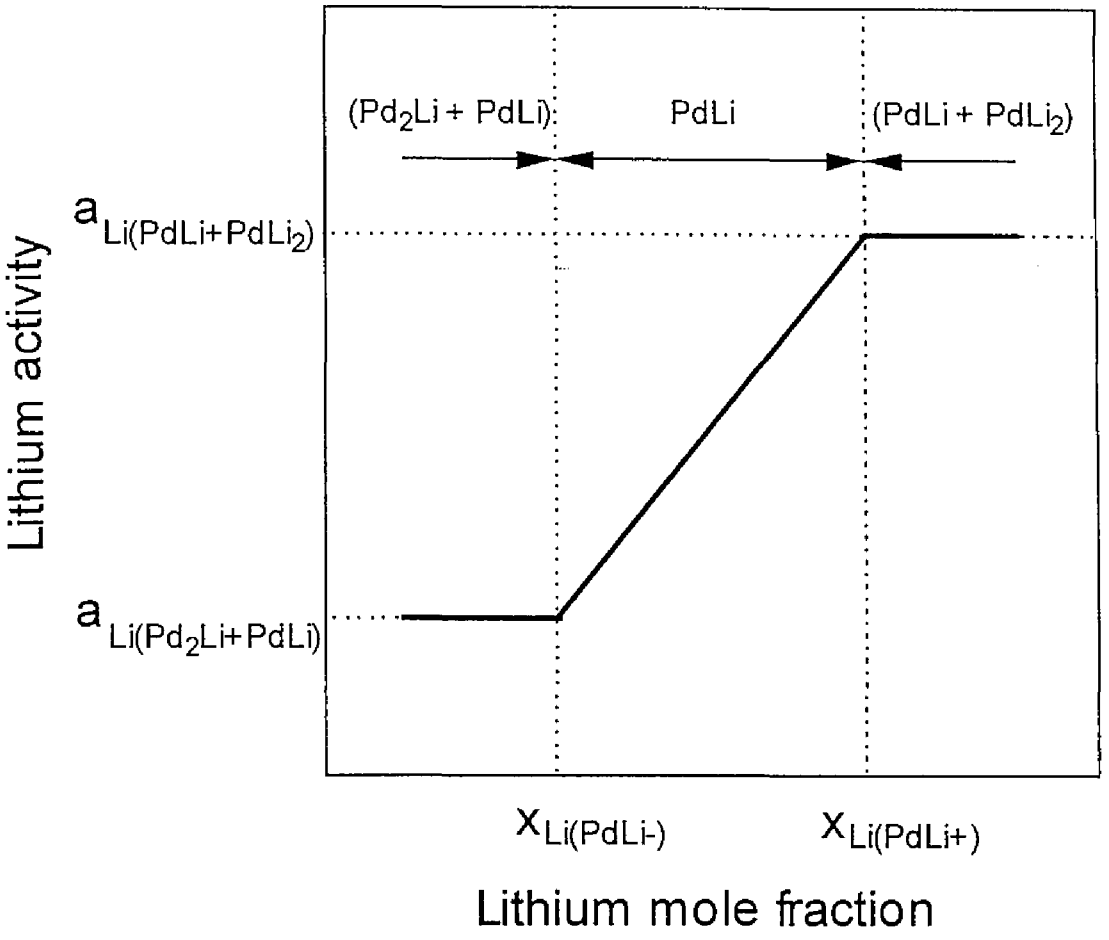

Fig. 4.3. Schematic representation of the linear approximation for the lithium activity dependence on the lithium mole fraction in a single PdLi phase.

The actual integrating calculations were carried out using the computer software "Mathematica" (Wolfram Research, Inc.). The calculated Pd activities, a_{Pd}, and the relative partial molar Gibbs free energies of Pd in the Pd-Li alloy, $\Delta\overline{G_{Pd}}$, obtained using the relation,

$$\Delta\overline{G_{Pd}} = RT\ln a_{Pd} \qquad (6)$$

are given at various temperatures in Table 4.3.

Table 4.3. Thermodynamic properties of Pd for Pd-Li alloys in coexisting phase states at various temperatures.

T K	$\Delta\overline{G_{Pd}}$ kJ mol^{-1}	a_{Pd}
In the coexisting phase state between Pd and Pd_7Li		
673	-0.346*	0.94*
698	-0.359*	0.94*
723	-0.372*	0.94*
748	-0.384*	0.94*
773	-0.398*	0.94*
In the coexisting phase state between Pd_7Li and Pd_2Li		
673	-6.04±0.09	0.340±0.006
698	-5.93±0.06	0.360±0.003
723	-5.9±0.2	0.374±0.009
748	-5.88±0.06	0.389±0.004
773	-5.83±0.08	0.403±0.005
In the coexisting phase state between Pd_2Li and PdLi		
673	-11.9±0.4	0.120±0.009
698	-11.9±0.4	0.128±0.008
723	-11.7±0.3	0.142±0.006
748	-11.3±0.2	0.162±0.006
773	-11.4±0.2	0.171±0.004
In the coexisting phase state between PdLi and $PdLi_2$		
673	-43.5±0.6	$4.2(\pm0.5) \times 10^{-4}$
698	-43.2±0.6	$5.9(\pm0.6) \times 10^{-4}$
723	-42.5±0.3	$8.5(\pm0.5) \times 10^{-4}$
748	-42.61± 0.3	$1.06(\pm0.05) \times 10^{-3}$
773	-41.8±0.2	$1.50(\pm0.05) \times 10^{-3}$
In the coexisting phase state between $PdLi_2$ and liquid Pd-Li alloy		
673	-73.1±0.7	$2.1(\pm0.3) \times 10^{-6}$
698	-71.6±0.6	$4.4(\pm0.5) \times 10^{-6}$
723	-69.3±0.4	$9.9(\pm0.7) \times 10^{-6}$
748	-67.7±0.6	$1.9(\pm0.2) \times 10^{-5}$
773	-64.7±0.7	$4.2(\pm0.5) \times 10^{-5}$

*Assumed value from Raoul's law.

To calculate the relative molar entropies of Li in Pd-Li alloys, $\Delta\overline{S_{Li}}$, the electrode potentials of the Pd-Li alloy, E, were plotted against temperature for various coexisting phases as presented in Figs. 4.4 to 4.8. They are represented by the following relations in the temperature range of 673-773 K:

$$E = (1.40 \pm 0.04) - (5.0 \pm 0.5) \times 10^{-4}T \qquad (Pd + Pd_7Li) \qquad (7)$$

$$E = (0.90 \pm 0.03) - (3.44 \pm 0.38) \times 10^{-4}T \qquad (Pd_7Li + Pd_2Li) \qquad (8)$$

$$E = (0.68 \pm 0.02) - (2.0 \pm 0.3) \times 10^{-4}T \qquad (Pd_2Li + PdLi) \qquad (9)$$

$$E = (0.201 \pm 0.004) + (3 \pm 5) \times 10^{-6}T \qquad (PdLi + PdLi_2) \qquad (10)^*$$

$$E = (0.6 \pm 0.4) - (2 \pm 1) \times 10^{-3}T + (1.4 \pm 0.8) \times 10^{-6}T^2 \qquad (PdLi_2 + \text{liq.-phase}) \qquad (11)$$

The relative partial molar entropies of Li, $\Delta\overline{S_{Li}}$, were calculated from the relation

$$\Delta\overline{S_{Li}} = F\frac{dE}{dT} \qquad (12)$$

where dE/dT were obtained from Eqs. (7) to (11), respectively. Since the temperature dependence of the potential for the coexisting ($PdLi_2$ + liq.-phase) seemed to have a parabolic relation, the dE/dT value at 723 K was used for the calculation for this phase. The results are summarized in Table 4.4.

---

* The gradient, $(3 \pm 5) \times 10^{-6}$ (V K^{-1}), does not have much statistically important meaning, because the error value is fairly large. However, the result has shown that the potential values scarcely change against temperature for the coexisting ($PdLi+PdLi_2$) phase.

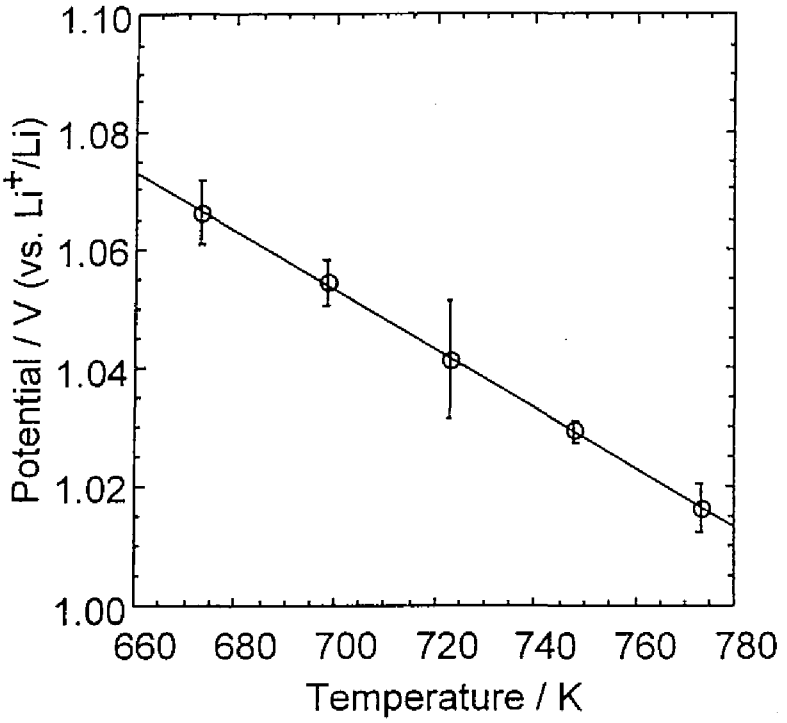

Fig. 4.4. Temperature dependence of the potential for Pd-Li alloy in the coexisting (Pd + Pd_7Li) phase state.

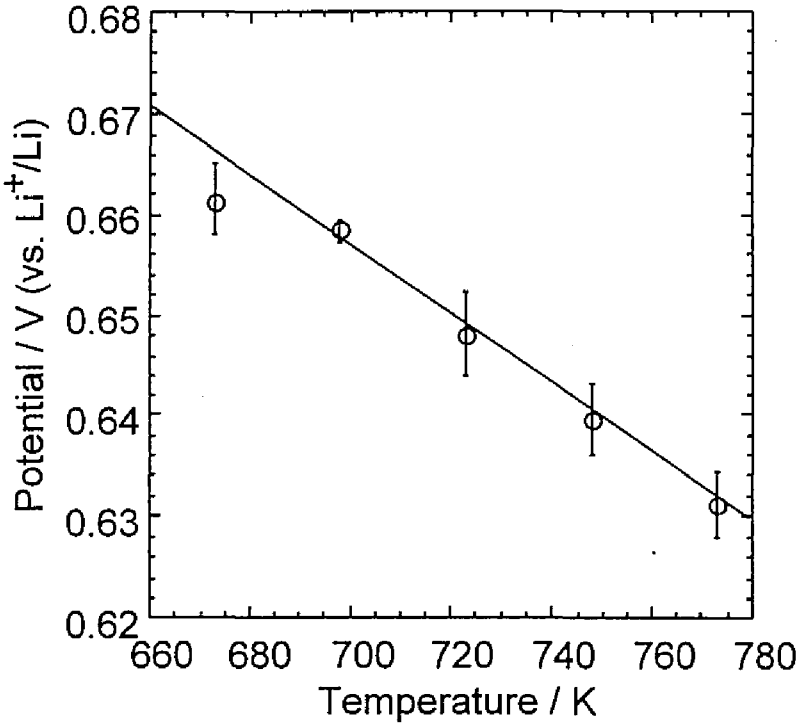

Fig. 4.5. Temperature dependence of the potential for Pd-Li alloy in the coexisting (Pd_7Li + Pd_2Li) phase state.

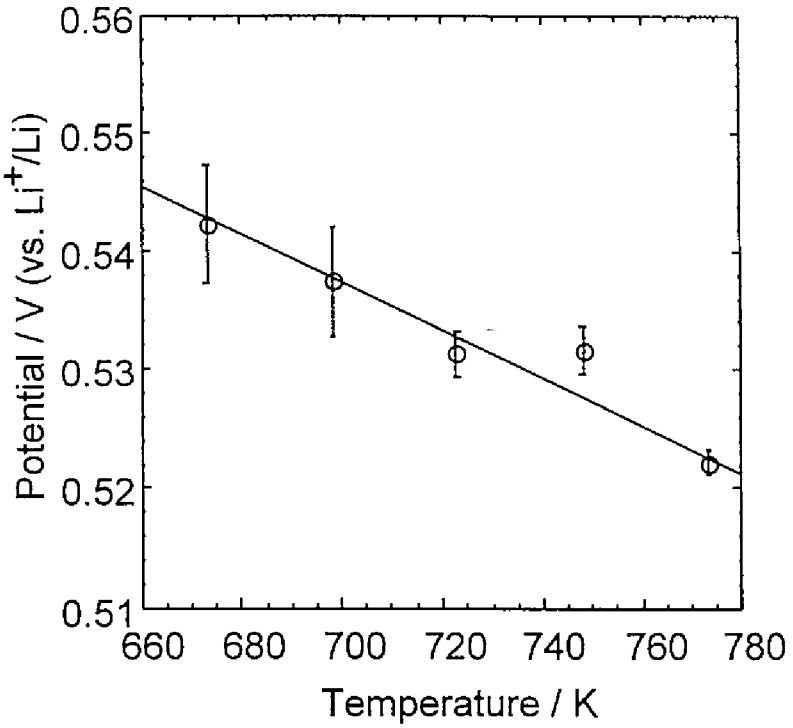

Fig. 4.6. Temperature dependence of the potential for Pd-Li alloy in the coexisting (Pd_2Li + PdLi) phase state.

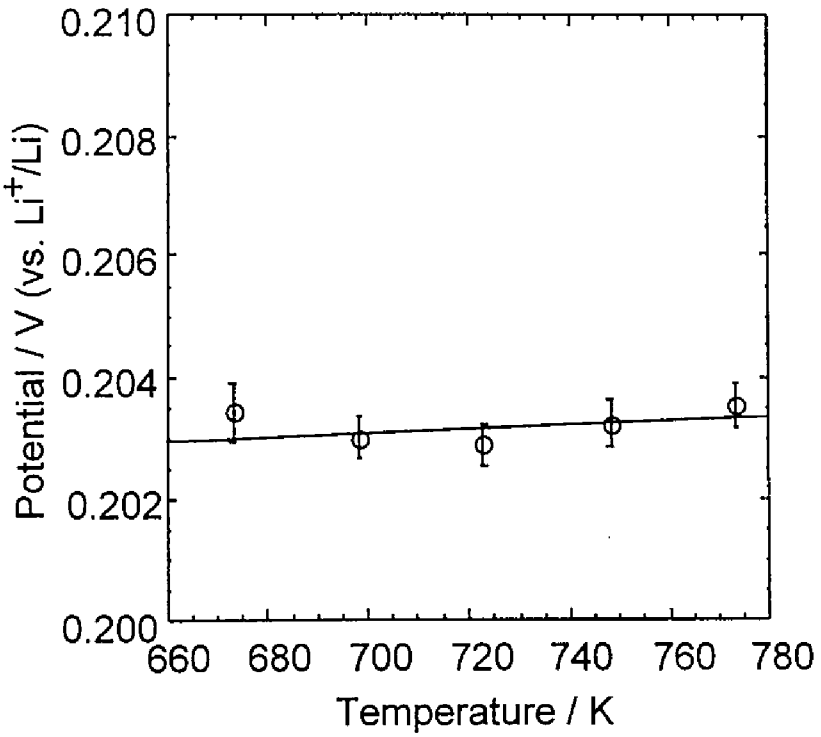

Fig. 4.7. Temperature dependence of the potential for Pd-Li alloy in the coexisting (PdLi + $PdLi_2$) phase state.

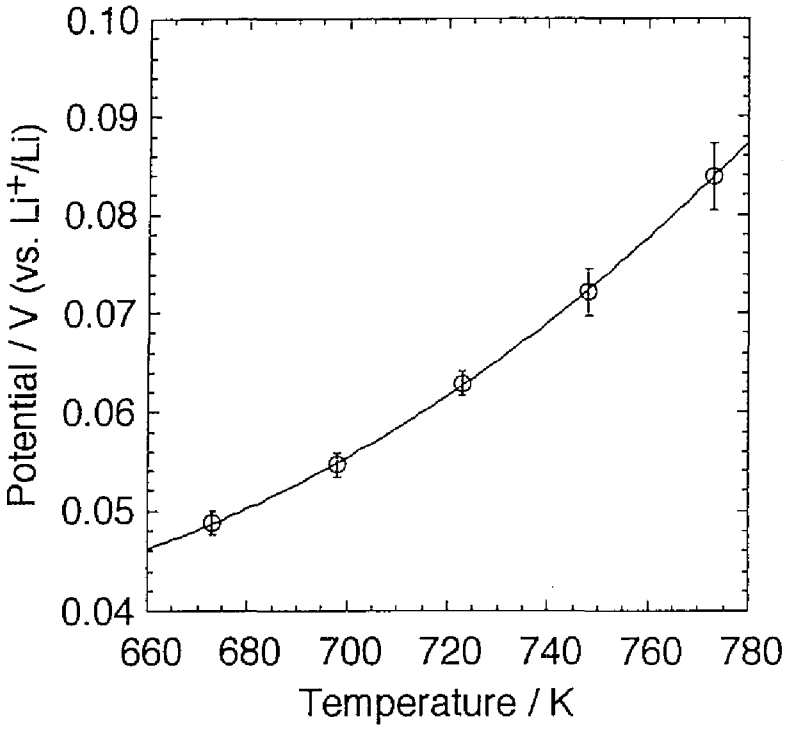

Fig. 4.8. Temperature dependence of the potential for Pd-Li alloy in the coexisting ($PdLi_2$ + liq.) phase state.

Table 4.4. Relative partial molar entropy and enthalpy of Li and Pd for Pd-Li alloys in coexisting phase states.

Phase	$\Delta\overline{S_{Li}}$ J mol^{-1}	$\Delta\overline{S_{Pd}}$ J mol^{-1}	$\Delta\overline{H_{Li}}$* kJ mol^{-1}	$\Delta\overline{H_{Pd}}$* kJ mol^{-1}
Pd + Pd_7Li	-48±5	-	-135±4	-
Pd_7Li + Pd_2Li	-33±4	-1.6±1.0	-86±3	-7.1±0.7
Pd_2Li + PdLi	-19±3	-6±4	-65±2	-16±3
PdLi + $PdLi_2$	0.3±0.5	-16±5	-19.4±0.5	-54±3
$PdLi_2$ + liq.-phase	34*	82*	18	-10

*Values at 723 K.

The relative partial molar enthalpies of Li, $\Delta\overline{H_{Li}}$, were calculated at 723 K from the relation:

$$\Delta\overline{H_{Li}} = \Delta\overline{G_{Li}} + T\Delta\overline{S_{Li}} \quad (13)$$

They are also given in Table 4.4.

Then the relative partial molar entropies of Pd, $\Delta\overline{S_{Pd}}$, were calculated from plots of $\Delta\overline{G_{Pd}}$ against temperature, and the relative partial molar enthalpies of Pd, $\Delta\overline{H_{Pd}}$, were calculated at 723 K from the relation:

$$\Delta\overline{H_{Pd}} = \Delta\overline{G_{Pd}} + T\Delta\overline{S_{Pd}} \quad (14)$$

The calculated values of $\Delta\overline{S_{Pd}}$, and $\Delta\overline{H_{Pd}}$ are also given in Table 4.4.

Then the standard Gibbs free energies of formation, ΔG_f^0, for Pd_7Li, Pd_2Li, PdLi, $PdLi_2$ and liquid phase alloy in the unit of per gram atom of Li were obtained from the following relation,

$$\Delta G_f^0 = \Delta\overline{G_{Li}} + \frac{X_{Pd}}{X_{Li}}\Delta\overline{G_{Pd}} \quad (15)$$

at 673, 698, 723, 748 and 773 K, and are summarized in Table 4.5.

Table 4.5. Standard Gibbs free energy of formation for Pd-Li alloys at various temperatures.

Temperature K	ΔG_f^0 kJ mol^{-1}				
	Pd_7Li	Pd_2Li	PdLi	$PdLi_2$	liq.-phase*
673	-105.3±0.5	-75.9±0.4	-64.2±0.6	-41.4±0.3	-27.8±0.2
698	-104.3±0.4	-75.4±0.2	-63.8±0.6	-41.2±0.3	-29.8±0.2
723	-103±1	-74.4±0.5	-63.0±0.3	-40.8±0.2	-31.7±0.2
748	-102.0±0.2	-73.5±0.4	-62.6±0.3	-40.9±0.2	-33.3±0.3
773	-100.9±0.4	-72.6±0.4	-61.8±0.2	-40.5±0.1	-34.5±0.4

*Lithium mole fractions in the liquid phase alloys are 0.760, 0.745, 0.73, 0.72 and 0.71 at 673, 698, 723, 748 and 773 K, respectively.

Finally, the obtained thermodynamic data were extrapolated to 298.15 K for comparison with the literature [2], as shown in Table 4.6. The extrapolation was carried out assuming temperature independent heat capacity and correcting for the heat of fusion of Li, 3.0 kJ mol^{-1}. There is a substantial discrepancy between the values of this work and the previous estimates in reference 2. Since the values of this work were obtained by calculations from directly measured potential data, errors in these values mainly seem to be due to a temperature dependence of the heat capacities, in disagreement with the assumption above. In reference 2, the computer calculation was carried out from minimal thermodynamic data, *i.e.*, the partial molar excess free energy of Li in an α-Pd phase between 1073 and 1373 K [1] and thermodynamic values of pure Pd and Li. Therefore, errors may be brought from the estimation of some parameters, *e.g.*, interaction parameters (or Redlich-Kister coefficients in ref. 2). However, the essential cause of the discrepancy is not clear yet. The explanation of this substantial discrepancy is interesting future subject.

Table 4.6. Thermodynamic data extrapolated to 298.15 K for comparison with the literature [2].

Compound	ΔG_f^0 kJ (mol Li)$^{-1}$		ΔH_f^0 kJ (mol Li)$^{-1}$	
	This work	Ref. 2	This work	Ref. 2
Pd_7Li	-125	-39.9	-138	-38.9
Pd_2Li	-92.9	-24.2	-104	-21.6
PdLi	-77.0	-14.7	-84.6	-11.6
$PdLi_2$	-47.2	-6.32	-49.6	-2.34

4.4 Conclusion

A series of open-circuit potentiometry and constant current chronopotentiometry were carried out to measure the potentials for the various Pd-Li alloys in coexisting phase states in the temperature range of 673-773 K. These values were used to calculate the activities and relative partial molar properties of both Li and Pd. The standard Gibbs free energies of formation for Pd_7Li, Pd_2Li, PdLi, $PdLi_2$ and liquid phase alloy were also determined over the specified temperature range.

Nomenclature

a_i	activity of component i (i=Li, Pd)
E	potential (V vs. Li^+/Li)
F	Faraday constant (96487 C mol^{-1})
ΔG_f^0	standard Gibbs free energy of formation (J mol^{-1})
$\Delta \overline{G_i}$	relative partial molar Gibbs free energy of component i (i=Li, Pd) (J mol^{-1})
$\Delta \overline{H_i}$	relative partial molar enthalpy of component i (i=Li, Pd) (J mol^{-1})
R	gas constant (8.314 J K^{-1} mol^{-1})
$\Delta \overline{S_i}$	relative partial molar entropy of component i (i=Li, Pd) (J K^{-1} mol^{-1})
T	temperature (K)
X_i	mole fraction of component i (i=Li, Pd)

References

[1] H. Brodowsky and H. Schumacher, *Report at CALPHAD XI,* Argonne, IL(1980), Summary in L. Kaufman, *CALPHAD* **6**, 178(1982).

[2] R. A. Howald, *CALPHAD* **14,** 1(1990).

[3] Y. Sakamoto, T. Hisamoto, M. Ura and R. Nakamura, *J. Alloys Comp.* **200,** 141(1993).

[4] O. Yamazaki, H. Yoshitake, N. Kamiya and K. Ota, *J. Electroanal. Chem.* **390,** 127(1995).

[5] K. Amezawa, Y. Tomii and Y. Ito, *J. Electrochem. Soc.* **141,** 3096(1994).

[6] R. A. Sharma and R. N. Seefurth, *J. Electrochem. Soc.* **123,** 1763(1976).

[7] C. J. Wen, B. A. Boukamp, R. A. Huggins and W. Weppner, *J. Electrochem. Soc.***126,** 2258(1979).

[8] J. H. N. Van Vucht and K. H. J. Buschow, *J. Less-Common Met.* **48,** 345(1976).

Chapter 5

Electrochemical Hydrogen Absorbing Behavior of Pd and Pd-Li Alloys in a Molten LiCl-KCl-LiH System*

5.1 Introduction

Hydrogen behavior in metals at high temperature are worth investigating from various reasons. For hydrogen energy systems, which have attracted much attention because of their cleanness and permanence, higher operating temperatures have the advantages of higher reactivity. Furthermore, if the total generated heat is efficiently utilized in the system, higher overall energy efficiency can be expected. These high temperature operations require the development of new hydrogen absorbing alloys which work at the required temperatures. At the same time, understanding of hydrogen behavior in structural materials at high temperature is necessary to prevent hydrogen embrittlement. For a D-T neutron generator, the development of new metal-tritide targets is important because the desorption of tritium caused by generated heat prevents high neutron output and long term operation for conventional Ti-T targets [1]. This can be overcome by developing a hydrogen absorbing alloy with a very low hydrogen desorption pressure at high temperatures. Metal alloys having high hydrogen permeability at high temperatures are promising both as cathode materials for a Li-H_2 thermally regenerative fuel cell [2, 3] and as a hydrogen diffusion membrane for hydrogen purification [4].

Despite these potential uses, few studies on high temperature hydrogen absorbing alloys

---

*Published in *J. Electrochem. Soc.* **144,** 2290(1997).

exist. Therefore, high temperature hydrogen absorbing alloys were investigated by electrochemical methods using a molten LiCl-KCl-LiH system. When LiH is dissolved in a LiCl-KCl eutectic melt, it ionizes to form Li^+ and H^- ions, as described in chapter 2. Therefore, it is possible to investigate hydrogen behavior in the alloys by using the half-cell reactions of M-H/H^- systems [5, 6]. Electrochemical methods have several advantages; high sensitivity, simple apparatus, safe handling of hydrogen gas, possibility to change hydrogen pressure instantaneously by controlling electrode potential, etc.

As a first step of an electrochemical study concerning hydrogen behavior in metals at high temperature, Pd and Pd-Li alloys were selected to be investigated from the following reasons. Firstly, Pd is well known as a hydrogen absorbing metal, and has been studied intensively at room temperature [7]. Also, Pd-Li alloys seemed to have high hydrogen absorbing ability at high temperatures according to Nacken *et al.* who reported that PdLi absorbs hydrogen to form $PdLiH_x$ (x=0.73-0.82) at 873 K [8].

Furthermore, the knowledge obtained through the present study seems to be useful in considering the following interesting hydrogen absorbing behaviors of Pd-Li alloys at moderate temperature (298-348 K). Sakamoto *et al.* reported that Pd_7Li dissolves considerable amounts of hydrogen to form a more stable hydride phase than Pd despite the lattice contraction which occurs on alloying Pd with Li [9]. Yamazaki *et al.* found that the deposition of Li onto Pd and the formation of Pd-Li alloy during cathodic hydrogen charging in aqueous LiOH solution are likely to occur at a much more positive potential than the reported UPD potential [10].

From the conclusions in chapter 3 chapter 4, formation potentials of various Pd-Li alloy phases have been clarified. Thus, Pd-Li alloy samples were produced by electrochemical method using Pd electrode in a LiCl-KCl eutectic melt. The electrochemical techniques, cyclic voltammetry and chronopotentiometry were used in this study. The hydrogen amounts in Pd, Pd_7Li, Pd_2Li and PdLi were estimated in order to discuss the Li alloying effect on the hydrogen absorbing ability.

5.2 Experimental

The apparatus and experimental method have been described in chapter 3. Thus, several important points will be mentioned specially.

The experiments were performed in a molten LiCl-KCl-LiH system (5 mol% LiH added) under a dry argon atmosphere at 673 K. After LiH (Wako Pure Chemical Co., Ltd., 95 %) was added, the melt was stirred for about half an hour by dry argon gas bubbling to dissolve LiH completely. The introduction of LiH provides a very reducing chemical environment with extremely low levels of water and oxygen, as it has been shown by Deublein et al. [11].

A potentio/galvanostat (SI1287; Solartron) connected to a personal computer (FMV46CES; Fujitsu) were used to obtain voltammetric and chronopotentiometric data. Ohmic drops were compensated during the electrochemical measurements by using the measured solution resistance.

The working electrodes were square-shaped sheets of Pd (5 mm x 5 mm x 0.2 mm, The Nilaco Corporation, 99.95 %) or Mo (5 mm x 5 mm x 0.2 mm, The Nilaco Corporation, 99.95 %). The reference electrode was an Al-Li alloy in the coexisting (α+β) phase state.

Analyses of the Pd-Li-H alloy samples were carried out by powder XRD, using an X-ray generator (CN4012K; Rigaku Co., Ltd., CuKα line, 1.5418 Å) and a Debye-Scherrer camera (CN1111B1; Rigaku Co., Ltd.). The measured XRD data were compared with the calculated data based on the reported structure and lattice constant of Pd-Li-H compounds [8,12].

5.3 Results and discussion

5.3.1 Cyclic voltammetry

Cyclic voltammetry was carried out on a Mo electrode in a molten LiCl-KCl-LiH system (5 mol% LiH added). The hydrogen solubility in Mo is so small that the amount of hydrogen absorbing into the electrode is negligible [13]. Before adding LiH, a blank measurement was performed, as shown with the solid line in Fig. 5.1. Only the currents due to deposition and dissolution of Li are observed because there exists no chemical species except Li^+ ion which reacts in this potential region. Typical voltammograms obtained after adding LiH (5 mol%) are also shown in Fig. 5.1. The potential scan rates were 0.05 V s^{-1} (dashed line) and 0.1 V s^{-1} (solid line). In both voltammograms, the anodic currents start flowing from about 0.55 V, which are based on the following half-cell reaction [4]:

$$H^- \rightarrow \frac{1}{2}H_2 + e^- \qquad (1)$$

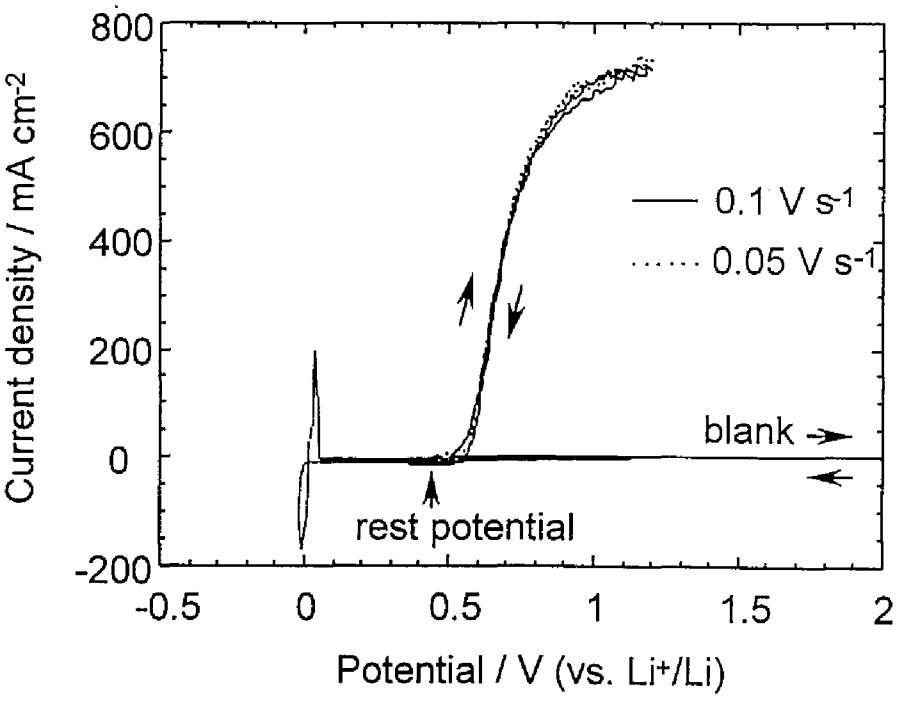

Fig. 5.1. Cyclic voltammograms for a Mo electrode in molten LiCl-KCl (blank) and in a molten LiCl-KCl-LiH system (5 mol% LiH added) at 673K. The potential scan rate: 0.1 V s^{-1} (blank), 0.1 V s^{-1} (solid line) and 0.05 V s^{-1} (dashed line).

Then, the currents increase rapidly to reach approximately 700 mA cm^{-2} at 1.2 V. There is almost no difference between the voltammograms with the two different scan rates, which indicates that nearly steady states are observed. Since the cathodic current is much smaller than the anodic current, the evolving hydrogen is considered to escape from the surface of the Mo electrode as gas. Considering the values of the anodic current densities, a molten LiCl-KCl-LiH system (5 mol% LiH added) was chosen in the further experiments to have high enough hydrogen supplying ability for studying the hydrogen absorbing behavior of the electrodes. Incidentally, a little amount of added LiH may have been consumed by reaction with residual contamination in the salt. Therefore, the actual amount of LiH may have been not precisely equal to 5 mol%. However, the consumed amount of LiH was considered to be less than 0.1 mol% because cyclic voltammograms showed the existence of H^- ion after the addition of even 0.1 mol% LiH. It is important to keep the initial concentration of LiH during the measurements. For every experiments, the concentration of LiH in the salt was checked by cyclic voltammetry using a Mo electrode before and after the measurements, and it was confirmed that the current densities had almost the same values.

Cyclic voltammetry was also performed for a Pd electrode. Before adding LiH, a blank measurement was performed, as shown with the dashed line in Fig. 5.2. In this voltammogram, the cathodic current starting from around 0.6 V is due to the Li alloy formation reaction:

$$Pd + x\,Li^+ + x\,e^- \rightarrow PdLi_x \qquad (2)$$

The anodic current is based on the Li dissolution from the Pd-Li alloy, as described in chapter 3. The solid line in Fig. 5.2 shows a typical voltammogram after adding LiH (5 mol%). The anodic part of the voltammogram consists of two waves with a first wave starting at about 0.52 V and a second wave starting at about 0.85 V. The first wave is supposed to correspond to the oxidation of H^- ion followed by hydrogen absorption into the electrode:

$$H^- \rightarrow H(Pd) + e^- \qquad (3)$$

At the second wave region, H_2 gas evolution reaction seems to occur in addition to the hydrogen absorption reaction. On the other hand, the cathodic current is supposed to be due to

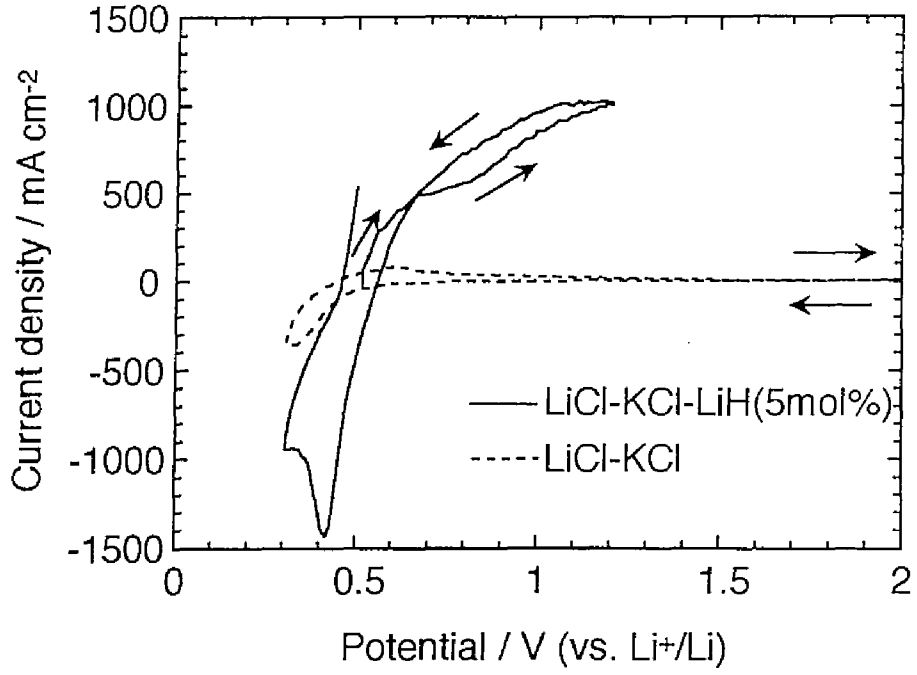

Fig. 5.2. Cyclic voltammograms for a Pd electrode in a LiCl-KCl eutectic melt (dashed line) and in a LiCl-KCl-LiH system (5 mol% LiH added) (solid line) at 673 K. Potential scan rate: 0.1 V s^{-1}.

the electrochemical hydrogen desorption. Considering the blank measurement for Pd, the current in the molten LiCl-KCl-LiH system is supposed also to include the current based on the Li alloying and the Li dissolution as shown in reaction (2). However, the hydrogen related reaction seems to dominate in the current contribution, because the current density corresponding to the solid line is much higher than for the dashed line.

5.3.2 X-ray diffraction analysis

The preceding results show that the reduction of Li^+ ion and the oxidation of H^- ion occurs in the same potential region on a Pd electrode. These data suggest the possibility of spontaneous formation of a Pd-Li-H compound:

$$Pd + Li^{+} + H^{-} \rightarrow Pd\text{-}Li\text{-}H \qquad (4)$$

To confirm this reaction, Pd was immersed in the molten LiCl-KCl-LiH system (5 mol% LiH added) for 10 hours. The potential at the open circuit was around 0.44 V during the immersion. After the immersion, the Pd sheet became rather thick and, the color changed into gray. The electrode seemed to have been completely alloyed because it was easily ground into powder. The sample was analyzed by powder XRD, and was identified as $PdLiH_x$ (Table 5.1). This result proves reaction (4) which represents a spontaneous formation of a $PdLiH_x$ compound.

Using a Pd electrode, potentiostatic electrolysis was conducted at 0.60 V for 1 hour in the molten LiCl-KCl-LiH system (5 mol% LiH added) in order to confirm the reaction at this potential. During the electrolysis, an anodic current was observed at current density of around

Table 5.1. X-ray powder data for the alloy made by immersion of Pd for 10 hours in a molten LiCl-KCl-LiH system (5 mol% LiH added) at 673 K. CuKα 1.5418 Å.

Intensity (S, M, W)	d / Å	h k l for $PdLiH_x$*
S	3.774	0 0 1
M	2.786	1 0 0
S	2.249	1 0 1
W	1.979	1 1 0
VW	1.888	0 0 2
M	1.752	1 1 1
W	1.364	1 1 2
W	1.312	2 0 1
VW	1.252	2 1 0
W	1.190	2 1 1
VW	1.124	2 0 2

* Tetragonal unit cell with a=2.80 Å, c=3.77 Å.

200 mA cm^{-2}. After the electrolysis, there seemed to be no change in the electrode except at the surface. The XRD data for the electrode, as shown in Table 5.2, showed that the main phase was α-Pd. The data also showed the existence of residual amounts of $PdLiH_x$, which were considered to have been formed at the surface. This result shows that the ternary $PdLiH_x$ phase forms at 0.60 V. However, the formation rate of the ternary phase from Pd is very slow at 0.60 V. This seems to be mainly because the slow diffusion rate of Li in Pd. Accordingly, the reactions during the electrolysis are mainly H_2 gas evolution due to H^- ion oxidation and partly the formation of $PdLiH_x$.

Table 5.2. X-ray powder data for the alloy made by potentiostatic electrolysis of Pd at 0.60 V for 1 hour in a molten LiCl-KCl-LiH system (5 mol% LiH added) at 673 K. CuKα 1.5418 Å.

Intensity (S, M, W)	d / Å	h k l for $PdLiH_x$*	h k l for Pd**
W	3.921	0 0 1	
W	2.765	1 0 0	
M	2.269	1 0 1	
VS	2.230		1 0 0
W	1.971	1 1 0	
S	1.939	(0 0 2)	2 0 0
W	1.761	1 1 1	
S	1.374	(1 1 2)	2 2 0
VS	1.173	(1 0 3)	3 1 1
M	1.122	2 0 2	2 2 2
S	0.893		3 3 1
S	0.870		4 2 0

* Tetragonal unit cell with a=2.79 Å, c=3.91 Å.

** Face centered cubic unit cell with a=3.89 Å.

A PdLi electrode was used instead of a Pd electrode to investigate the difference in hydrogen absorbing behavior. The PdLi electrode was prepared by potentiostatic electrolysis of Pd at 0.30 V for 20 hours in a LiCl-KCl eutectic melt. This PdLi electrode was also polarized at 0.60 V for 1 hour in a molten LiCl-KCl-LiH system (5 mol% LiH added). The results from the XRD analysis of this sample, as shown in Table 5.3, suggest that PdLi is changed into $PdLiH_x$ by an electrochemical hydrogen absorption reaction:

$$PdLi + x\,H^- \rightarrow PdLiH_x + x\,e^- \qquad (5)$$

The total charge observed here was around 7 times larger than the value required to form stoichiometric PdLiH. This suggests that the hydrogen absorption was the main reaction in the earlier period of electrolysis and H_2 gas evolution was the main reaction after hydrogen saturation of the electrode.

Incidentally, the observed c-axis length of $PdLiH_x$ sample made by electrolysis was 3.95 Å, and that for immersed sample was 3.77 Å. Since the c-axis length for $PdLiH_x$ is influenced by the hydrogen concentration [13], it can be used to estimate the hydrogen concentration. Assuming that the c-axis length changes linearly with the hydrogen concentration, x value is 0.96 for the sample electrolyzed at 0.60 V and 0.73 for the immersed sample. These results indicate that the hydrogen concentration is higher for $PdLiH_x$ obtained by electrolysis than $PdLiH_x$ obtained by immersion.

Table 5.3. X-ray powder data for the alloy made by potentiostatic electrolysis of PdLi at 0.60 V for 1 hour in a molten LiCl-KCl-LiH system (5 mol% LiH added) at 673 K. CuKα 1.5418 Å.

Intensity (S, M, W)	d / Å	h k l for $PdLiH_x$*
M	3.938	0 0 1
S	2.778	1 0 0
VS	2.276	1 0 1
S	1.970	1 1 0
M	1.762	1 1 1
W	1.611	1 0 2
S	1.397	(2 0 0)
W	1.318	2 0 1
W	1.245	2 1 0
S	1.191	2 1 1
M	0.908	3 0 1

* Tetragonal unit cell with a=2.79 Å, c=3.95 Å.

5.3.3 Chronopotentiometry

By chronopotentiometry, it is possible to quantitatively evaluate the hydrogen absorbing capacity of alloys. The amount of electrochemically absorbed or desorbed hydrogen can be calculated from the charge. Therefore, chronopotentiometry was applied for Pd and Pd-Li alloys to study the hydrogen absorbing ability. To investigate the effect of the Li concentration on the hydrogen absorbing ability systematically, several phases of Pd-Li alloy were prepared, i.e., PdLi phase (46-52 a/o Pd), Pd_2Li phase (56-72 a/o Pd) and Pd_7Li phase (86-87.5 a/o Pd).

These Pd-Li alloys were all formed by electrolysis of LiCl-KCl using a Pd electrode at 723 K. From the results in chapter 3 and chapter 4, the stable potential range of PdLi, Pd_2Li and Pd_7Li are 0.20-0.53, 0.53-0.64 and 0.64-1.05 V in a LiCl-KCl eutectic melt at 723 K. PdLi was prepared by potentiostatic electrolysis at 0.30 V for 20 hours using a Pd cathode. However, for Pd_2Li and Pd_7Li, it takes a very long time to form them completely through the whole electrode by using a Pd cathode. The reason for this is that the growth rates of Pd_2Li and Pd_7Li are very slow when the Li alloying reaction is utilized. On the other hand, it was found that the formation of Pd_2Li or Pd_7Li by the Li dissolution from a PdLi electrode was possible and required less time. Therefore, Pd_2Li and Pd_7Li were made by potentiostatic electrolysis at 0.60 and 0.80 V, respectively, for 20 hours using a PdLi anode. In addition to these phases, another stoichiometric phase, $PdLi_2$, is present according to the phase diagram [14]. The stable potential range of $PdLi_2$ is 0.05-0.20 V according to the previous experiments described in chapter 3. However, $PdLi_2$ was not chosen to be investigated, because it changes to PdLi rapidly at potentials more positive than 0.20 V. This means that $PdLi_2$ is not stable at the hydrogen charging potential.

For each anodic hydrogen charging, potentiostatic electrolysis was performed at 0.60 V for 0.5 hour, which was considered to have saturated the electrode with hydrogen. Then, chronopotentiometry was conducted under galvanostatic hydrogen discharging at 10 mA cm^{-2}.

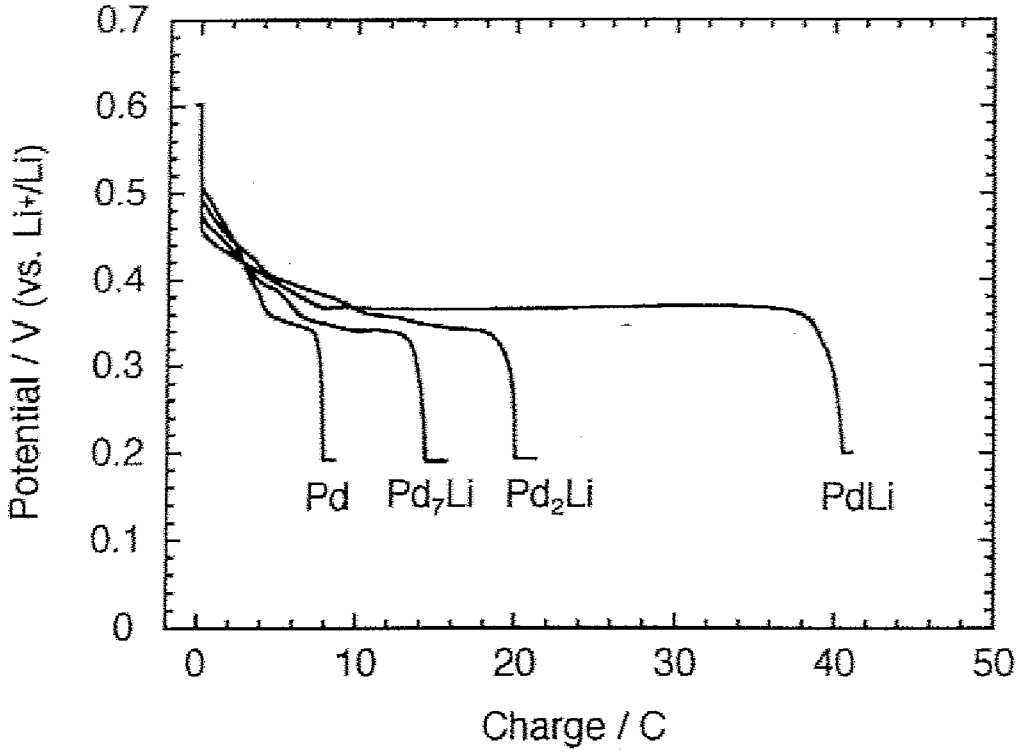

Fig. 5.3. Potential-charge curves for Pd, Pd_7Li, Pd_2Li and PdLi electrodes under cathodic hydrogen discharging in a molten LiCl-KCl-LiH (5 mol% LiH added) system at 673 K. After potentiostatic hydrogen charging at 0.6 V for 0.5 hour. Discharging current density: 10 mA cm^{-2}.

Figure 5.3 shows each potential-charge curve for Pd, Pd_7Li, Pd_2Li and PdLi, respectively. The cathodic current was terminated when the potential plateau appeared at approximately 0.20 V, which corresponds to the formation potential of $PdLi_2$. The curve for PdLi shows a flat potential plateau at 0.37 V, indicating the presence of a co-existing phase. Since the alloy sample obtained just after the flat plateau was identified as PdLi by XRD analysis, the co-existing phases are considered to be $PdLiH_x$ and PdLi. Thus, the reaction can be described as

$$PdLiH_x + x\,e^- \rightarrow PdLi + x\,H^- \qquad (6)$$

The curves for Pd, Pd_7Li and Pd_2Li also show potential plateaus, but they do not have very flat regions. This means that the hydrogen activity in Pd, Pd_7Li and Pd_2Li changes during the

hydrogen discharge. The results show that charges are obviously larger for electrodes with higher lithium concentration. Therefore, the order of hydrogen absorbing ability is PdLi > Pd_2Li > Pd_7Li > Pd.

However, the cathodic current seem to include not only discharging of hydrogen, but also a small amount of Li alloying of the electrode as described above. So, the amount of hydrogen calculated from the integration of the cathodic current seems to be an overestimation. To evaluate the contribution of the lithium alloying to the current, potential-charge curve was measured for each electrode without hydrogen charging, as shown in Fig. 5.4. The charges needed for attaining an electrode potential of 0.20 V at 10 mA cm^{-2} are 5.0, 10, 5.4 and 0.4 C for Pd, Pd_7Li, Pd_2Li and PdLi electrodes, respectively. These values are smaller than the values observed in Fig. 5.3 because of the absence of hydrogen in the electrodes. Furthermore, these values are smaller than the value of 54.4 C which corresponds to the amount of Li to form a stoichiometric PdLi compound from the Pd electrode. This implies that the Li alloying reactions proceed only at the surface of the electrodes. Incidentally, the Li alloying reactions seem to be easier for the Pd_7Li electrode and the Pd_2Li electrode than for the Pd electrode. The main reason for this is that the Pd_7Li electrode and the Pd_2Li electrode were made by dissolution of lithium from PdLi electrodes. Table 5.4 shows the estimated composition and the H/Pd ratio for each electrode, after compensating for the charge resulting from the Li alloying. The Pd electrode shows a H/Pd ratio of 0.05. This value is larger than the reported value of 0.01 at a hydrogen pressure of 760 Torr at 673 K [15]. The difference is assumed to be due to the formation of a Pd-Li-H alloy at the surface layer. In Table 5.4, the H/Pd ratios for Pd_7Li, Pd_2Li and PdLi are 0.08, 0.27 and 0.74, respectively. These results show that a higher Li concentration enhances the hydrogen absorption. These characteristics for Pd-Li alloys can be explained by the stronger interaction of Li-H than of Pd-H.

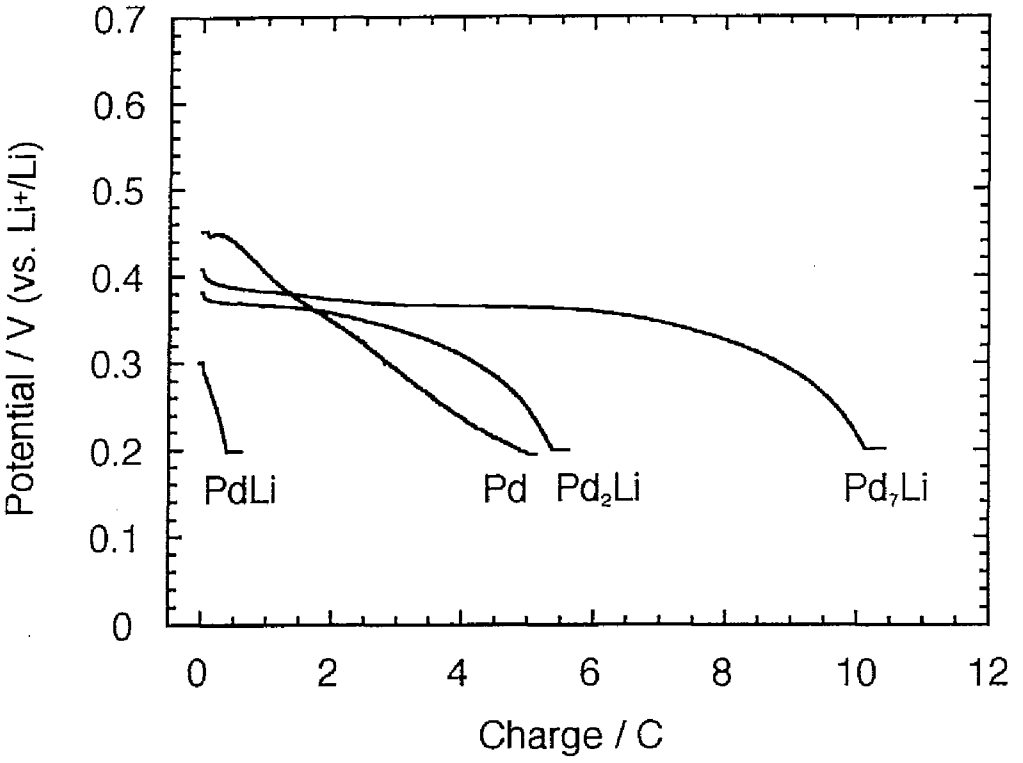

Fig. 5.5. Potential-charge curves for Pd, Pd_7Li, Pd_2Li and PdLi electrodes under a galvanostatic cathodic electrolysis in a molten LiCl-KCl-LiH system (5 mol% LiH added) at 673 K. Cathodic current density: 10 mA cm^{-2}.

Table 5.4. Hydrogen amounts in Pd and Pd-Li alloy electrodes after charging by potentiostatic electrolysis at 0.6 V for 0.5 hour.

Electrode	Composition	H / Pd
Pd	$PdH_{0.05}$	0.05
Pd_7Li	$Pd_7LiH_{0.56}$	0.08
Pd_2Li	$Pd_2LiH_{0.54}$	0.27
PdLi	$PdLiH_{0.74}$	0.74

Further studies were focused on the PdLi electrode which showed the best hydrogen absorbing ability. To discuss the rate of the electrochemical hydrogen desorption, chronopotentiometry was conducted at several discharging current densities. Hydrogen chargings were performed by potentiostatic electrolysis at 0.6 V for 0.5 hour. Figure 5.5 shows the obtained potential-charge curves at discharging current densities of 5, 10, 20 and 40 mA cm^{-2}. For curve a (5 mA cm^{-2}), curve b (10 mA cm^{-2}) and curve c (20 mA cm^{-2}), flat potential plateaus are observed at 0.38, 0.37 and 0.34 V, respectively. The potential difference among these plateaus are considered to arise from the overpotentials which are necessary to discharge hydrogen at the specific rates. Therefore, the value of the flat plateau potential is more negative for larger discharging current densities. Since a flat potential plateau means a presence of a co-existing phase of $PdLiH_x$ and PdLi at the surface of the electrode, as we descried earlier, the result indicates that the rate of hydrogen diffusion in the bulk alloy overtakes the rate of electrochemical hydrogen desorption at the surface. Supporting this, the amount of discharged hydrogen is almost the same value for the three different current densities. If one defines the hydrogen amount as 100 for curve a (5 mA cm^{-2}), then the hydrogen amount for curve b (10 mA cm^{-2}) and curve c (20 mA cm^{-2}) can be expressed as 97 and 96. On the contrary, the observed potential plateau for curve d (40 mA cm^{-2}) is not stable, and the hydrogen amount for the curve d is expressed as 70 referring to curve a (100). In curve d, the rate of hydrogen diffusion in the bulk alloy cannot overtake the rate of electrochemical hydrogen desorption at the surface. Therefore, the limiting value seems to be between 20 and 40 mA cm^{-2} for continuous electrochemical desorption of hydrogen. Accordingly, these results imply that the hydrogen amount estimated from a discharging current density of 10 mA cm^{-2} has a good accuracy.

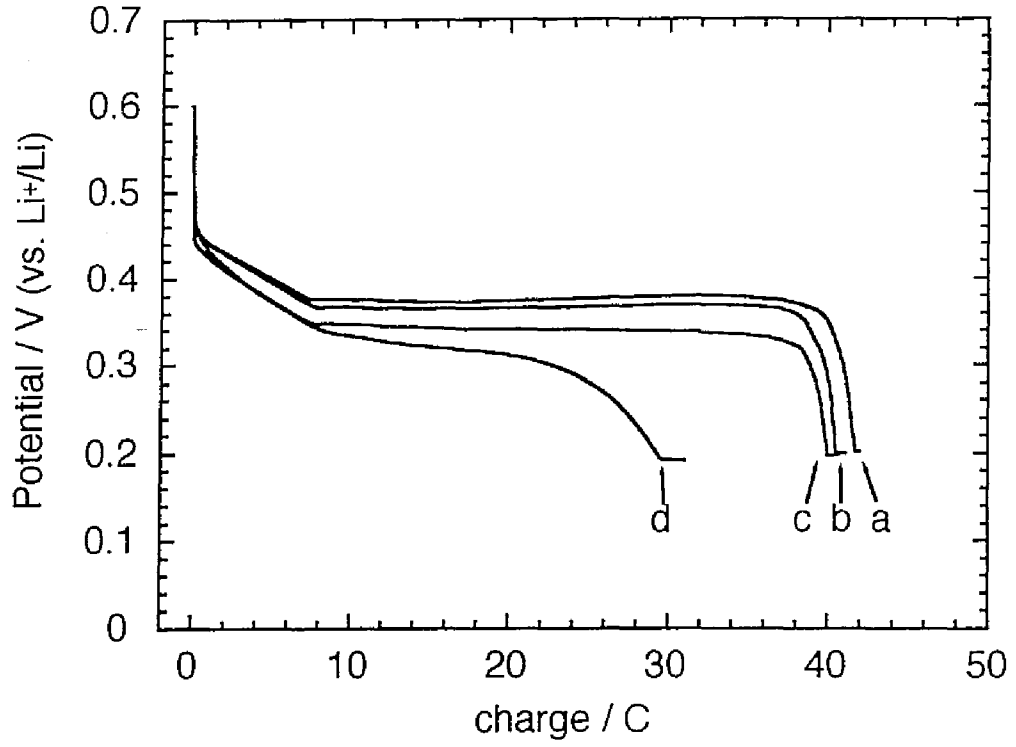

Fig. 5.5. Potential-charge curves for PdLi electrodes at various cathodic current densities in a molten LiCl-KCl-LiH system (5 mol% LiH added) at 673 K. After potentiostatic hydrogen charging at 0.6 V for 0.5 hour. Cathodic current density: (a) 5 mA cm^{-2}, (b) 10 mA cm^{-2}, (c) 20 mA cm^{-2} and (d) 40 mA cm^{-2}.

The effect of the charging potential on the amount of absorbed hydrogen was also studied for the PdLi electrode. Figure 5.6 shows the potential-charge curves at a discharging current density of 10 mA cm^{-2}, after charged by potentiostatic electrolysis at 0.55 V (curve a), 0.60 V (curve b) and 0.65 V (curve c) for 0.5 hour. Since curve a shows an almost flat potential plateau at around 0.39 V, the phase formed at 0.55 V is considered to be $PdLiH_x$. However, the amounts of hydrogen given by the H/Pd ratio is 0.56 for curve a, which is smaller than the value of 0.74 for curve b. This discrepancy is related to the fact that the total charges during anodic hydrogen charging were around 30 C and 250 C for curve a and curve b. That is, the electrochemical absorption of hydrogen into the PdLi electrode proceeds more

slowly at 0.55 V than at 0.60 V. This is consistent with that the hydrogen gas evolution starts at around 0.55 V as shown in Fig. 5.1. On the other hand, curve c has the first potential plateau at around 0.44 V and does not have a very flat region at around 0.38 V. This suggests the existence of hydrogen with higher activity or lithium with lower activity in the electrode at 0.65 V than those in the electrode at 0.60 V. A possible explanation is formation of $PdLi_yH_x$ ($y<1$), but this has not been reported. This issue is an interesting future subject.

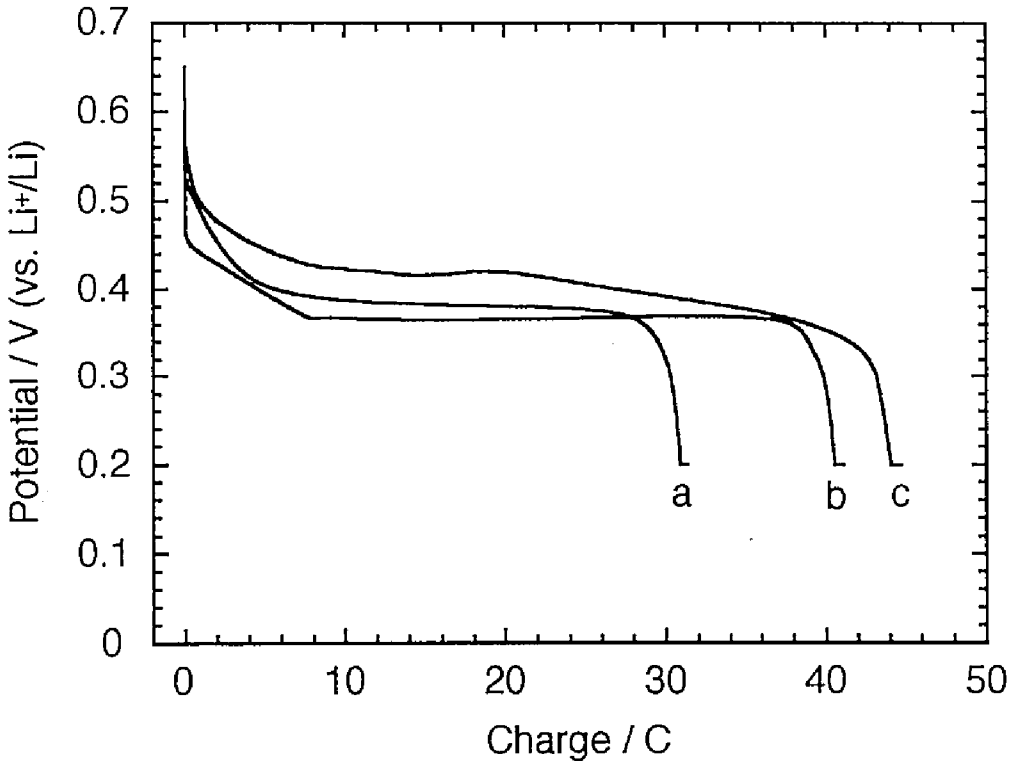

Fig. 5.6. Potential-charge curves for PdLi electrodes under a galvanostatic cathodic electrolysis in a molten LiCl-KCl-LiH system (5 mol% LiH added) at 673 K. After potentiostatic hydrogen charging at (a) 0.55 V, (b) 0.60 V and (c) 0.65 V for 0.5 hour. Cathodic current density: 10 mA cm^{-2}.

Since a flat potential plateau appears around 0.38 V during the electrochemical hydrogen desorption from $PdLiH_x$, the stable potential limit on the negative side for $PdLiH_x$ seems to be around 0.40 V considering the effect of overpotential. On the other hand, $PdLiH_x$ phase is stable at least to 0.60V from XRD analysis. The limit on the positive side seems to be between 0.60-0.65 V from the difference in the shapes of potential-charge curves.

5.4 Conclusions

Electrochemical hydrogen absorption and desorption into/from Pd and Pd-Li alloys were studied in a molten LiCl-KCl-LiH system. The results confirmed the validity of the electrochemical method using a molten LiCl-KCl-LiH system for studying the hydrogen behavior in the alloys at high temperature. The conclusions in this chapter can be summarized as follows:

(1) 5 mol% LiH gives sufficient hydrogen supplying ability for studying the hydrogen absorbing behavior of the electrodes.

(2) Pd spontaneously changes into $PdLiH_x$ by immersion into a molten LiCl-KCl-LiH system since anodic hydrogen absorption and cathodic lithium deposition occurs in the same potential range on a Pd electrode.

(3) From chronopotentiometry under hydrogen discharging, values of the H/Pd ratio for Pd, Pd_7Li, Pd_2Li and PdLi electrodes were found to be 0.05, 0.08, 0.27 and 0.74, respectively. These values show that the hydrogen absorbing ability for Pd-Li alloys is enhanced by increase of Li concentration in the alloy. This tendency can be explained by the stronger interaction of Li-H than of Pd-H.

(4) There seemed to be a limiting value between 20 and 40 mA cm^{-2} for continuous electrochemical desorption of hydrogen from a $PdLiH_x$ electrode.

(5) The rate of electrochemical hydrogen absorption into PdLi at 0.55 V is slower than that at

0.60 V. This is related to that hydrogen gas evolution starts around 0.55 V.

(6) $PdLiH_x$ phase is stable from around 0.40 to at least 0.60V. The stable potential limit for the positive side seems to be between 0.60-0.65 V.

References

[1] H. H. Barschall, in *Neutron Sources for Basic Physics and Applications*, S. Cierjacks, Editor, p. 57, Pergamon Press (1983).

[2] R. E. Shearer and R. C. Werner, J. Electrochem. Soc. **105,** 693 (1958).

[3] P. Roy, S. A. Salamah, J. Maldonado and R. S. Narkiewicz, AIP Conf. Proc. **271,** 913 (1993).

[4] M. L. Doyle and I. R. Harris, *Platinum Metals Rev.* **32,** 130(1988).

[5] B. Y. Liaw, P.-L. Tao, P. Turner and B. E. Liebert, *J. Electroanal. Chem.* **319,** 161(1991).

[6] B. Y. Liaw, G. Deublein and R. A. Huggins, *J. Electrochem. Soc.* **142,** 2196(1995).

[7] Y. Fukai, *The Metal-Hydrogen System*, Springer-Verlag (1993).

[8] B. Nacken and W. Bronger, *J. Less-Common Met.* **52,** 323(1977).

[9] Y. Sakamoto, T. Hisamoto, M. Ura and R. Nakamura, *J. Alloys Comp.* **200,** 141(1993).

[10] O. Yamazaki, H. Yoshitake, N. Kamiya and K. Ota, *J. Electroanal. Chem.* **390,** 127(1995).

[11] G. Deublein and R. A. Huggins, *J. Electrochem. Soc.* **136,** 2234(1989).

[12] D. Noreus and O. Rapp, *Physical Review B* **42,** 10730(1990).

[13] S. Yamanaka, T. Matsuura and M. Miyake, *Z. Phys. Chem.* **179,** 103(1993).

[14] O. Loebich, Jr. and Ch. J. Raub, *J. Less-Common Met.* **55,** 67(1977).

[15] R. Burch and N. B. Francis, *J. Chem. Soc.* **69,** 1978(1973).

Chapter 6

Electrode Behavior of Si and Evolution of SiH_4 in Molten LiCl-KCl-LiH Systems*

6.1 Introduction

6.1.1 SiH_4

Monosilane, SiH_4, is important material gas in the field of Si semiconductors, because purification of Si is conducted by decomposition of SiH_4 gas [1]. Especially, low cost SiH_4 production is crucial for mass production of inexpensive Si solar cells.

The melting and boiling points of SiH_4 are 88 K and 161 K, respectively [2]. SiH_4 gas is colorless, odorous and toxic. Since SiH_4 gas explosively reacts with O_2 or Cl_2, the handling of SiH_4 requires special cautions. The SiH_4 molecule has a tetrahedral structure with a Si-H bond length of 1.48 Å [2]. The Si-H bond is covalent, however, the bond strength is weak. Therefore, SiH_4 decomposes nearly completely into Si and H_2 at temperatures higher than 873 K [1]

$$SiH_4 \rightarrow Si + 2\,H_2 \qquad (1)$$

The purification of Si is carried out by utilizing this reaction.

6.1.2 Conventional methods of SiH_4 production

In this section, the major conventional method of SiH_4 production (Union Carbide

---

* To be submitted to *J. Electrochem. Soc.*

Method) is first mentioned as a reference. A conventional method using molten chloride, which is related to the novel method presented in the following section, is described next.

The method using catalytic disproportionation of chlorosilane

The method was developed into practical use by Union Carbide Corporation. It is the largest scale method of SiH_4 production in the world at present [3].

A mixture of H_2 and $SiCl_4$ reacts with a metal grade Si (98%) in a fluidized bed at 773 K using a copper catalyst:

$$3\ SiCl_4 + Si + 2\ H_2 \rightleftharpoons 4\ SiHCl_3 \qquad (2)$$

Gas mixture is separated into $SiCl_4$ and $SiHCl_3$ by a rectifier. Then, the $SiHCl_3$ is transported to the first disproportionation reactor which has an amine catalyst. The following reaction progresses at around 600 K:

$$2\ SiHCl_3 \rightleftharpoons SiCl_4 + SiH_2Cl_2 \qquad (3)$$

SiH_2Cl_2 is subsequently conveyed to a second disproportionation reactor, also with an amine catalyst. The disproportionation reaction is expressed as

$$3\ SiH_2Cl_2 \rightleftharpoons 2SiHCl_3 + SiH_4 \qquad (4)$$

Finally, SiH_4 is extracted and $SiHCl_3$ is returned to the former rectifier.

Since this method is conducted by a chemical plant, it is suitable for mass production. However, it requires a lot of energy and a large space, because it proceeds by a multistage reaction of gas materials at high temperatures. Furthermore, since there is a large amount of chlorosilane to be taken care of, a special disposal facility is necessary to handle the large amount of chlorides.

The conventional molten salt method

The conventional SiH_4 production method using molten salt electrolysis was first proposed by Sundermeyer in 1965 [4]. When $SiCl_4$ is introduced to molten LiCl-KCl-LiH, SiH_4 is produced by the following reaction:

$$4\,LiH + SiCl_4 \rightarrow SiH_4 + 4\,LiCl \qquad (5)$$

The consumed LiH and $SiCl_4$ are produced by hydrogenation of Li and chlorination of Si, respectively. Thus, if Li and Cl_2 are prepared by electrolysis of molten LiCl-KCl, a completely closed recycling system can be constructed. The method has advantages due to its high reaction rate and high SiH_4 purity.

Industrialization of the method was attempted by Yatsurugi *et al.* in 1980s [5]. Figure 6.1 shows the test apparatus for commercializing investigation of the method. However, the practical use has not yet been attained because of the complexity of the apparatus.

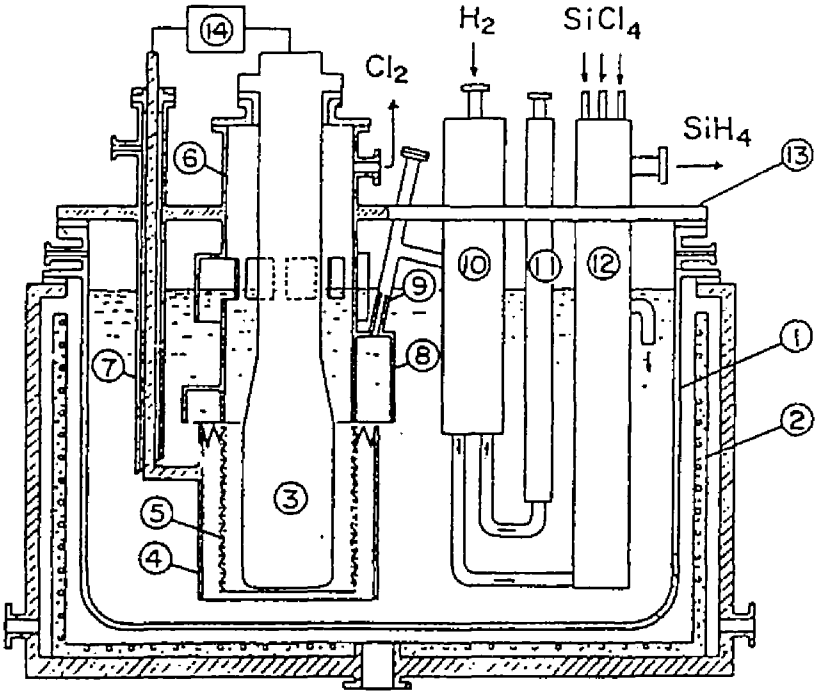

Fig. 6.1. Test apparatus for the conventional molten salt method developed by Yatsurugi *et al.* [5]. (1) molten salt vessel, (2) heater, (3) anode, (4) cathode, (5) diaphragm, (6) anode chamber, (7) outer jacket and cathode lead bar, (8) Li collector, (9) Li transport tube, (10) hydrogenation chamber, (11) salt pump, (12) silane reactor, (13) salt bath rid and (14) electrolytic power source.

6.1.3 A novel method of SiH_4 production

6.1.3.1 Principle

Based on the principle of the conventional SiH_4 production method using molten salts, the author examined the possibility of developing a novel SiH_4 production method. Figure 6.2 illustrates a conceptual principle of the novel SiH_4 production method. A metal grade Si electrode is used as an anode in a molten LiCl-KCl-LiH system. SiH_4 is thought to evolve directly by anodic oxidation of H^- ion on a Si electrode. In addition, chlorosilanes (SiH_3Cl, SiH_2Cl_2, $SiHCl_3$ and $SiCl_4$) might be produced by anodic oxidation of H^- ion and Cl^- ion. In this case, the chlorosilanes are thought to immediately react with H^- ion to produce SiH_4.

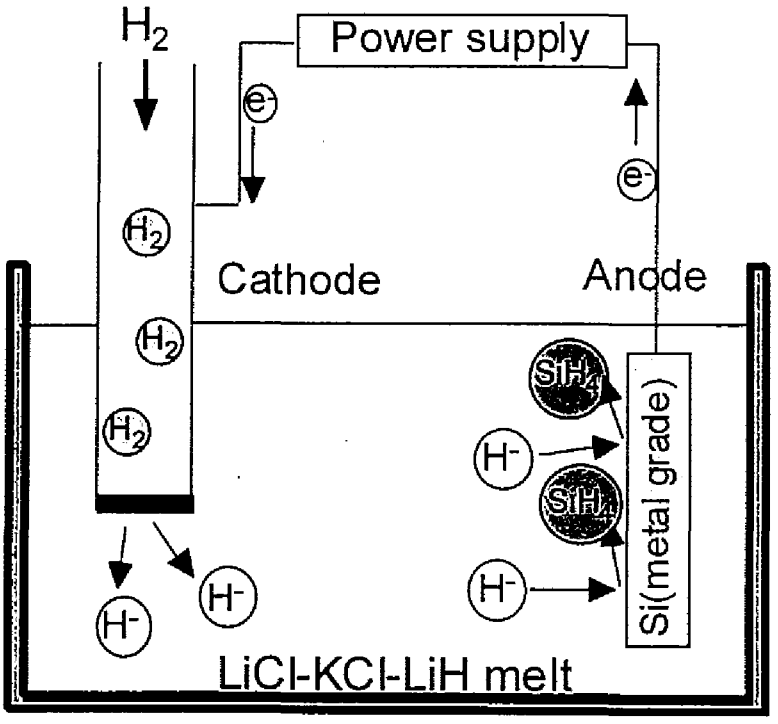

Fig. 6.2. Conceptual representation of a novel SiH_4 production method.

Therefore, a resultant reaction at the anode side can be expressed as

$$Si + 4\,H^- \rightarrow SiH_4 + 4\,e^- \quad (6)$$

The consumed H^- ion is directly supplied by the cathodic reduction of H_2 gas using a gas electrode:

$$H_2 + 2\,e^- \rightarrow 2\,H^- \quad (7)$$

Thus, total reaction is

$$Si + 2\,H_2 \rightarrow SiH_4 \quad (8)$$

The special feature of the method is the simplicity of the apparatus because SiH_4 is directly produced at the anode and H^- ion are directly supplied from the cathode. Furthermore, lower energy consumption than the conventional molten salt method can be expected because the reaction proceeds without Li deposition nor Cl_2 evolution. Therefore, the method seems very promising and worth studying as a novel and low cost SiH_4 production method.

6.1.3.2 Thermodynamic consideration

The possibility of the novel SiH_4 production method is examined from a thermodynamical point of view. From the analogy with a potential-pH diagram (Pourbaix diagram) in an aqueous solution, a potential-pH^- diagram is constructed for the Si system in a LiCl-KCl eutectic melt at 723 K. Standard free energies of formation for silane and chlorosilane gases at 723 K are estimated from reported values at 700 K and 800 K [6], assuming temperature independent entropy. They are listed in Table 6.1. The equilibrium potential of the H_2/H^- couple, $E^0_{H_2/H^-} = 0.25$ V (vs. Li^+/Li), is from the result presented in chapter 2. The equilibrium potential of the Cl_2/Cl^- couple, $E^0_{Cl_2/Cl^-} = 3.626$ V, is from the literature [7] (The pressure and concentration units are *atm* and *mole fraction* in all cases). Using these data, the following equations are obtained for corresponding reactions:

(1) $SiH_4 + 4\,e^- \rightleftharpoons Si + 4\,H^-$ $\qquad E = 0.494 + 0.143\ pH^-$

(2) $SiHCl_3 + 4\,e^- \rightleftharpoons Si + 3\,H^- + Cl^-$ $\qquad E = 0.879 + 0.107\ pH^-$

(3) $SiH_2Cl_2 + 4\,e^- \rightleftharpoons Si + 2\,H^- + 2\,Cl^-$ $\qquad E = 1.276 + 0.0715\ pH^-$

(4) $SiHCl_3 + 4\ e^- \rightleftharpoons Si + H^- + 3\ Cl^-$ $E = 1.696 + 0.0358\ pH^-$

(5) $SiCl_4 + 4\ e^- \rightleftharpoons Si + 4\ Cl^-$ $E = 2.158$

(6) $Cl_2 + 2\ e^- \rightleftharpoons 2\ Cl^-$ $E = 3.626$ [7]

(7) $H_2 + 2\ e^- \rightleftharpoons 2\ H^-$ $E = 0.25 + 0.143\ pH^-$

where E is potential (V vs. Li^+/Li) and pH^- is $-\log(a_{H^-})$. a_{H^-} is the activity of H^- ion (mole fraction). The potential-pH^- diagram of the Si system is constructed as shown in Fig. 6.3. Each line with a specified number corresponds to one of the reactions described above. SiH_4 evolution, line (1), is about 0.25 V more positive than H_2 evolution, line (7), as seen in Fig. 6.3. When a Si electrode is anodically polarized, it is thought that H_2 evolution first occurs followed by evolution of SiH_4 and SiH_3Cl, etc. However, the actual current sharing ratio is determined by each reaction kinetics. Thus, SiH_4 evolution is thought to be affected by a surface state of the electrode, an electrode potential, a H^- ion concentration, etc.

Table 6.1. Standard free energy of formation for silane and chlorosilane gas at 723 K.

Gas	ΔG_f^0 (at 723 K) kJ mol^{-1}
SiH_4	94.9
SiH_3Cl	-82.4
SiH_2Cl_2	-255.3
$SiHCl_3$	-419.0
$SiCl_4$	-566.7

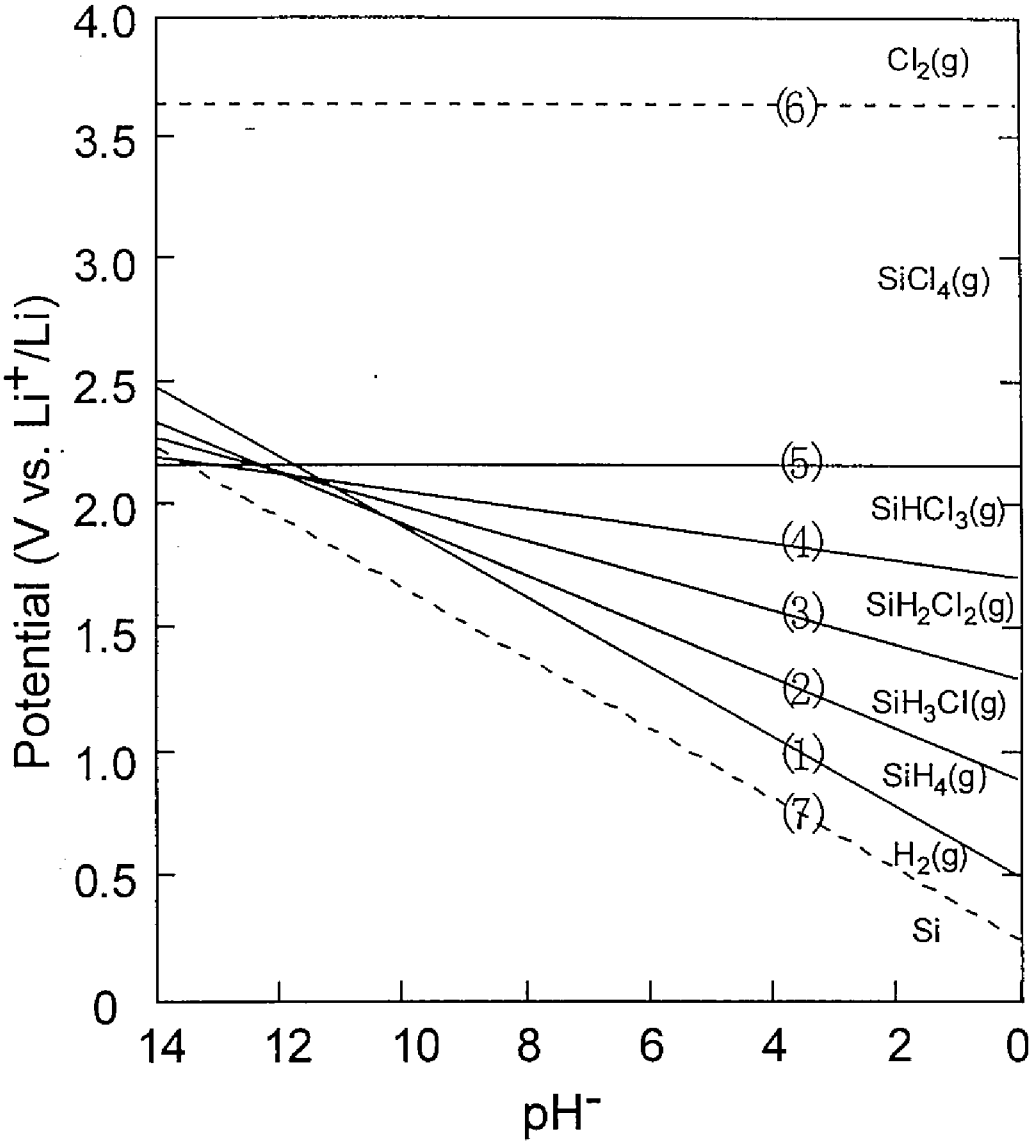

Fig. 6.3. Potential-pH$^-$ diagram of the Si system in a LiCl-KCl eutectic melt at 723 K. Unit: mole fraction.

There seems to be no report which deals with the anodic behavior of a Si electrode in a LiCl-KCl eutectic melt. In order to study the novel method of SiH_4 production, this chapter describes the electrode behavior of Si and the SiH_4 evolution in molten LiCl-KCl-LiH systems. Single crystal Si (Miller indices 100) was first used as working electrode to investigate the electrode behavior of pure Si. Furthermore, metal grade Si (98%) was studied due to its low cost and thereby following interest for practical applications. The effect of F^- ion addition on the SiH_4 evolution reaction was also examined. Finally, some considerations both on the reaction scheme and on current efficiency for the SiH_4 evolution were made.

6.2 Experimental

Electrolysis cell and chemicals

Figure 6.4 illustrates the electrolysis cell. The details concerning the experimental apparatus have already been described in chapter 2. Therefore, some points are described below. The LiCl-KCl eutectic melt (LiCl:KCl = 58.5:41.5 mol%, m.p. 625 K; reagent grade, Wako Pure Chemical Co., Ltd.) was used as a solvent and LiH (Wako Pure Chemical Co., Ltd., 95 %) was directly added to the melt as a H^- ion source. LiF (Wako Pure Chemical Co., Ltd., 98 %) was also added as a F^- ion source.

Electrodes

Figure 6.5 shows schematic drawing of the electrode structure. The working electrode was either a square-shaped sheet of single crystal Si (ca. 30 mm x 5 mm x 0.2 mm, Miller indices 100, resistivity is 1.5-3.0 x 10^{-3} Ω cm) or a rod of metal grade Si (ca. 30 mm x ϕ5 mm, Wako Pure Chemical Co., Ltd., 98%). According to the supplier, impurities in the metal grade Si are thought to be Fe (<0.7 %), Al (<0.2 %), C (<0.1 %), P (<0.05 %) and S (<0.05 %). A Ni wire was used as a current lead and sufficient ohmic contact was achieved by winding an

Ag wire tightly around the Ni and Si. To prevent anodic dissolution of lead materials, only the tip of the Si electrodes was dipped into the melt. The counter electrode was a glassy carbon rod (70 mm x ϕ5 mm, Tokai Carbon Co., Ltd.) or an Al rod (70 mm x ϕ4 mm, Nilaco Corp., 99.99 %). The reference electrode was an Al-Li alloy in the coexisting (α+β) phase state prepared electrochemically from an Al wire (10 mm x ϕ1 mm, Nilaco Corp., 99.99 %).

Measurement and control systems

Figure 6.6 describes the measurement and control systems. The electrolysis cell was operated in a furnace attached to the base of an argon glove box with gas circulating purifier (MBN-R-07; Japan Pionics Co., Ltd.), resulting in a water contamination level less than 1 ppm. Chromel-Alumel thermocouples were used for both temperature measurement and control. The temperature was maintained within ± 1 K by a temperature control unit (DSM-2; Shimaden Co., Ltd.). A potentio/galvanostat (HZ-3000; Hokuto Denko Corp.) connected to a personal computer (FMVS31673; Fujitsu) was used for the cyclic voltammetry and potentiostatic electrolysis.

Analysis

The gas evolved by potentiostatic electrolysis was transported to the gas sampler. The sampled gas was analyzed by an infrared (IR) absorption spectrometer (BIORAD; FTS155). The concentration of SiH_4 in the sampled gas was conventionally measured by a gas detecting tube (Komyo Rikagaku Kogyo; 240 S). The principle of the gas detecting tube is

$$2\,HgCl_2 + SiH_4 \rightarrow 2\,Hg + Si + 4\,HCl \qquad (9)$$

When SiH_4 is introduced in the gas detecting tube which contains $HgCl_2$ and Methyl Orange, the extricated HCl changes the color of the Methyl Orange into red. Thus, the concentration of SiH_4 can be determined by the size of the red area. The surface of the Si electrode after electrolysis was examined by a scanning electron microscope (HITACHI; S-450).

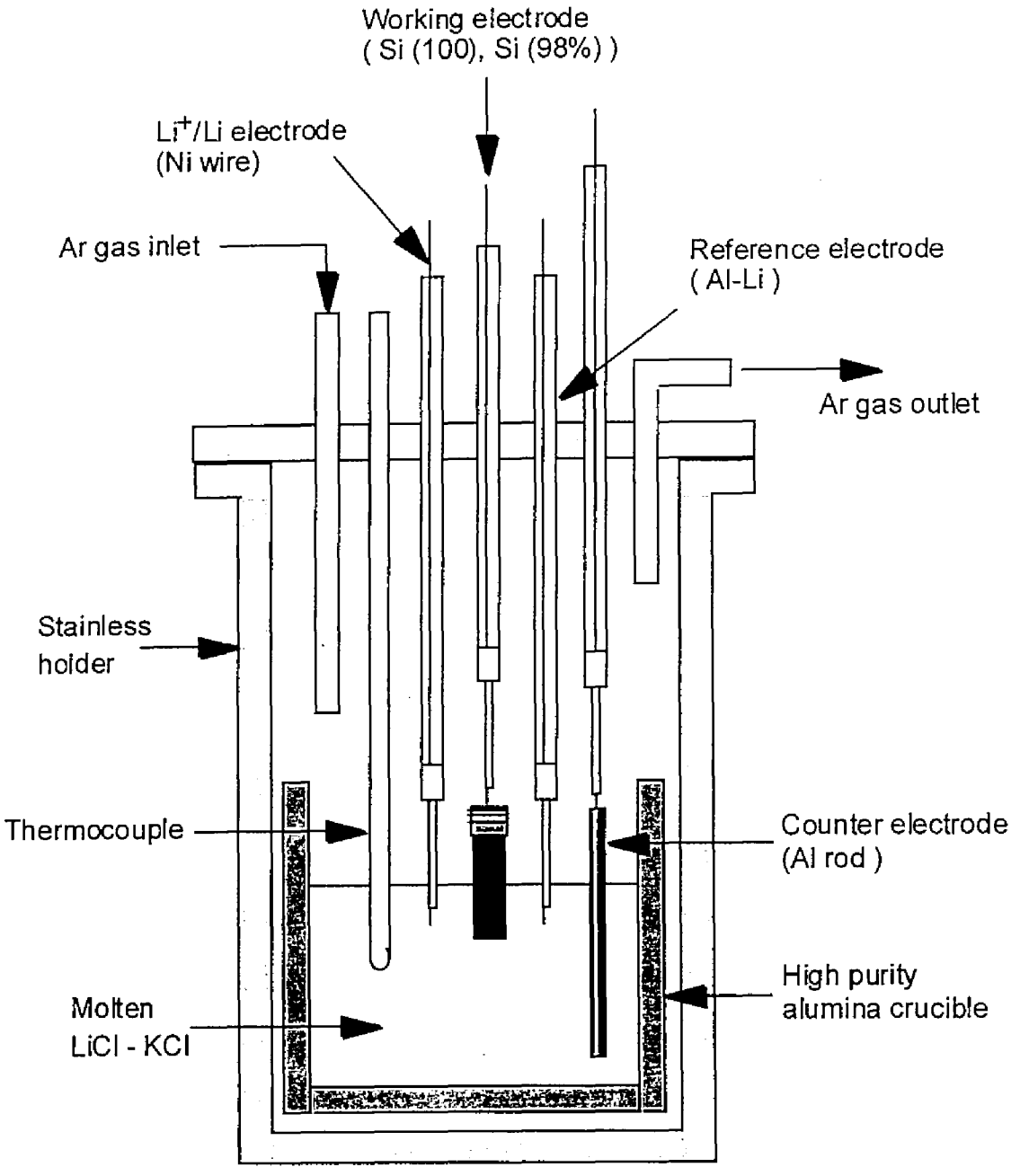

Fig. 6.4. Schematic drawing of the electrolysis cell.

(1) Working electrode

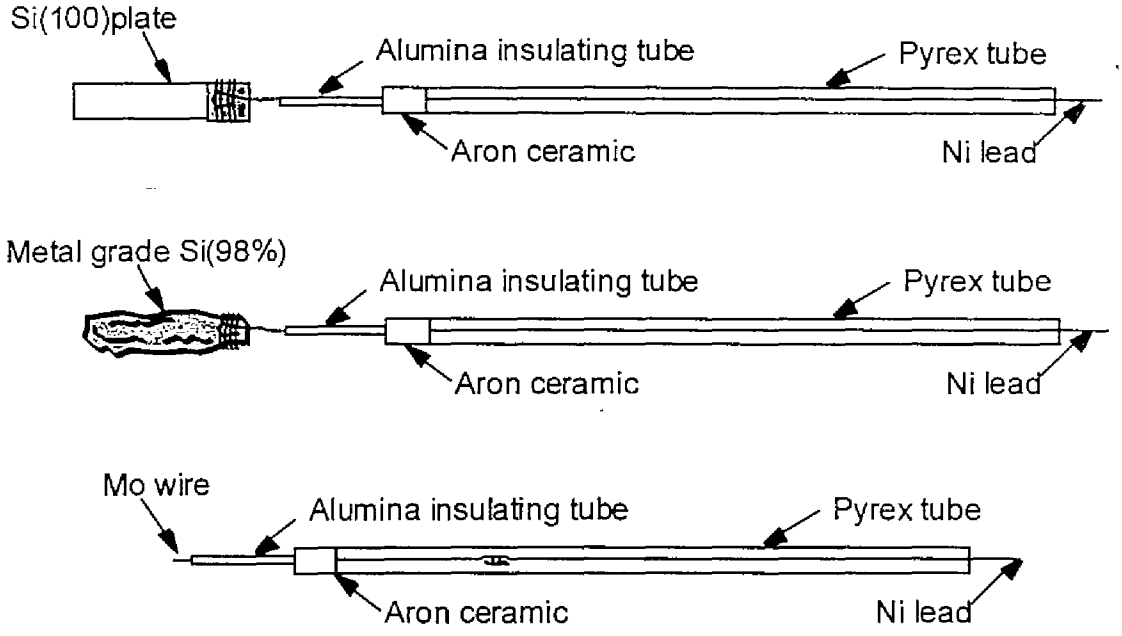

(2) Counter electrode

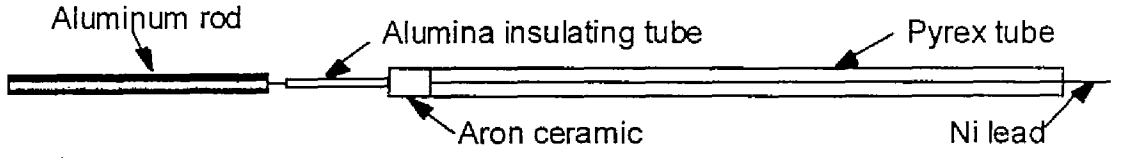

(3) Reference electrode (AlLi)

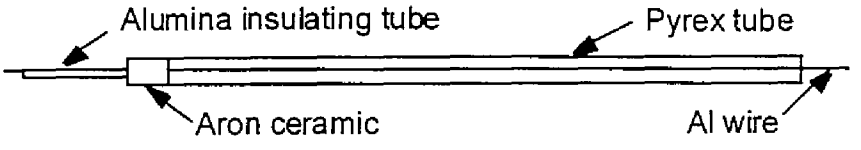

(4) Li^+/Li electrode

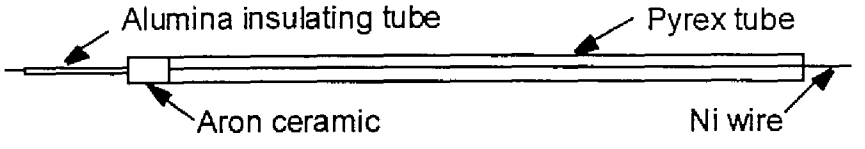

Fig. 6.5. Schematic drawing of the electrodes.

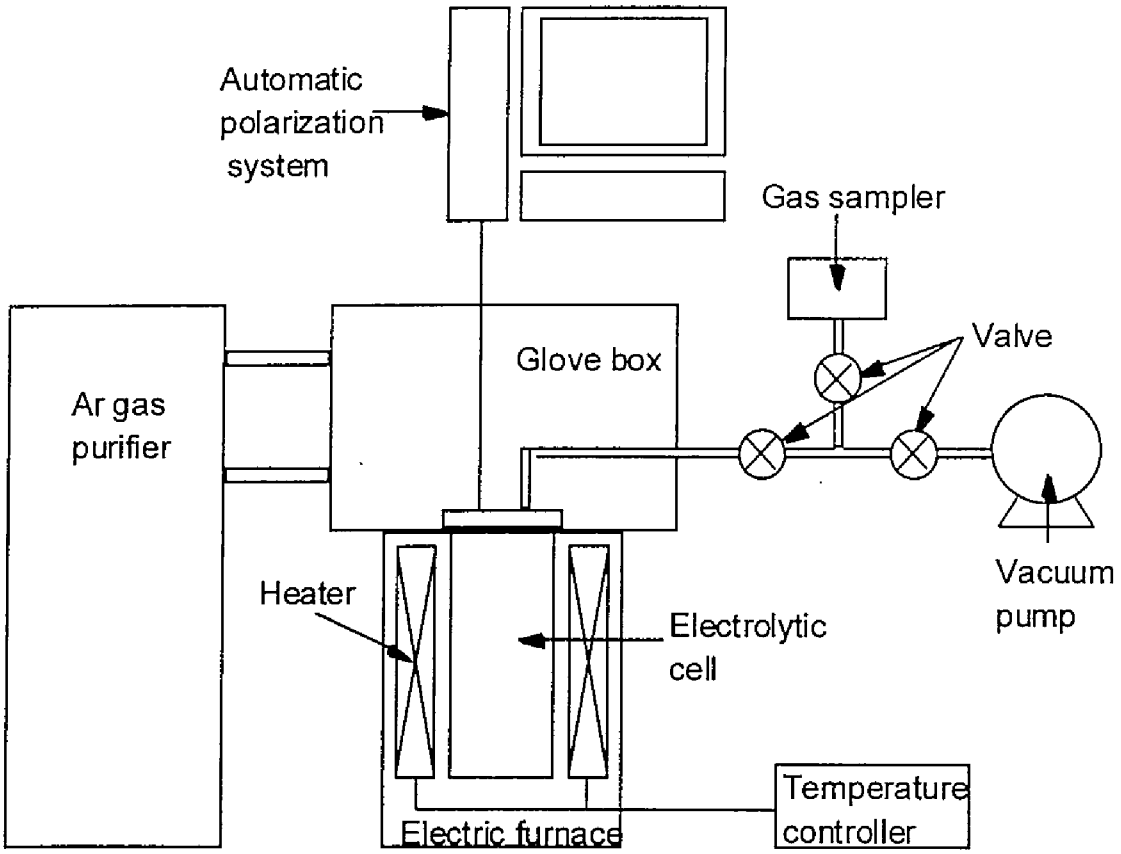

Fig. 6.6. Schematic drawing of the measurement and the control system.

6.3 Results and discussion

6.3.1 Behavior of a single crystal Si electrode

A single crystal Si was first used as a working electrode to investigate the electrode behavior of pure Si. Analysis methods employed were cyclic voltammetry for the electrode, IR absorption spectroscopy for the evolved gas and SEM measurement for the electrode surface.

6.3.1.1 Cyclic voltammetry

For all cyclic voltammograms obtained in this study, the potential scan started from the rest potential in positive direction. The direction was reversed at 6.8 V (vs. Li^+/Li). A new Si electrode was used for each experiment. Cyclic voltammograms were continuously measured for five cycles for the same electrode. The scan rate was kept constant at 0.05 V s^{-1}.

Blank

As a blank measurement, cyclic voltammetry was conducted in a LiCl-KCl eutectic melt at 673 K (Fig. 6.7). There are hardly any anodic currents even in the region more positive than the Cl_2/Cl^- potential (3.63 V). This might be explained by the formation of a Si-Cl passivation film on the electrode. Single crystal Si has been reported to produce a Si-Cl passivation film in a Cl_2 gas atmosphere [8].

In a molten LiCl-KCl-LiH(5 mol%) system

Figure 6.7 also shows cyclic voltammograms obtained after the addition of 5 mol% LiH. In the forward scan of the first cycle, the anodic currents increase until 1.2 V, which is thought to correspond to the anodic oxidation of H^- ion and thereby following H_2 gas evolution. The anodic currents then decrease rapidly, indicating the formation of a passivation

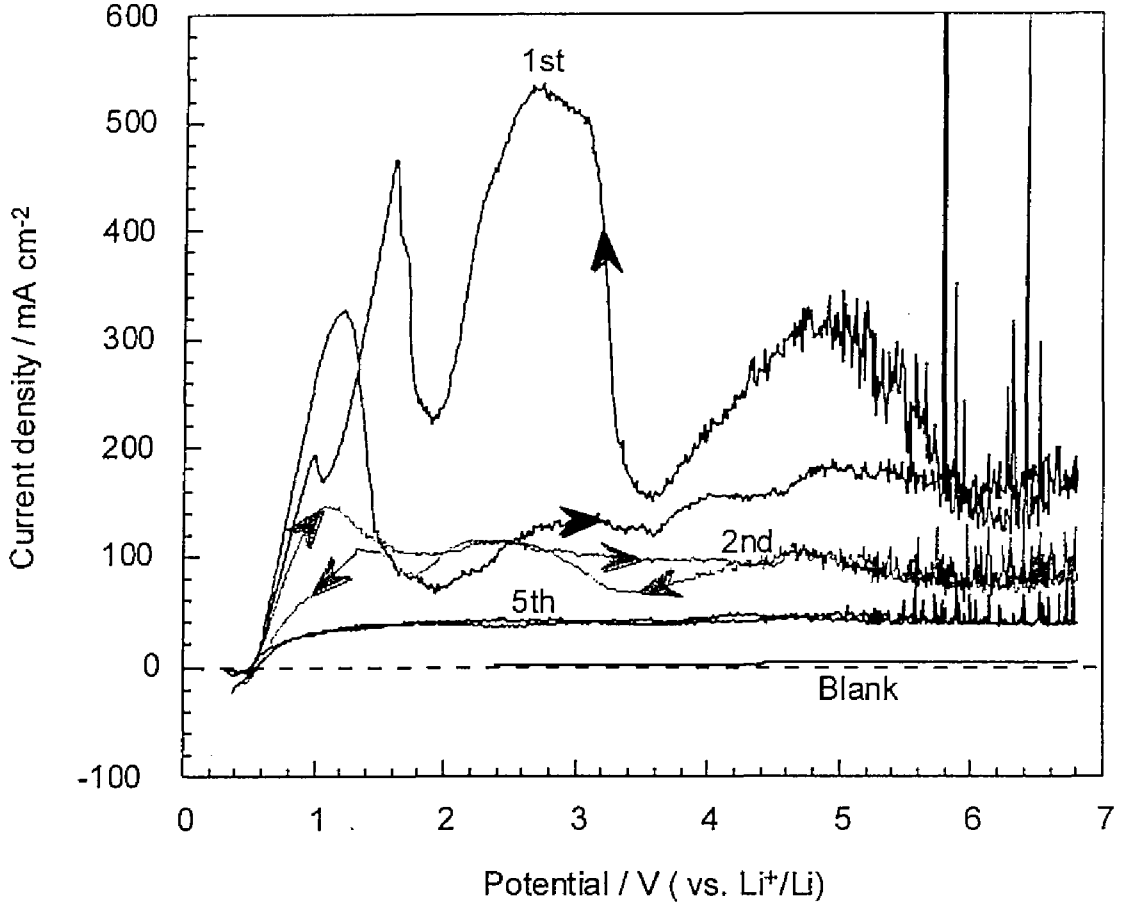

Fig. 6.7. Cyclic voltammograms for a single crystal Si (100) electrode in a LiCl-KCl eutectic melt and a molten LiCl-KCl-LiH(5 mol%) system at 673 K. Scan rate: 0.05 V s^{-1}.

film. There is evidence in the literature that Si absorbs a certain amount of hydrogen, and then the electrical conductivity of the Si-H layer decreases as the H concentration increases [9]. Thus, the Si-H passivation film was probably formed in addition to the Si-Cl passivation film. From around 5.8 V, the currents start fluctuating largely, which suggests the breakdown of the passivation film. This breakdown is thought to be due to the reaction of Cl^- ion. Subsequently, the newly produced surface is thought to electrochemically react with H^- and Cl^- ions, which is seen as the large current increase in Fig. 6.7. After the reversal of the scan direction, anodic current peaks appear at around 5.0, 2.7 and 1.6 V, respectively. Though the actual corresponding reactions have not been cleared yet, they might correspond to any formation of

$SiHCl_3$, SiH_2Cl_2, SiH_3Cl or SiH_4. These currents are thought to appear in the reverse scan because the surface state changed by the breakdown of the passivation film in the most positive potential region. In the second voltammogram cycle, the anodic currents and also the fluctuations decrease at all potentials (gray curve in Fig. 6.7). This can be explained by the growth of the passivation film. In the fifth and final cycle, the currents decrease further to around 40 mA cm^{-2} (Fig. 6.7).

In a molten LiCl-KCl-LiF(1 mol%)-LiH(5 mol%) system

In order to investigate the effect of F^- ion addition, 1 mol% LiF was added to the melt, and cyclic voltammograms were measured, shown in Fig. 6.8. In the forward scan of the first

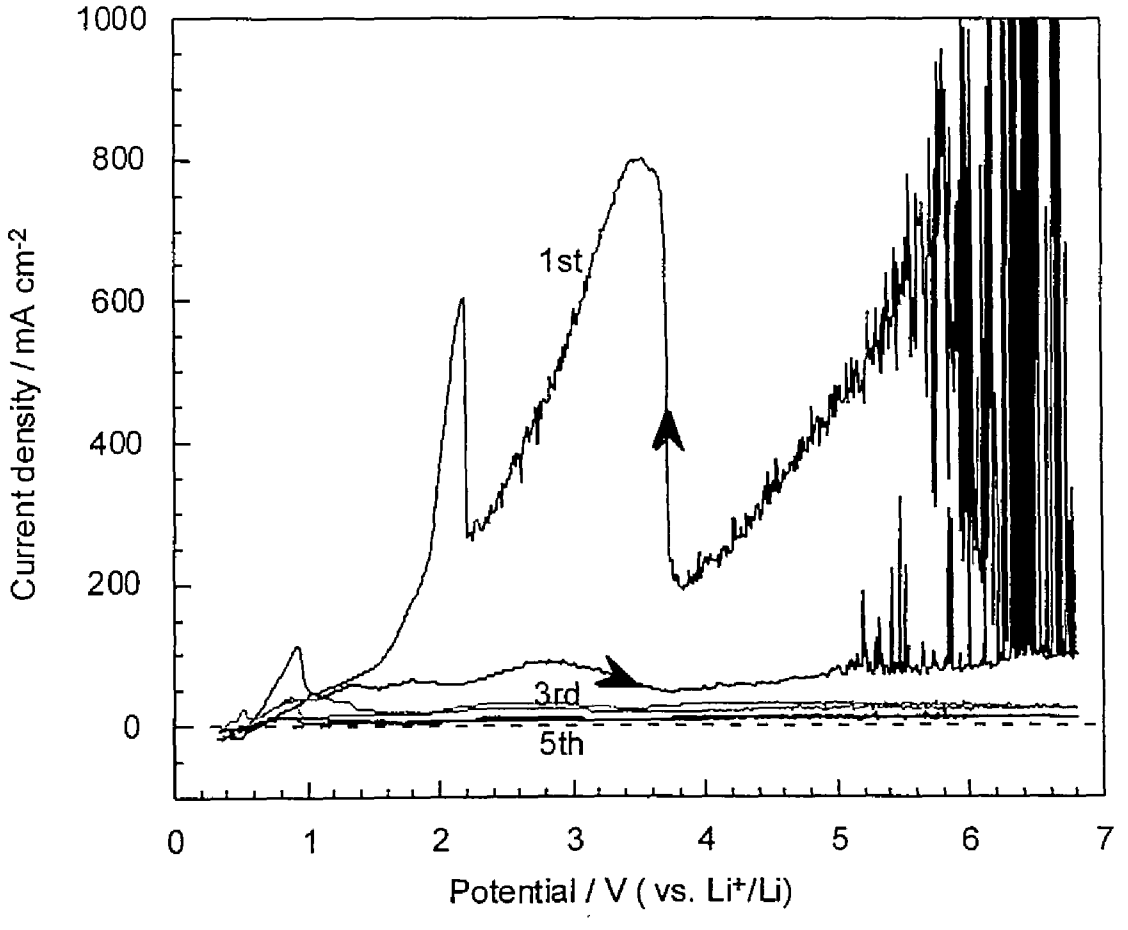

Fig. 6.8. Cyclic voltammograms for a single crystal Si (100) electrode in a molten LiCl-KCl-LiF(1 mol%)-LiH(5 mol%) system at 673 K. Scan rate: 0.05 V s^{-1}.

cycle, an anodic current peak is observed around 0.9 V, which is regarded as the oxidation of H^- ion to H_2 gas. After the peak, anodic currents decrease to around 50 mA cm^{-2}, indicating the formation of a passivation film. From 5.0 V, current fluctuations start and gradually become larger. After reversing the scan direction, fluctuations larger than 1 A cm^{-2} are observed until 5.0 V, suggesting the intense breakdown of the passivation film. In the reverse scan, there are anodic current peaks at around 5.6, 3.5 and 2.2 V, despite they did not appear in the forward scan. They might correspond to formation of $SiHCl_3$, SiH_2Cl_2, SiH_3Cl or SiH_4, being similar to the case shown in Fig. 6.7. The third and fifth cyclic voltammograms are also shown in Fig. 6.8. As the cycles are repeated, the currents decrease more drastically than for the case with no F^- ion addition. Therefore, the passivation film is thought to grow faster when F^- ion is added.

Comparison

To clarify the effect of F^- ion addition, two of the obtained voltammograms are compared, as shown in Fig. 6.9. The major difference is that current fluctuations at most positive regions are larger and more intensive in the case of F^- ion addition. Moreover, the anodic current peaks in the reverse scan for the F^- ion addition case are around 1.5 times larger than the peaks for the no addition case. These differences show that the breakdown and dissolution of the Si electrode are promoted by the F^- ion addition.

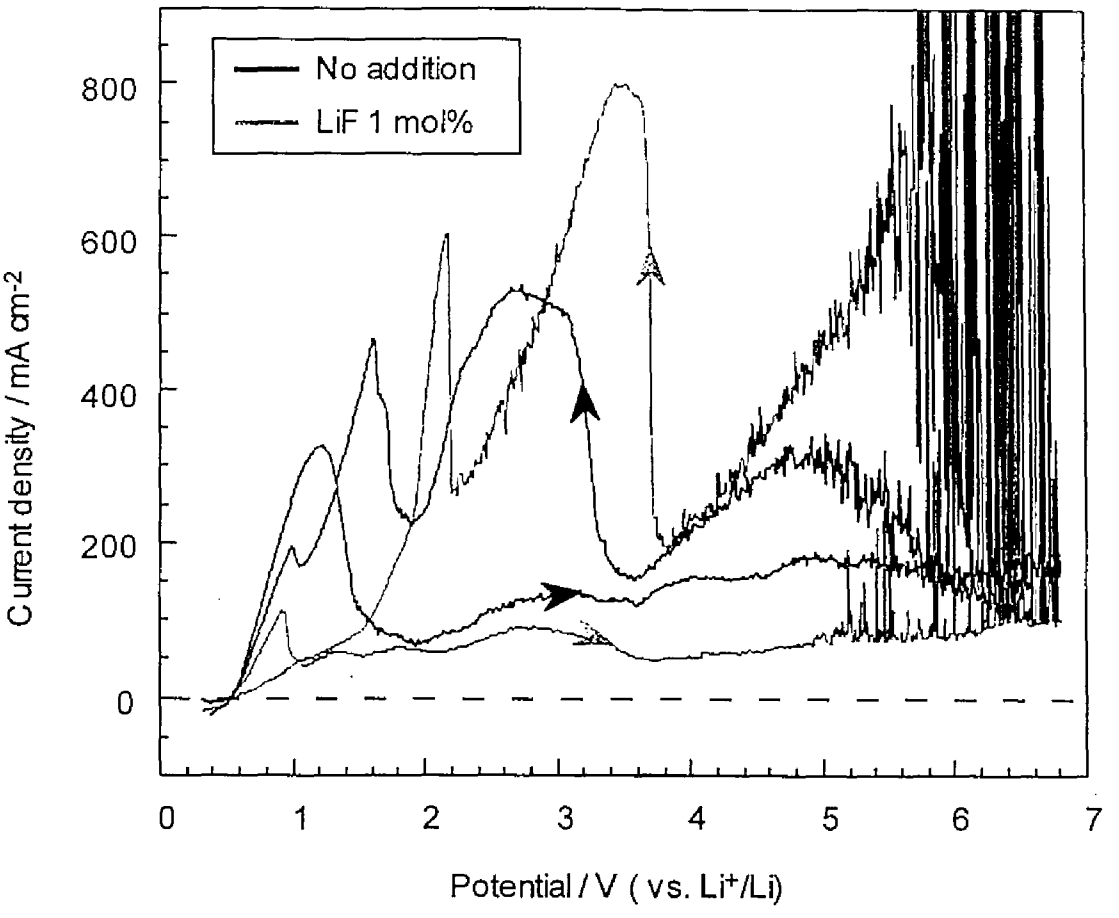

Fig. 6.9. Comparison of first cycle voltammograms for a single crystal Si (100) electrode in a molten LiCl-KCl-LiH(5 mol%) system and in a molten LiCl-KCl-LiF(1 mol%)-LiH(5 mol%) system. Scan rate: 0.05 V s^{-1}.

6.3.1.2 Gas analysis by IR absorption spectroscopy

Based on the cyclic voltammetry results, the gas samples were prepared by potentiostatic electrolysis at several selected potentials (1.8, 2.8, 3.8, 4.8 and 6.8 V). The gas samples were then analyzed by IR absorption spectroscopy. All figures have the same transmittance scale making direct comparisons of the transmittance possible. The total quantity of electricity during each electrolysis was adjusted to 100 C for direct comparison of the results.

It is worth noting the condition of the Si electrode. From several experiments, the

following phenomenon has been confirmed: if the electrode is once passivated, anodic currents do not flow intensively even in the most positive potential region. On the other hand, after the electrode has been kept at current fluctuating regions, the behavior of the electrode is again similar to a new Si electrode. Therefore, a Si electrode which was regarded as not being passivated was used in all experiments described below.

In a molten LiCl-KCl-LiH(5 mol%) system

Figure 6.10 shows the IR spectra of the gas samples obtained in a molten LiCl-KCl-LiH(5 mol%) system. IR spectra for 3.8, 4.8 and 6.8 V show the absorption peaks at 2190 and

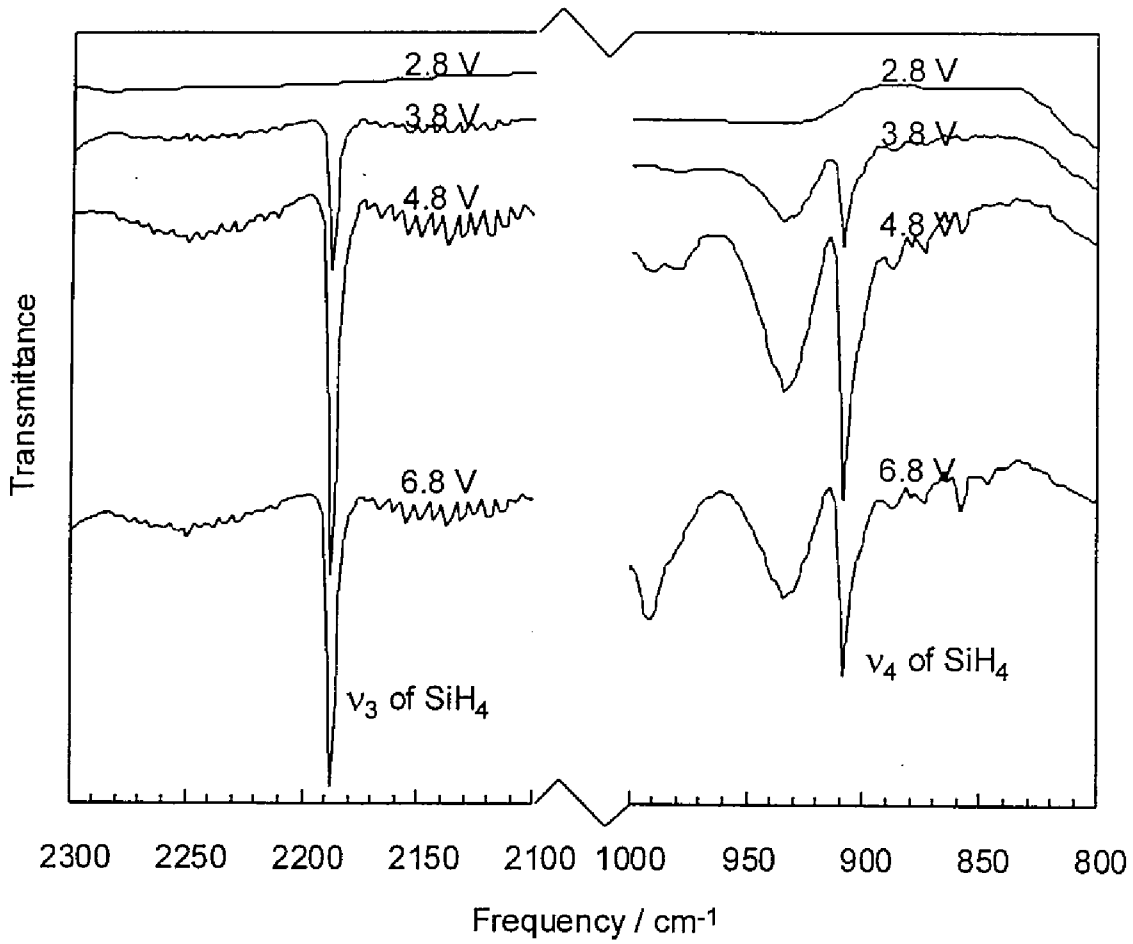

Fig. 6.10. IR spectra of gas samples obtained after potentiostatic electrolysis of a single crystal Si (100) electrode in a molten LiCl-KCl-LiH(5 mol%) system at 673 K. Total charge of each electrolysis is 100 C.

910 cm^{-1}. They correspond to the ν_3 (2192 cm^{-1}) and ν_4 (910 cm^{-1}) modes of SiH_4 vibration [10]. However, absorption peaks for SiH_3Cl, SiH_2Cl_2, $SiHCl_3$ and $SiCl_4$ are not observed in the spectra. This might be due to the fast SiH_4 producing reactions from chlorosilanes and H^- ion. Judging from the height of the absorption peaks, the amount of SiH_4 is considered to be larger for 4.8 and 6.8 V than for the other potentials.

In a molten LiCl-KCl-LiF(1 mol%)-LiH(5 mol%) system

The analysis was repeated after the addition of 1 mol% LiF to the melt (Fig. 6.11). In this case, a very small amount of SiH_4 was confirmed even at 2.8 V. Furthermore, large SiH_4 absorption peaks are observed also at potentials more positive than 3.8 V. The heights of these peaks are about 1.5 times larger than the heights in the no addition cases. The results indicate that the F^- ion addition is advantageous for the SiH_4 evolution, consistent with the cyclic voltammetry results.

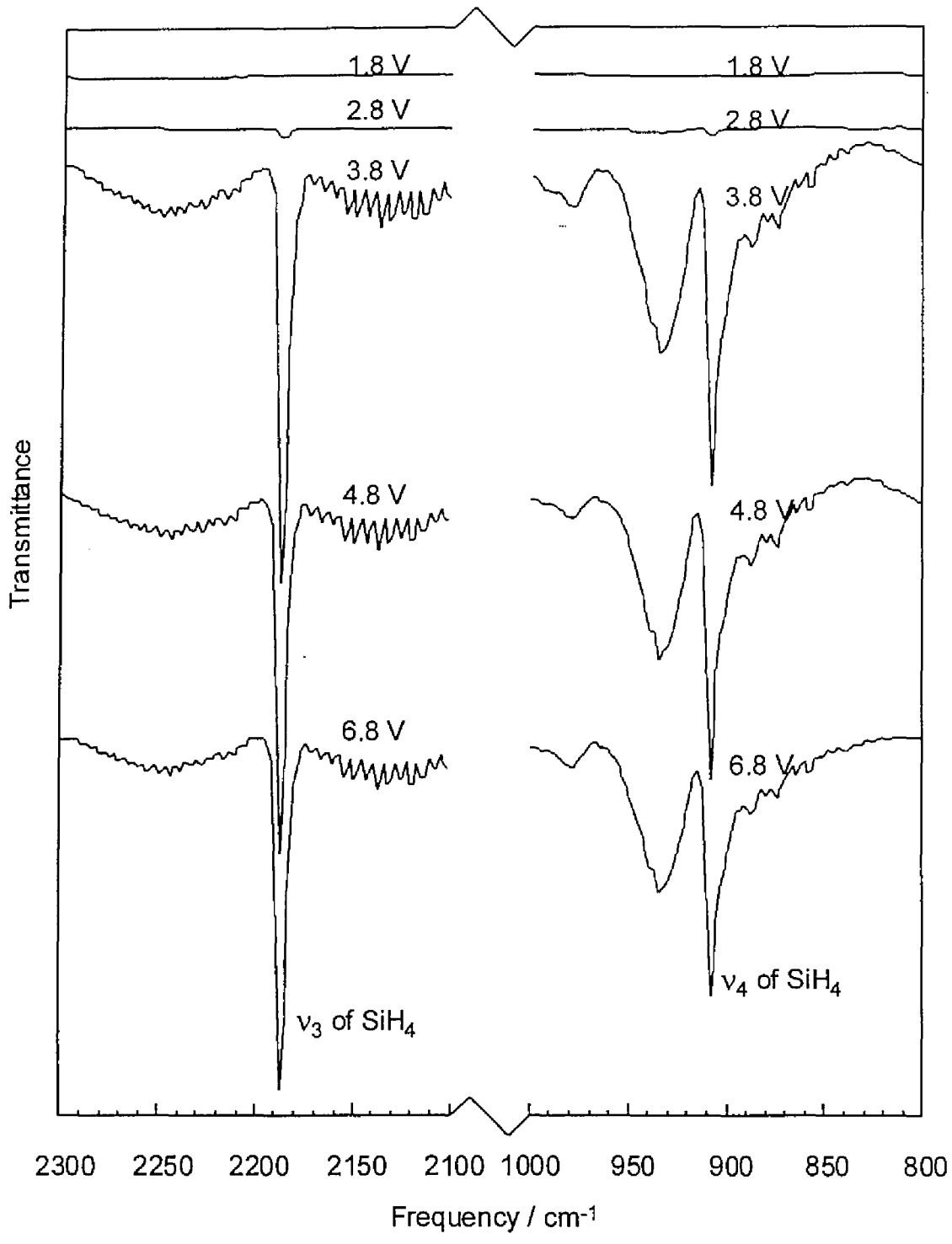

Fig. 6.11 IR spectra of gas samples obtained after potentiostatic electrolysis of a single crystal Si (100) electrode in a molten LiCl-KCl-LiF(1 mol%)-LiH(5 mol%) system at 673 K. Total charge of each electrolysis is 100 C.

6.3.1.3 Observation of electrode surface by SEM

The surface of the Si(100) electrode was studied after potentiostatic electrolysis. The electrolysis was performed at 4.8 V for 30 minutes in four different melts, *i.e.*, LiCl-KCl, LiCl-KCl-LiH(5 mol%), LiCl-KCl-LiF(0.1 mol%)-LiH(5 mol%) and LiCl-KCl-LiF(1 mol%)-LiH(5 mol%), respectively.

For comparison, a SEM image of the Si electrode prepared in a LiCl-KCl eutectic melt was obtained, as shown in Fig. 6.12 (a). No change from the initial Si is seen in the surface, which is consistent with the fact that very small current, order of mA cm^{-2}, was observed during the electrolysis. On the other hand, breakdown and dissolution of the electrode surface can be seen in the molten LiCl-KCl-LiH(5 mol%) case, Fig. 6.12 (b). The diameter of the remaining Si column is about 2-3 μm. There are also the larger falling traces, having the size of 20-30 μm.

To investigate the effect of F^- ion addition, 0.1 mol% LiF was added to the melt. Figure 6.13 (a) shows the SEM image. The traces of the breakdown and dissolution are finer than the traces in Fig. 6. 12 (b). There are also some pores of the size of 5-10 μm. The morphological difference between the F^- ion addition case and the no addition case indicates that the dissolution scheme of the Si electrode is different for each case. Combining the results of voltammetry and IR absorption spectroscopy, the dissolution of Si is considered to be easier for the F^- ion addition case. Furthermore, the result of 1.0 mol% LiF addition was also examined, as shown in Fig. 6.13 (b). The surface seems to be similar to the case of 0.1 mol% addition. Thus, the effect of F^- ion concentration has not been clarified from the SEM measurements.

(a) in a LiCl-KCl eutectic melt

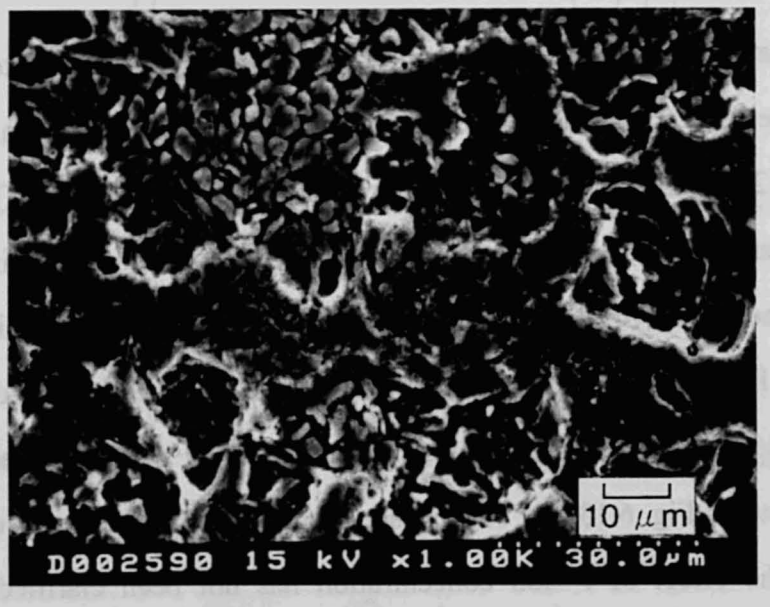

(b) in a molten LiCl-KCl-LiH(5 mol%) system

Fig. 6.12. SEM images of a single crystal Si (100) electrode after potentiostatic electrolysis at 4.8 V (vs. Li^+/Li) for 30 min. (a) in a LiCl-KCl eutectic melt and (b) in a molten LiCl-KCl-LiH(5 mol%) system.

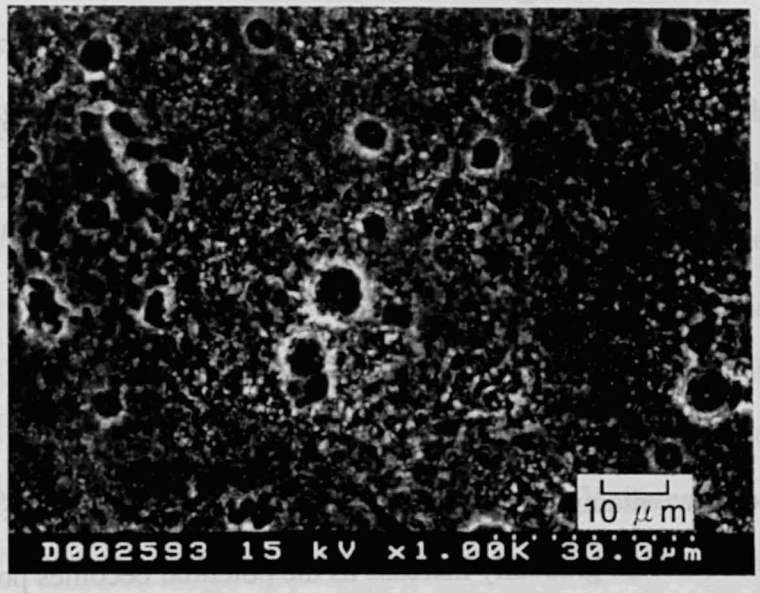

(a) in a molten LiCl-KCl-LiF(0.1 mol%)-LiH(5 mol%) system

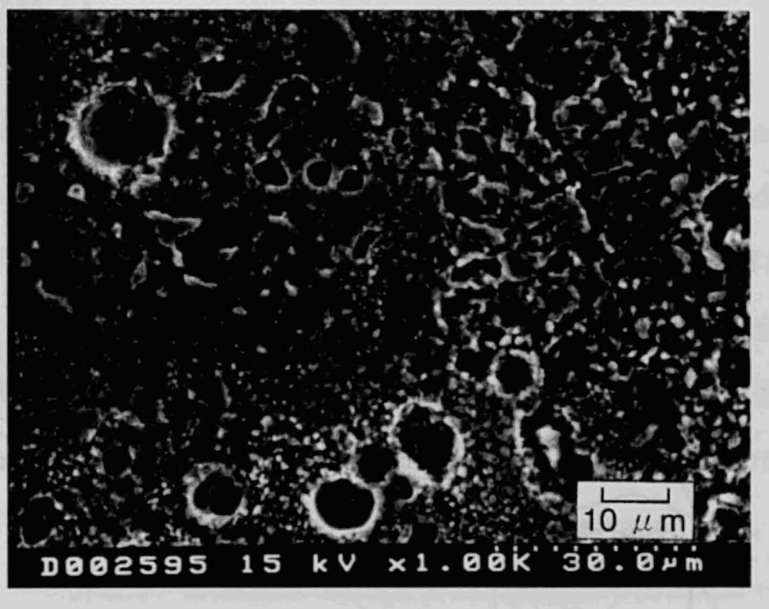

(b) in a molten LiCl-KCl-LiF(1 mol%)-LiH(5 mol%) system

Fig. 6.13. SEM images of a single crystal Si (100) electrode after potentiostatic electrolysis at 4.8 V (vs. Li^+/Li) for 30 min. (a) in a molten LiCl-KCl-LiF(0.1 mol%)-LiH(5 mol%) system and (b) in a molten LiCl-KCl-LiF(1 mol%)-LiH(5 mol%) system.

6.3.2 Behavior of a metal grade Si electrode

Since metal grade Si (98%) is supposed to be used for practical applications, a metal grade Si electrode was also investigated by cyclic voltammetry, and the evolved gas was analyzed by IR absorption spectroscopy.

6.3.2.1 Cyclic voltammetry

Blank

As a blank, cyclic voltammetry was performed in a LiCl-KCl eutectic melt (black curve in Fig. 6.14). Anodic currents gradually increase as the potential becomes positive and reach

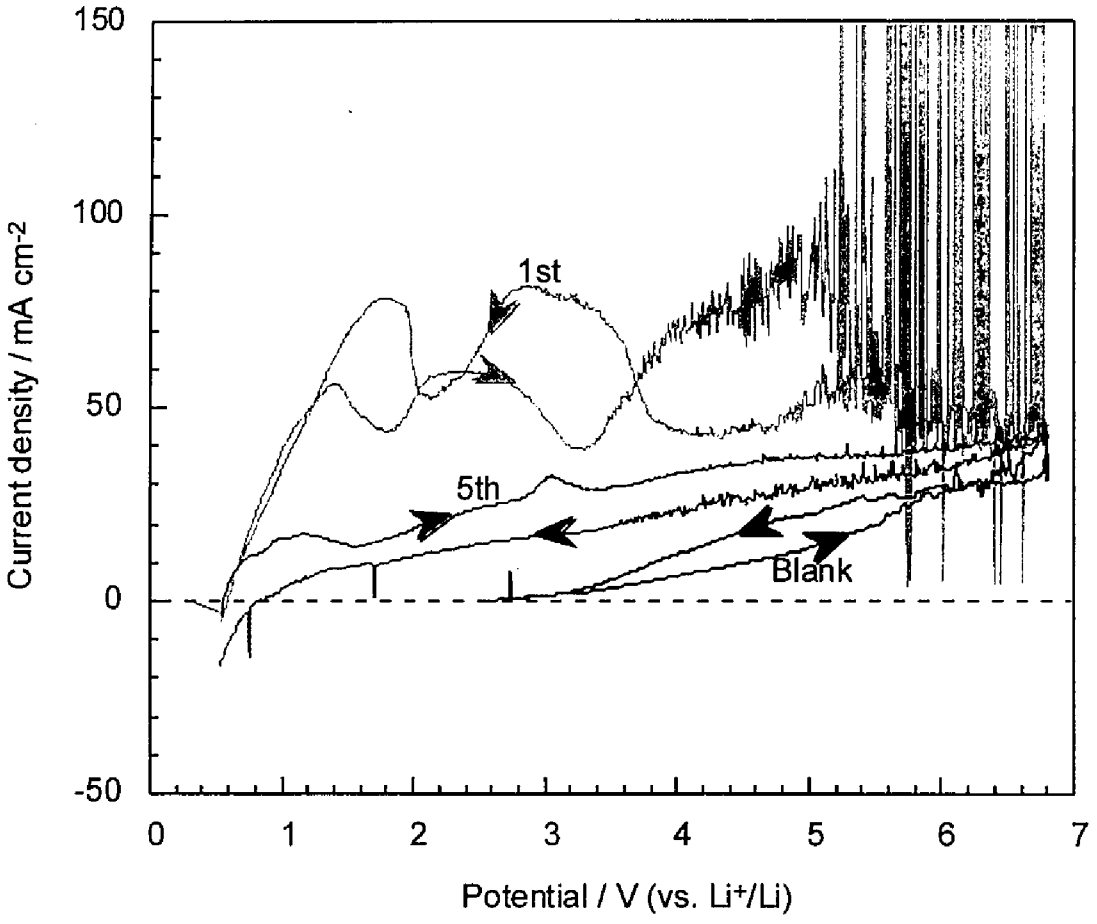

Fig. 6.14. Cyclic voltammograms for a metal grade Si (98%) electrode in a LiCl-KCl eutectic melt and a molten LiCl-KCl-LiH(5 mol%) system at 673 K. Scan rate: 0.05 V s^{-1}.

around 40 mA cm^{-2} at 6.8 V. Compared to the single crystal Si electrode, larger anodic currents are observed. This might be explained by the impurities in the electrode preventing the rigid passivation film growth.

In a molten LiCl-KCl-LiH(5 mol%) system

Figure 6.14 also shows cyclic voltammograms obtained in a molten LiCl-KCl-LiH(5 mol%) system. In the first cycle (a light gray curve), there are several anodic current peaks in both forward and reverse scans, which is similar to the case of a single crystal Si. Current fluctuations can be seen at potentials more positive than 4.0 V. However, the anodic current densities are only about one fifth of the current densities for single crystal Si. This suggests that metal grade Si is less reactive than single crystal Si.

In a molten LiCl-KCl-LiF(1 mol%)-LiH(5 mol%) system

In order to examine the effect of F^- ion addition, 1 mol% LiF was added to the melt. Figure 6.15 shows the measured cyclic voltammograms in the first, second and fifth cycles. Almost similar behavior to that of single crystal Si, see Fig. 6.8, is observed for the first cycle. Nevertheless, anodic current densities are approximately only one third of the current densities for single crystal Si, indicating the lower reactivity of metal grade Si. For the second and fifth cycles, the anodic currents become much smaller, which is similar to the behavior of single crystal Si. This is probably due to the formation of a passivation film.

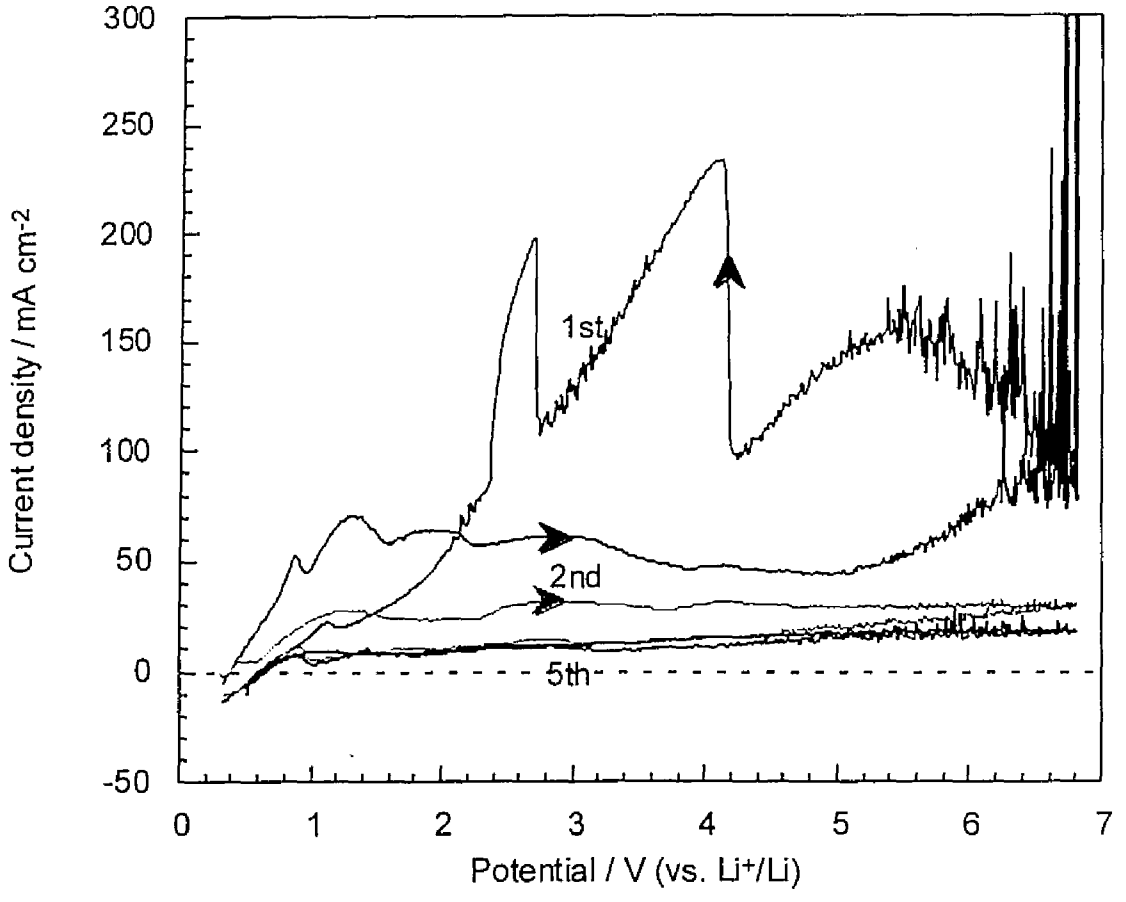

Fig. 6.15. Cyclic voltammograms for a metal grade Si (98%) electrode in a molten LiCl-KCl-LiF(1 mol%)-LiH(5 mol%) system at 673K. Scan rate: 0.05 V s^{-1}.

Comparison

To make clear the effect of F^- ion addition, the two measured voltammograms are compared in Fig. 6.16. Obviously, anodic currents are larger for the case of F^- ion addition, being similar to the case of single crystal Si. Furthermore, sharp anodic current peaks at 2.5 and 4.0 V can be seen only for the case of F^- ion addition. Though the actual reaction corresponding to the sharp current peaks has not been clarified yet, the existence of several peaks indicates the possibility of different reaction schemes. The overall tendency resembles the case of single crystal Si, *i.e.*, the anodic reactions are promoted by F^- ion addition.

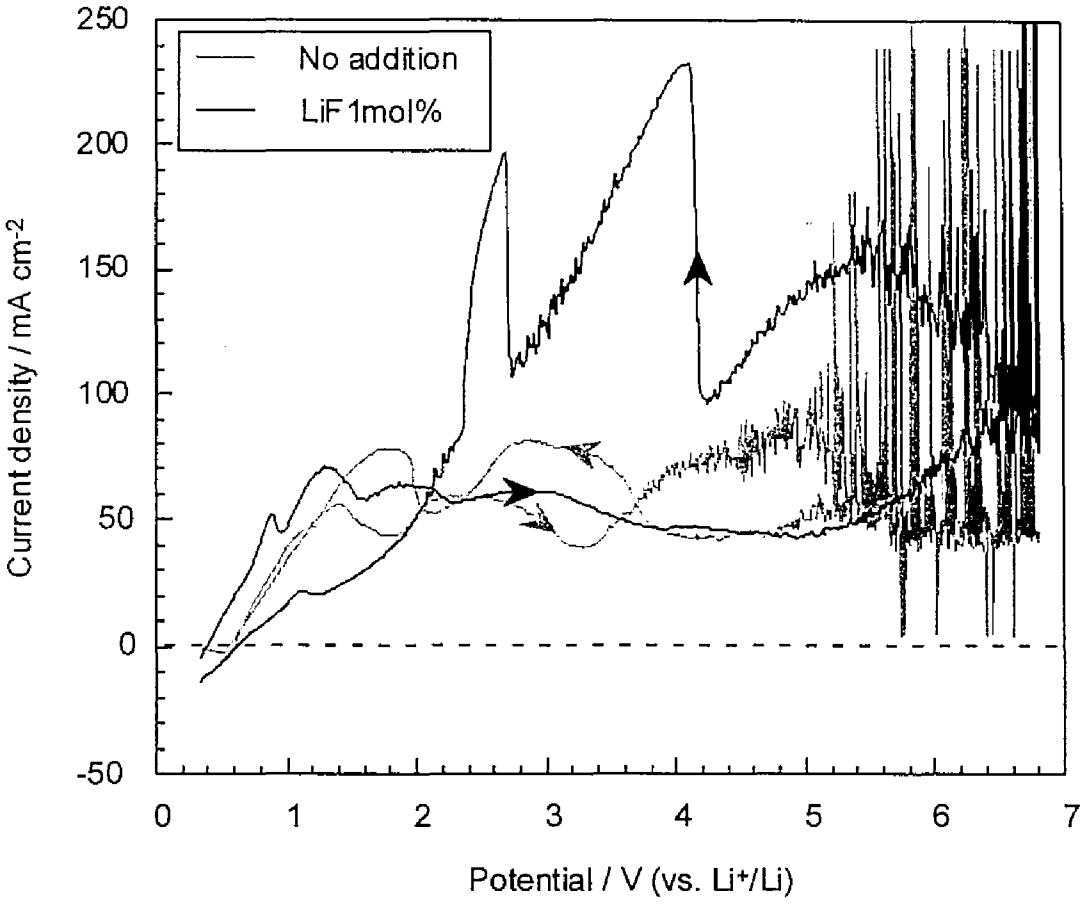

Fig. 6.16. Comparison of first cycle voltammograms for a metal grade Si electrode in a molten LiCl-KCl-LiH(5 mol%) system and in a molten LiCl-KCl-LiF(1mol%)-LiH(5 mol%) system. Scan rate: 0.05 V s^{-1}.

6.3.2.2 Gas analysis by IR absorption spectroscopy

Based on the results obtained by using cyclic voltammetry, potentiostatic electrolysis were conducted to prepare gas samples. The gas samples were then analyzed by IR absorption spectroscopy. For each electrolysis, the total charge was adjusted to 100 C in order to make direct comparison possible.

In a molten LiCl-KCl-LiH(5 mol%) system

Figure 6.17 shows the measured IR spectra for the gas samples obtained in a molten LiCl-KCl-LiH(5 mol%) system. The existence of SiH_4 is confirmed in the samples obtained at potentials more positive than 2.8 V. Nevertheless, judging from the heights of the absorption peaks, the amount of evolved SiH_4 is considered to be smaller than the amount obtained using a single crystal Si electrode (Fig. 6.10). This suggests that the reactivity of metal grade Si is lower than that of single crystal Si, in consistency with the cyclic voltammetry result.

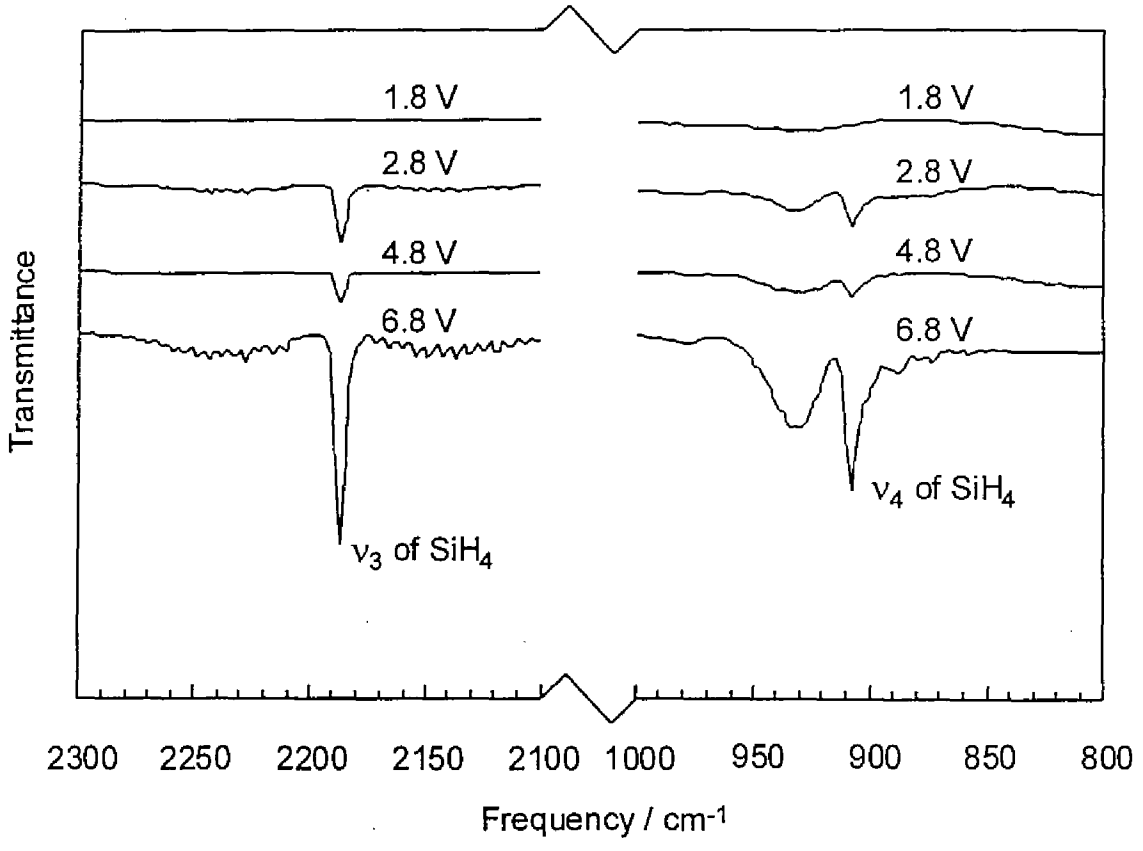

Fig. 6.17. IR spectra of gas samples obtained after potentiostatic electrolysis of a metal grade Si (98%) electrode in a molten LiCl-KCl-LiH(5 mol%) system at 673 K. Total charge of each electrolysis is 100 C.

In a molten LiCl-KCl-LiF(1 mol%)-LiH(5 mol%) system

The experiments were repeated after the addition of 1 mol% LiF to the melt. Figure 6.18 shows the results of the IR absorption spectroscopy. The presence of SiH_4 is confirmed in the samples obtained at potentials more positive than 2.8 V. The major difference from the no F^- ion addition case is much larger absorption peaks for 4.8 and 6.8V. The result shows that the F^- ion addition accelerates the SiH_4 evolution for metal grade Si as well as for single crystal Si.

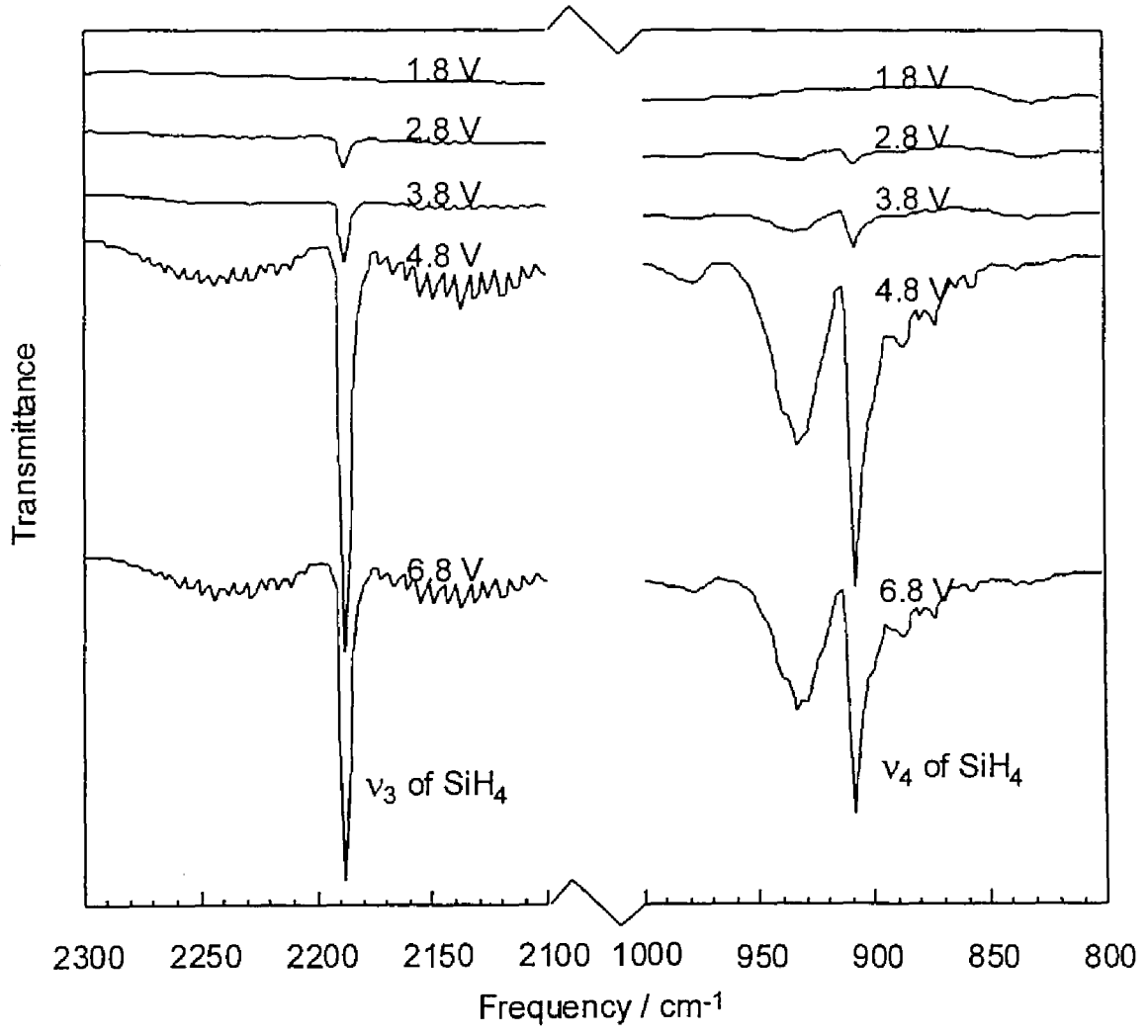

Fig. 6.18 IR spectra of gas samples obtained after potentiostatic electrolysis of a metal grade Si (98%) electrode in a molten LiCl-KCl-LiF(1 mol%)-LiH(5 mol%) system at 673 K. Total charge of each electrolysis is 100 C.

6.3.3 Considerations on current efficiency and reaction scheme

In the previous sections, it was qualitatively shown that SiH_4 evolves by anodic polarization of a Si electrode. In the present section, a semi-quantitative consideration is given. In the following discussion, current efficiency, η, is defined as

$$\eta = \frac{\text{charge corresponding to the evolved } SiH_4}{\text{total charge consumed}} \times 100 \qquad (10)$$

Since the addition of F^- ion has been found to be advantageous for SiH_4 evolution, experiments were conducted in the melts using a LiCl-KCl-LiF(1 mol%) system.

6.3.3.1 In molten LiCl-KCl-LiF(1 mol%)-LiH(5 mol%)

Estimation of current efficiency

The current efficiency was estimated for a single crystal Si electrode electrolyzed at 3.8, 4.8 and 6.8 V. These values were chosen because they seemed to have the highest SiH_4 concentrations, judging from the IR absorption spectra. The gas samples were the same as used for the IR spectroscopy experiments. The SiH_4 concentration was measured by a gas detecting tube. The results showed about 100 ppm of SiH_4 for all cases. Using both the total volume of the system, 1000 cm^3, and the total charge during electrolysis, 100 C, the current efficiency for SiH_4 evolution was calculated to be about 2%.

Possible reaction scheme

That the estimated current efficiency was as low as about 2% requires other current contributions than the SiH_4 evolution. The most likely reaction is H_2 evolution:

$$H^- \rightarrow \frac{1}{2} H_2 + e^- \qquad (11)$$

Since the presence of a large amount of H_2 in the gas samples was confirmed by gas chromatography, the reaction is thought to be the main electricity consuming reaction.

For the SiH_4 evolution, the following direct reaction is desirable due to the smallest

energy consumption:

$$Si + 4\,H^- \rightarrow SiH_4 + 4\,e^- \quad (12)$$

However, the requirement of positive potentials for SiH_4 evolution in the experiments suggests that the SiH_4 evolution mostly proceeds by indirect reactions, *i.e.*, the reactions of chlorosilanes, for example,

$$Si + 4\,Cl^- \rightarrow SiCl_4 + 4\,e^- \quad (13\text{-a})$$

$$SiCl_4 + 4\,H^- \rightarrow SiH_4 + 4\,Cl^- \quad (13\text{-b})$$

The similar reactions are also thought to be possible for SiH_3Cl, SiH_2Cl_2 and $SiHCl_3$ in addition to $SiCl_4$. Moreover, in the F^- ion addition case, the following fluorosilane reaction seems to be possible:

$$Si + 4\,F^- \rightarrow SiF_4 + 4\,e^- \quad (14\text{-a})$$

$$SiF_4 + 4\,H^- \rightarrow SiH_4 + 4\,F^- \quad (14\text{-b})$$

Strategy to improve current efficiency

From the above presented results and discussions, the SiH_4 evolution seems to mostly proceed by the reactions of chlorosilanes and H^- ion, and the H_2 gas evolution is considered to be the main electricity consuming reaction. Based on this, a strategy was thought out to improve the current efficiency. In the following discussion, the reactions being considered are limited to the H_2 evolution (reaction 11) and the $SiCl_4$ evolution (reaction 13-a) to simplify the explanation. In addition to this, whole evolved $SiCl_4$ is assumed to react with H^- ion to form SiH_4. Figure 6.19 (a) describes the conceptual representation of a concentration profile of H^- ion and a volume concentration profile of $SiCl_4$ gas for an ideal case. In this case, H^- ion and $SiCl_4$ completely react each other in the reaction zone. Thus, the H^- ion concentration is zero in the vicinity of the anode, resulting in no current consumption by H_2 gas evolution. Also, SiH_4 evolution rate, v_{SiH_4}, as a function of the distance from anode is drawn in Fig. 6.19 (b), in which the integrated area, S_v, is directly related to a nominal SiH_4 evolution current, $i_{SiH_4}(\text{nominal})$. After all, $i_{SiH_4}(\text{nominal})$ is regarded as equal to i_{SiCl_4}, thus, the

expected current efficiency is 100% in this case. However, the present experiment situation is thought to be different. Figure 6.20 (a) and (b) describe the assumed situation for a high H^- ion concentration case such as in molten LiCl-KCl-LiF(1 mol%)-LiH(5 mol%). In this case, since $SiCl_4$ evolution rate is not so high and H^- ion concentration in the bulk melt is high, H^- ion concentrations are considered to be high near the anode. That is, a H^- ion diffusion layer with large concentration gradient is thought to be exist. Consequently, H_2 gas evolution current becomes large, which results in the low current efficiency for SiH_4 production. On the other hand, low H^- ion concentration case is described in Fig. 6. 20 (c) and (d). In this case, a concentration gradient of a H^- ion diffusion layer is thought to be smaller than the gradient for the high concentration case, which means the smaller H_2 gas evolution current. Therefore, the melt with low H^- ion concentration is expected to give higher current efficiency, assuming the same $SiCl_4$ evolution rate for both cases.

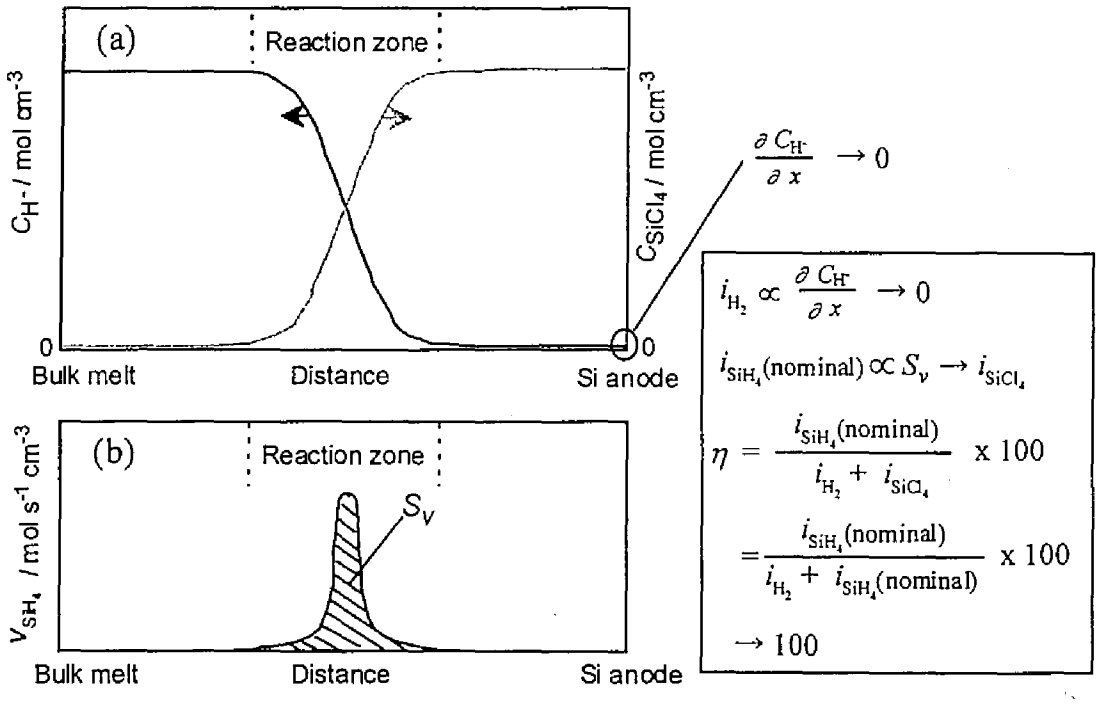

Fig. 6.19. Conceptual representation of (a) the concentration profiles of H^- ion and $SiCl_4$ (b) SiH_4 evolution rate as a function of the distance from anode, and explanation for the expected current efficiency for an ideal case.

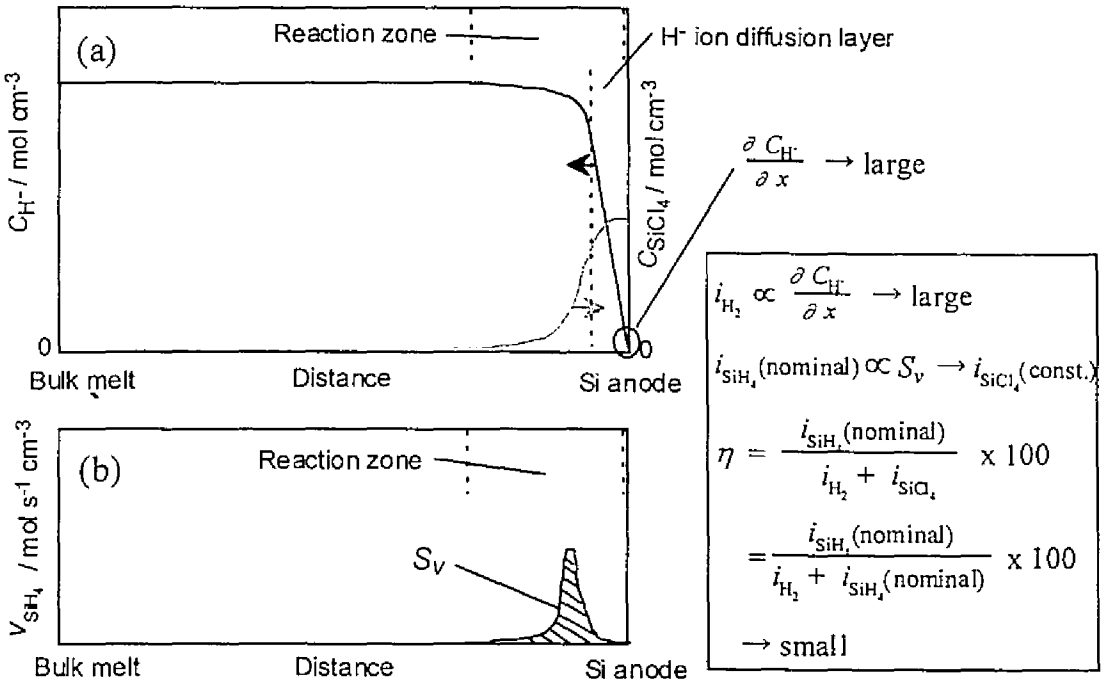

High H^- ion concentration case

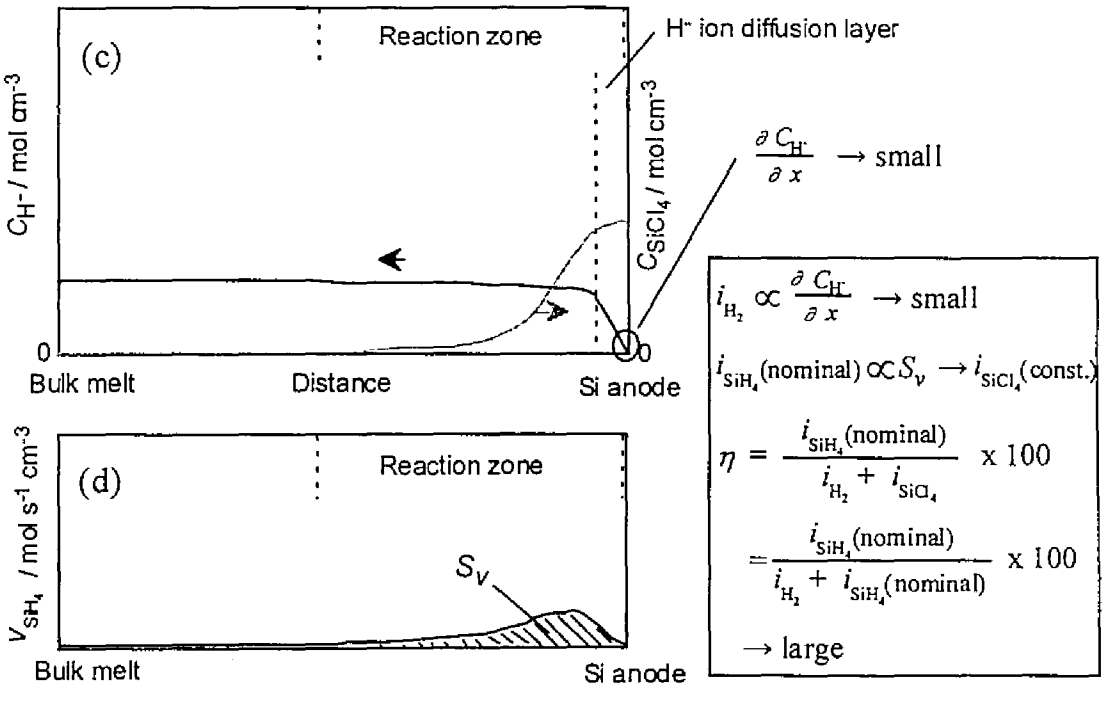

Low H^- ion concentration case

Fig. 6.20. Conceptual representation of the concentration profiles of H^- ion and $SiCl_4$ and explanation for the expected current efficiency for (a), (b) high H^- ion concentration case and (c), (d) low H^- ion concentration case.

6.3.3.2 In molten LiCl-KCl-LiF(1 mol%)-LiH (0.8 mol%)

Based on the strategy described in the previous section, the melt containing 0.8 mol% LiH was investigated.

Cyclic voltammetry

Figure 6.21 shows the cyclic voltammograms for a single crystal Si electrode. In the first forward scan, a sharp anodic current peak of 30 mA cm^{-2} is observed around 0.5 V. This

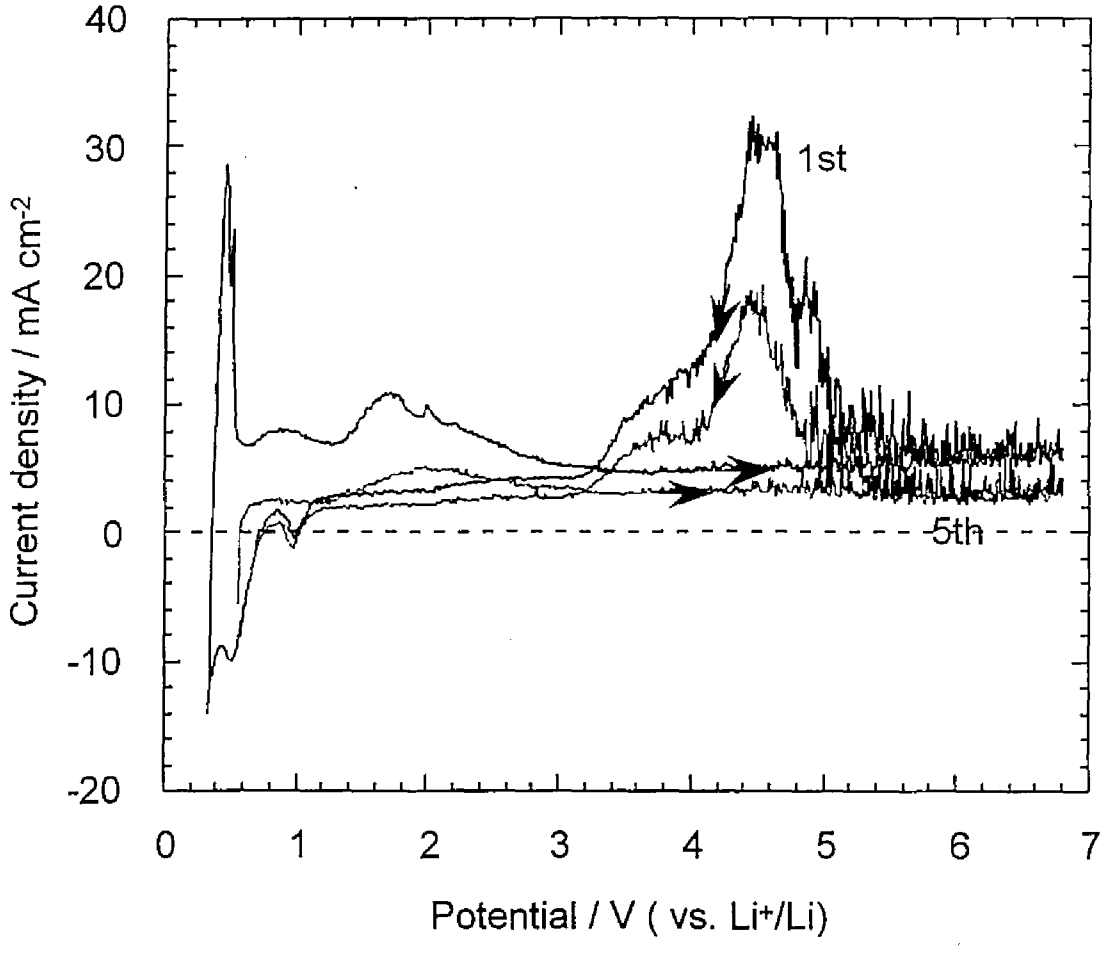

Fig. 6.21. Cyclic voltammograms for a single crystal Si (100) electrode in a molten LiCl-KCl-LiF(1 mol%)-LiH (0.8 mol%) system at 673 K. Scan rate: 0.05 V s^{-1}.

is thought to correspond to the oxidation of H^- ion to H_2 gas. Then anodic currents rapidly decrease to about 8 mA cm^{-2}, indicating passivation film formation. Current fluctuations start from 5.0 V, but they are not intensive. In the reverse scan, an anodic current peak appears around 4.5 V, which was not observed in the forward scan. This anodic current peak indicates the reaction of the Si electrode. Nevertheless, the anodic currents are only about one twentieth of the currents for the 5 mol% LiH system (Fig. 6.8). The small size of the current is thought to be due both to the diffusion control of H^- ion and to the decrease of the electrode area caused by the passivation film formation. In the fifth cycle, anodic currents become smaller, suggesting further growth of the passivation film. However, the anodic current peak at 4.5 V is still observed in the reverse scan.

IR absorption spectroscopy

Potentiostatic electrolysis was conducted at 3.5, 4.5 and 5.5 V until the quantity of electricity reached 10 C. The gas evolved during electrolysis was then analyzed by IR absorption spectroscopy (Fig. 6.22). The presence of SiH_4 is confirmed for all cases. However, the amounts of SiH_4 are larger for 4.5 and 5.5 V than for 3.5 V. The existence of a small amount of SiF_4 is also verified for the cases of 4.5 V and 5.5 V. The result supports the validity of the reaction scheme via SiF_4 (reaction 14-a and 14-b). Furthermore, the heights of the absorption peaks are similar to the heights for the 5 mol% LiH case (Fig. 6.8). Since the charge during electrolysis was only one tenth of the charge for the 5 mol% LiH case, higher current efficiency is indicated.

It is worth noting that the anodic currents during the electrolysis were as large as about 100 mA cm^{-2} for the case of 4.5 and 5.5 V. If this is compared with the current values found in the cyclic voltammetry, a large difference is observed. This is probably due to the absence of a passivation film in the potentiostatic case, which in turn might be explained by the potential step being directly applied to a new Si electrode.

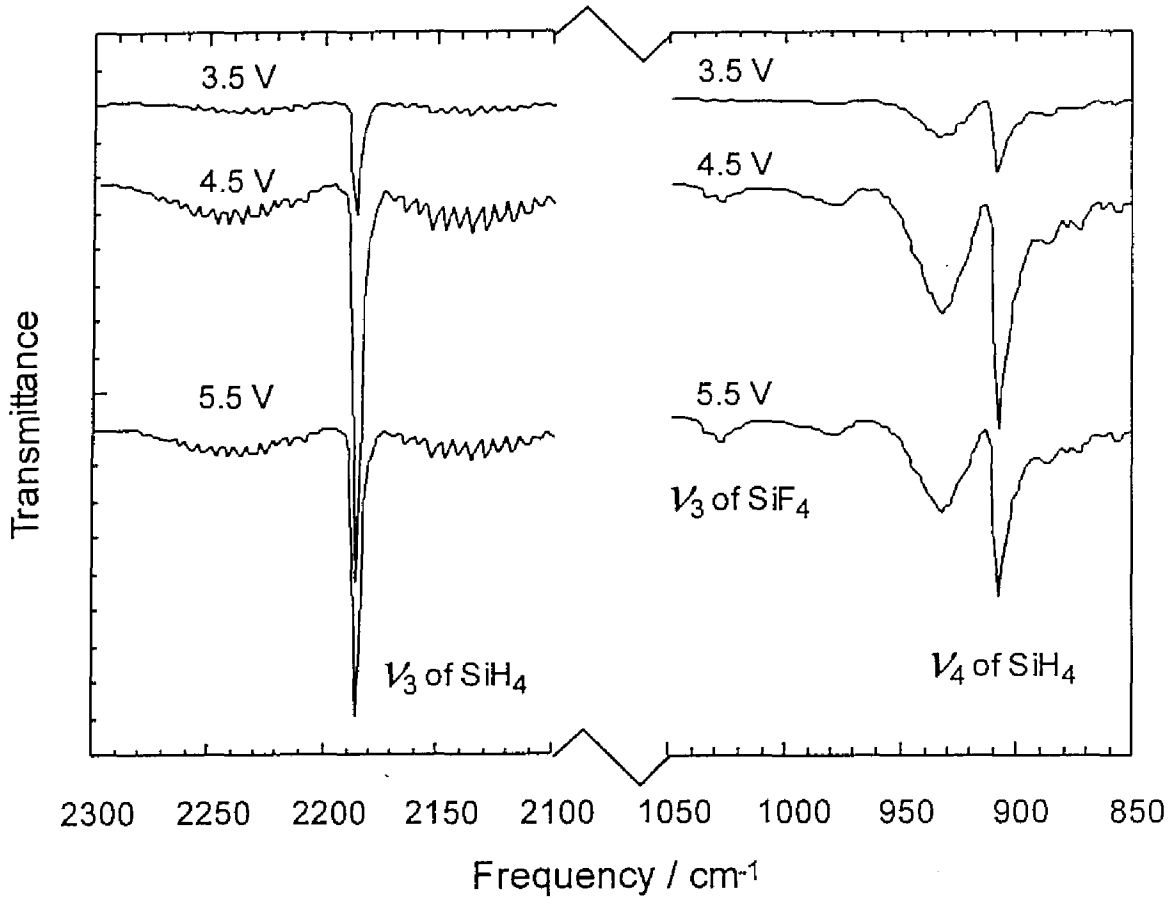

Fig. 6.22. IR spectra of gas samples obtained after potentiostatic electrolysis of a single crystal Si (100) electrode in a molten LiCl-KCl-LiF (1 mol%)-LiH(0.8 mol%) system at 673 K. Total charge of each electrolysis is 10 C.

Estimation of current efficiency

The gas samples were prepared in the same potentiostatic electrolysis for the IR measurements, then the concentrations of SiH_4 were measured by a gas detecting tube. The values were 20 ppm for 3.5 V, and 100 ppm for 4.5 and 5.5 V. The current efficiencies are estimated to be about 4 % for 3.5 V, and about 20 % for 4.5 and 5.5 V. The obtained current efficiency of 20 % is ten times higher than for the 5 mol% LiH case. This shows that a low H^- ion concentration is effective to improve the current efficiency of SiH_4 evolution.

6.4 Conclusions

In order to develop a novel method for SiH_4 production, electrode behavior of single crystal Si and metal grade Si was investigated in molten LiCl-KCl-LiH systems. The conclusions obtained through the study are summarized below.

(1) Anodic currents hardly flow on a single crystal Si electrode in a LiCl-KCl eutectic melt. This is thought to be due to the formation of a Si-Cl passivation film.

(2) The cyclic voltammograms obtained in a molten LiCl-KCl-LiH(5 mol%) system showed several anodic current peaks and current fluctuations, indicating the reactions of the Si electrode. However, after several scan cycles, the anodic currents decreased, suggesting growth of a passivation film consisting of Si-H or Si-Cl.

(3) The gas samples obtained by potentiostatic electrolysis in a molten LiCl-KCl-LiH(5 mol%) system were analyzed by IR absorption spectroscopy. The result showed the existence of SiH_4 at potentials more positive than 3.8 V.

(4) When F^- ion is added to the melt, the anodic reactions are promoted. The amount of evolved SiH_4 also increases.

(5) Metal grade Si shows similar behavior as single crystal Si. The evolution of SiH_4 is possible at potentials more positive than 2.8 V.

(6) The current efficiency of SiH_4 evolution was estimated to be around 2% for a single crystal Si electrode in a molten LiCl-KCl-LiF(1 mol%)-LiH(5 mol%) system.

(7) The main current consuming reaction is regarded as H_2 gas evolution:

$$H^- \rightarrow \frac{1}{2} H_2 + e^-$$

(8) The requirement of positive potentials for SiH_4 evolution in the experiments suggests that the SiH_4 evolution proceeds by indirect reactions, *i.e.*, the reaction of chlorosilanes, for example,

$$Si + 4\,Cl^- \rightarrow SiCl_4 + 4\,e^-$$

$$SiCl_4 + 4\,H^- \rightarrow SiH_4 + 4\,Cl^-$$

This reaction is also thought to be possible for SiH_3Cl, SiH_2Cl_2 and $SiHCl_3$ in addition to $SiCl_4$.

(9) Based on the strategy to improve current efficiency, the low H^- ion concentration system, *i.e.*, a molten LiCl-KCl-LiF(1 mol%)-LiH(0.8 mol%) system was investigated. The result showed current efficiencies of about 20%.

(10) In the case of a molten LiCl-KCl-LiF(1 mol%)-LiH(0.8 mol%) system, a small amount of SiF_4 was founded. Thus, the following fluorosilane reaction is suggested:

$$Si + 4\,F^- \rightarrow SiF_4 + 4\,e^-$$

$$SiF_4 + 4\,H^- \rightarrow SiH_4 + 4\,F^-$$

(11) The novel method of SiH_4 production was confirmed to have the feasibility of developing into a practical process in the future.

References

[1] W. Simmler, in *Ullmann's Encyclopedia of Industrial Chemistry*, Vol. A24, p.1, VCH Publishers (1993).

[2] E. Hengge et al., in *Gmelin Handbook of Inorganic Chemistry, Silicon, Supplement Volume B1, Silicon and Noble Gases, Silicon and Hydrogen,* p. 105, Springer-Verlag (1982).

[3] R. Hayashi, in *Surface Science Technology Series Vol. 3, Science of Silicon,* ed. UCS study group on semiconductor basic technology, Realize Corporation (1996), in Japanese.

[4] W. Sundermeyer and L. M. Litz, *Chem. Ing.Tech.*, **37,** 14(1965).

[5] Y. Yatsurugi, *Molten Salt*, **31,** 77(1988), in Japanese.

[6] Chase et al., *J. Phys. Chem. Ref. Data,* **14,** Suppl. 1, (1985).

[7] J. A. Plambeck, in *Encyclopedia of Electrochemistry of the Elements, volume X, Fused Salt Systems*, ed., A. J. Bard, p.18, Marcel Dekker, New York (1976).

[8] W. Sesselmann, E. Hudeczek and F. Bachmann, *J. Vac. Sci. Technol. B,* **7,** 1284(1989).

[9] F. Gaspari, S. K. O'Leary and S. Zukotynski, *J. Non-Cryst. Solids,* **155,** 149(1993).

[10] R. E. Wilde, T. K. K. Srinivasan, R. W. Harral and S. G. Sankar, *J. Chem. Phys.*, **55,** 5681(1971).

Chapter 7

General Conclusion

Electrochemical reactions involving hydride (H^-) ion in molten salts were investigated with the scope of developing some useful applications. The obtained results are summarized below.

In chapter 2, the author presented the electrochemical behavior of H^- ion including both anodic and cathodic reactions to obtain fundamental data. Investigations were conducted on a Mo electrode in a molten LiCl-KCl-LiH system by cyclic voltammetry, chronopotentiometry and double potential step chronoamperometry. Using a Mo electrode the hydrogen absorption into the electrode could be neglected, which made possible the investigation of the reverse cathodic reaction without any influence of absorbed hydrogen. Cyclic voltammetry showed that the electrode reaction of H^- ion proceeds by a reversible electrochemical reaction followed by a chemical reaction. The observed voltammograms were analyzed by conventional methods including a convolution technique, which gave $E_{1/2}$ = 0.755 V (vs. Li^+/Li) and $n \sim 1$ for the anodic oxidation of hydride ion. The chronopotentiometry results also indicated reversible behavior with $E_{\tau/4}$ = 0.75 V and $n \sim 1$ for the anodic oxidation of H^- ion. Double potential step chronoamperometry was conducted to study the chemical reaction steps, and the results point to the following reaction scheme:

$$H^- \rightarrow H_{ad} + e^- \qquad \text{(Reversible)}$$

$$H_{ad} + H_{ad} \rightarrow H_{2,sol} \qquad \text{(Reversible)}$$

$$H_{2,sol} \rightarrow H_{2,bubble} \qquad \text{(Irreversible)}$$

Diffusion coefficients of H^- ion were estimated by different methods and found to be in the range of 1.4-2.2 x 10^{-5} cm^2 s^{-1} at 673 K. The values show good agreement with literature data.

Finally, cathodic polarization curves for gas electrodes showed that the electrochemical reduction of H_2 gas is possible in a molten LiCl-KCl-LiH(2.0 mol%) system. It was also shown that Ni is superior to Mo for cathodic reduction of H_2 gas.

The author then attempted to investigate the hydrogen absorbing behavior of metals at high temperature using electrochemical reactions involving H^- ion. And as a first step, Pd and Pd-Li alloys were selected to be investigated.

In chapter 3, to provide fundamental information concerning the electrochemical formation of Pd-Li alloys in the molten LiCl-KCl system, electrodeposition of lithium on palladium was investigated by electroanalytical techniques. Electrochemical formation of various phases of Pd-Li alloy was achieved using cathodic polarization of the palladium electrode at various potentials in a LiCl-KCl eutectic melt at 723 K. The formation reactions and the corresponding formation potentials of each Pd-Li alloy phase were determined as follows:

$7\,Pd + Li^+ + e^- \rightleftharpoons Pd_7Li$	1.05 V (vs. Li^+/Li)
$2\,Pd_7Li + 5\,Li^+ + 5\,e^- \rightleftharpoons 7Pd_2Li$	0.64 V (vs. Li^+/Li)
$Pd_2Li + Li^+ + e^- \rightleftharpoons 2\,PdLi$	0.53 V (vs. Li^+/Li)
$PdLi + Li^+ + e^- \rightleftharpoons PdLi_2$	0.20 V (vs. Li^+/Li)
$PdLi_2 + x\,Li^+ + x\,e^- \rightleftharpoons$ liq. phase	0.06 V (vs. Li^+/Li)

These results also provide useful information concerning the electrochemical window of the molten LiCl-KCl system, which is of importance for the electrochemical formation reactions of palladium-rare earth alloys.

In chapter 4, the electrochemical study was continued for the Pd-Li alloy. A series of open-circuit potentiometry and constant current chronopotentiometry were carried out to determine the potentials for the various coexisting Pd-Li phase in the temperature range of 673-773 K. These potential values were used to calculate the activities and relative partial molar properties of both Li and Pd. The standard Gibbs free energies of the formation of Pd_7Li, Pd_2Li, PdLi, $PdLi_2$ and liquid phase alloy were also determined in the specified

temperature range. The obtained results are the first measured thermodynamic data for solid and liquid Pd-Li compounds.

In chapter 5, electrochemical hydrogen absorption and desorption into/from Pd and Pd-Li alloys were studied in a molten LiCl-KCl-LiH system. 5 mol% LiH showed to have sufficient hydrogen supplying ability for the investigation of the hydrogen absorbing behavior of the electrodes. It was shown that Pd spontaneously changes into $PdLiH_x$ by immersion into a molten LiCl-KCl-LiH system since anodic hydrogen absorption and cathodic lithium deposition occurs in the same potential range on a Pd electrode. From chronopotentiometry measurements performed under hydrogen discharging, values of the H/Pd ratio for Pd, Pd_7Li, Pd_2Li and PdLi electrodes were found to be 0.05, 0.08, 0.27 and 0.74, respectively. These values show that the hydrogen absorbing ability for Pd-Li alloys increases with increasing Li concentration. This tendency can be explained by the stronger interaction of Li-H than of Pd-H. The result obtained in chapter 5 confirmed the validity of the electrochemical method using a molten LiCl-KCl-LiH system.

In chapter 6, the electrode behavior of single crystal Si and metal grade Si were investigated in molten LiCl-KCl-LiH systems in order to develop a novel method for SiH_4 production. Anodic currents scarcely flowed on a single crystal Si electrode in a LiCl-KCl eutectic melt, which was thought to be due to the formation of a Si-Cl passivation film. The cyclic voltammograms in a molten LiCl-KCl-LiH(5 mol%) system showed several anodic current peaks and current fluctuations, indicating the reactions of the Si electrode. After several scan cycles, the anodic currents decreased, which was thought to be due to the growth of a passivation film consisting of Si-H or Si-Cl. The existence of SiH_4 in the gas samples obtained by potentiostatic electrolysis at more positive potentials than 3.8 V was confirmed by IR absorption spectroscopy. Addition of F^- ion to the melt was found to be effective for SiH_4 evolution. Metal grade Si showed similar behavior as single crystal Si. The evolution of SiH_4 was possible at more positive potentials than 2.8 V for metal grade Si. The current efficiency of SiH_4 evolution was estimated to be about 2% for a single crystal Si electrode in a

molten LiCl-KCl-LiF(1 mol%)-LiH(5 mol%) system. The main current consuming reaction is considered as H_2 gas evolution:

$$H^- \rightarrow \frac{1}{2} H_2 + e^-$$

The requirement of considerably positive potentials for SiH_4 evolution in the experiments suggests that the SiH_4 evolution proceeds by indirect reactions, *i.e.*, reactions of chlorosilanes, for example,

$$Si + 4\,Cl^- \rightarrow SiCl_4 + 4\,e^-$$

$$SiCl_4 + 4\,H^- \rightarrow SiH_4 + 4\,Cl^-$$

The reaction is also thought to be possible for SiH_3Cl, SiH_2Cl_2 and $SiHCl_3$ in addition to $SiCl_4$. In order to improve current efficiency, a molten LiCl-KCl-LiF(1 mol%)-LiH(0.8 mol%) system was investigated, which showed a current efficiency about 20%. In the case of a molten LiCl-KCl-LiF(1 mol%)-LiH(0.8 mol%) system, a small amount of SiF_4 was also found. Thus, the following reaction of fluorosilane is suggested:

$$Si + 4\,F^- \rightarrow SiF_4 + 4\,e^-$$

$$SiF_4 + 4\,H^- \rightarrow SiH_4 + 4\,F^-$$

In conclusion, the novel method of SiH_4 production was confirmed to have the feasibility of developing into a practical process in the future.

List of Publications

The main parts of this thesis are constructed from the following papers.

Chapter 2

1. T. Nohira and Y. Ito, to be submitted to *J. Electrochem. Soc.*

   "Electrochemical behavior of hydride ion on a Mo electrode in a LiCl-KCl eutectic melt"

Chapter 3

2. T. Nohira, K. Amezawa and Y. Ito, *J. Appl. Electrochem.* **25,** 48(1995).

   "Electrochemical formation of Pd-Li alloys in LiCl-KCl eutectic melts"

Chapter 4

3. T. Nohira and Y. Ito, *J. Electrochem. Soc.* **145,** 785(1998).

   "Thermodynamic properties of Pd-Li alloys"

Chapter 5

4. T. Nohira and Y. Ito, *J. Electrochem. Soc.* **144,** 2290(1997).

   "Electrochemical hydrogen absorbing behavior of Pd and Pd-Li alloys in a molten LiCl-KCl-LiH system"

Chapter 6

5. T. Nohira and Y. Ito, to be submitted to *J. Electrochem. Soc.*

   "Electrode behavior of Si and evolution of SiH_4 in molten LiCl-KCl-LiH systems"

Acknowledgment

The author wishes to express his sincere gratitude to Professor Yasuhiko Ito for his supervision, encouragement and important discussions throughout this study. He has provided a creative research environment, many chances to meet other researchers and his own outstanding wisdom.

Special acknowledgment is due to Associate Professor Rika Hagiwara for his kind guidance, helpful advice and continuos encouragement throughout the study. The author is especially grateful for his help and advice on X-ray diffraction analysis and IR absorption spectroscopy. The author would like to thank Mr. Takuya Goto for his stimulating discussions and valuable advice on the experimental techniques etc. throughout the study. Special thanks to Ms. Keiko Ema for her valuable advice on the experiments. The author is much indebted to Mr. Koji Amezawa. In the beginning of the study, the author was fortunate to have worked with him and learned many important things from him. The author wishes to express his appreciation to Mr. Masayuki Tada for his warm encouragement throughout the study. The author is also grateful to Mr. Takahiro Shiino for his collaboration for the study appearing in chapter 6.

The author would like to thank Associate Professor Yoichi Tomii for his stimulating discussions and warm encouragement to push the study forward. The author is also indebted to Associate Professor Yasuhiro Fukunaka for his kind suggestions and continuous encouragement. The author wishes to thank Professor Yukio Ogata for his valuable suggestions on the Si electrode and for providing the single crystal Si electrode.

Acknowledgment is due to Mr. Koji Yoshida for SEM appeared in chapter 2. The author would like to express his appreciation to Mr. I. Nakagawa for his technical assistance on the SEM study appeared in chapter 6.

Special thanks are due to Dr. Erik O. Ahlgren for his careful reading of the manuscript and valuable suggestions. The author also wishes to thank Mr. Lennart Olav Jerdal for

language corrections and useful suggestions. The author's experience in the lab has been enriched by these international friendships.

The author would like to thank to all the members of Professor Ito's laboratory, especially Messrs. Tokujiro Nishikiori, Qiao Huan and Akira Kinoshita for their great contribution to the study, and Messrs. Junya Kondoh, Hiroyuki Kawamura and Kan Hachiya for their stimulating discussions.

A part of the study was carried out with support from a Grant-in-Aid from the Japanese Ministry of Education, Science, Sports and Culture. The author is indebted to the Japan Society for the Promotion of Science for Young Scientists for financial support.

May 13th, 1998

Toshiyuki Nohira